SANDIA REPORT
SAND2008-4809
Unlimited Release
Printed July 2008

Active Load Control Techniques for Wind Turbines

Dale Berg, Scott J. Johnson, C.P. “Case” van Dam

Prepared by
Sandia National Laboratories
Albuquerque, New Mexico 87185 and Livermore, California 94550

Sandia is a multiprogram laboratory operated by Sandia Corporation,
a Lockheed Martin Company, for the United States Department of Energy’s
National Nuclear Security Administration under Contract DE-AC04-94AL85000.

Approved for public release; further dissemination unlimited.

Issued by Sandia National Laboratories, operated for the United States Department of Energy by Sandia Corporation.

NOTICE: This report was prepared as an account of work sponsored by an agency of the United States Government. Neither the United States Government, nor any agency thereof, nor any of their employees, nor any of their contractors, subcontractors, or their employees, make any warranty, express or implied, or assume any legal liability or responsibility for the accuracy, completeness, or usefulness of any information, apparatus, product, or process disclosed, or represent that its use would not infringe privately owned rights. Reference herein to any specific commercial product, process, or service by trade name, trademark, manufacturer, or otherwise, does not necessarily constitute or imply its endorsement, recommendation, or favoring by the United States Government, any agency thereof, or any of their contractors or subcontractors. The views and opinions expressed herein do not necessarily state or reflect those of the United States Government, any agency thereof, or any of their contractors.

Printed in the United States of America. This report has been reproduced directly from the best available copy.

Available to DOE and DOE contractors from
U.S. Department of Energy
Office of Scientific and Technical Information
P.O. Box 62
Oak Ridge, TN 37831

Telephone: (865) 576-8401
Facsimile: (865) 576-5728
E-Mail: reports@adonis.osti.gov
Online ordering: http://www.osti.gov/bridge

Available to the public from
U.S. Department of Commerce
National Technical Information Service
5285 Port Royal Rd.
Springfield, VA 22161

Telephone: (800) 553-6847
Facsimile: (703) 605-6900
E-Mail: orders@ntis.fedworld.gov
Online order: http://www.ntis.gov/help/ordermethods.asp?loc=7-4-0#online

SAND2008-4809
Unlimited Release
Printed July 2008

Active Load Control Techniques for Wind Turbines

Scott J. Johnson and C. P. "Case" van Dam
Department of Mechanical and Aeronautical Engineering
University of California
One Shields Avenue
Davis, CA 95616-5294

Dale E. Berg, Sandia National Laboratories Technical Manager

Sandia Contract No. 360473

ABSTRACT

This report provides an overview on the current state of wind turbine control and introduces a number of active techniques that could be potentially used for control of wind turbine blades. The focus is on research regarding active flow control (AFC) as it applies to wind turbine performance and loads. The techniques and concepts described here are often described as "smart structures" or "smart rotor control". This field is rapidly growing and there are numerous concepts currently being investigated around the world; some concepts already are focused on the wind energy industry and others are intended for use in other fields, but have the potential for wind turbine control. An AFC system can be broken into three categories: controls and sensors, actuators and devices, and the flow phenomena. This report focuses on the research involved with the actuators and devices and the generated flow phenomena caused by each device.

Disclaimer:

Given the nature of research in a progressive field such as wind energy, it is very difficult to mention every potential AFC device and to report precisely on all of the past and up-to-date findings. If a device or research paper is not mentioned within, it is because it was not found during the literature survey. Publications up through 2007 were used in this report.

TABLE OF CONTENTS

TABLE OF FIGURES

NOMENCLATURE

A_{jet}	Cross-sectional area of jet
A_f	Flap aspect ratio (L_f / L_g)
A_{ref}	Planform area of rotor blade, ref. area for momentum coef.
b	Airfoil span length / Turbine blade span
B	Blowing ratio
c	Airfoil chord length
C_D	Sectional drag coefficient
C_L	Sectional lift coefficient
C_M	Sectional pitching moment coefficient
C_P	Coefficient of pressure
C_μ	Momentum coefficient ($\dot{m}_{jet}V_{jet}$ / $0.5\rho V_{ref}^2 A_{ref}$)
d	Diameter of orifice
D	Duty cycle
f	Pulsing Frequency
F^+	Reduced pulsing frequency (f X / V)
F_A	Actuator force
h	Height of device from airfoil surface
i	Electric current
k	Reduced airfoil frequency ($\omega c/2U_\infty$)
L	Sectional lift ($L = 0.5\rho V^2 c C_L$)
L_f	Spanwise length of flap
L_g	Spanwise length of gap between flaps
L_{ref}	Reference length; chord = 1.0
L_T	Length of tab
Lx	Lever arm length in x direction
Ly	Lever arm length in y direction
M_∞	Freestream Mach number
$\dot{m}$	Mass flow rate of air
n	Rotational speed of blade
Re	Reynolds number ($\rho U_\infty L_{ref}/\mu$)
SR	Solidity ratio (span covered by device / total span of model)
t	Physical time (seconds)
T	Non-dimensional time ($U_\infty t/c$)
U_∞	Freestream velocity
V	Velocity over airfoil/blade
V_{AC}	Voltage (AC)
V_{DC}	Voltage (DC)
V_{jet}	Velocity of jet
V_{ref}	Rotor tip speed
V_{RMS}	Root mean squared voltage
x	Distance (along chord)
X	Representative lengthscale of separation zone

y	Distance (from airfoil surface)
z	Distance (along span)
α	Angle of attack (degrees)
α_m	Mean angle of attack (degrees)
α_{stall}	Angle of attack at stall (degrees)
β_{flap}	Flap angle (degrees)
δ	Boundary-layer thickness
Δ	Change or difference
θ	Angle of rotation (degrees)
θ_{pitch}	Blade incidence angle
ρ	Air density
ω	Frequency of pitch oscillation
Acronyms	
AFC	Active flow control
AFW	Active flexible wall
ATEG	Adaptive trailing edge geometry
CAD	Computer-aided design
CFD	Computational fluid dynamics
COE	Cost of Energy
CCW	Circulation control wing
DBD	Dielectric barrier discharge
DS	Delay stall
FCSD	Flexible composite surface deturbulator
HAWT	Horizontal axis wind turbine
HiMVG	High-frequency micro vortex generator
LPT	Low pressure turbine
MEM	Micro-electrical mechanical
MiTES	Miniature trailing-edge effectors
MVG	Micro vortex generator
NREL	National Renewable Energy Laboratory
O&M	Operations and maintenance
PIV	Particle imaging velocimetry
PVGJ	Pulsed vortex generator jet
RPM	Revolutions per minute
SVG	Smart vortex generator
UAV	Unmanned aerial vehicle
VG	Vortex generator
VGJ	Vortex generator jet
ZNMF	Zero net-mass flux

1 INTRODUCTION

1.1 Background

Wind energy is the fastest growing source of energy in the world today, with an average growth rate of nearly 30% per year for the past 10 years.[1] The U.S. installed capacity surged 45% in 2007, now totaling more than 16,800 MW, which generates an estimated 48 billion kilowatt-hours (KWh), enough to power 4.5 million homes.[2] For many utility companies, wind energy has become not only the renewable energy of choice, but also the least-cost option for new generation. With global warming, energy security, and rising fuel prices being main public concerns, it is feasible to assume that the growth of the wind energy industry will continue. However, it is still important to improve upon the technology in order to keep wind energy economically competitive with traditional and other renewable energy sources. This is done by lowering the cost of energy (COE), which can be accomplished in a number of different ways. There are three independent variables that go into calculating the cost of energy; the energy capture of the turbine over its lifetime, the capital cost of the turbine, and the operations and maintenance (O&M) costs. O&M costs can be further divided into scheduled and unscheduled costs.

$$COE = \frac{Lifetime\ Energy\ Capture}{Capital\ Cost + O\ \&\ M\ Cost} \qquad \textbf{(Eqn. 1)}$$

There are several different ways to lower the COE. By simply looking at the equation, one way is to make more reliable turbines, thereby reducing the downtime and O&M costs. Another is to decrease the amount of materials or improve manufacturing techniques that would allow the capital cost to drop. Technological advances to wind

turbines is becoming even more critical because capital costs are rising due to increasing raw material costs, high turbine demand, and increasing cost of energy inputs. Another technique used to reduce the COE is by increasing the rotor diameter and turbine size; this has been happening since the beginning of the commercial wind industry. A larger turbine can capture more energy throughout its lifetime, and although the cost of the turbine will increase and potentially O&M will increase as well, the COE has been able to decrease.

Significant growth of wind turbine size and weight over the past few decades has made it impossible to control turbines passively as they were controlled in the past. Modern turbines rely on sophisticated control systems that assure safe and optimal operation under a variety of atmospheric conditions. As turbines grow in size, the structural and fatigue loads become more pronounced. Implementing new and innovative load control techniques could decrease excessive loads, which affect the rotor and surrounding components. Extreme structural and fatigue loads are key factors in turbine design and the reduction of these loads could create a significant decrease in turbine cost by reducing required materials, lessening scheduled and unscheduled maintenance, and improving overall turbine reliability. This engineering challenge, which is economically driven by the push to lower the COE, has led to intensive research around the globe to improve the techniques of controlling rotor power and loads.

There are four areas that influence the control of rotor power and turbine loads for a given wind speed. They can all be addressed when analyzing the lift equation for a wind turbine blade.

$$L = \int_{r=0}^{b} \tfrac{1}{2} \rho \left[C_{L_\alpha} \left(\alpha + \theta_{pitch} - \alpha_o \right) \left\{ V_{wind}^2 + \left(2\pi n r \right)^2 \right\} c \right] dr \qquad \textbf{(Eqn. 2)}$$

1. Blade incidence angle (variable pitch) - θ_{pitch}
2. Flow velocity (variable speed rotor) - n
3. Blade size (variable blade length) - b
4. Blade section aerodynamics - C_{L_α}, α_o

The blade incidence angle, θ_{pitch}, can be controlled by pitching the blades and/or by designing an aeroelastic twist into the blade. Flow velocity is adjusted by using a variable-speed rotor, n, where n = RPM/60. These two control techniques (variable speed and blade pitch) are implemented on most modern machines. Variable diameter rotors, b, would allow control over the blade size and are being investigated as a means to increase energy capture and minimize loads during high winds. The fourth area, and the focus of this report, is the control of blade section aerodynamics, C_{L_α} and α_o, by implementing active flow control (AFC) methods.

The remaining portion of this chapter discusses the developments in wind turbine control and introduces some new control methods. *Chapter 2* provides a general background on active flow control. In *Chapter 3*, the various active flow control devices are presented and discussed.

1.2 Wind Turbine Control

Turbine control can be divided into two categories, passive control and active control. A considerable amount of research has been performed in these two areas. Passive techniques improve the turbine's performance and/or reduce loads without external

energy expenditure. Examples of this include the yaw movement of a free-to-yaw downwind rotor and aeroelastic blade twist.

Active control requires external energy, or auxiliary power. Therefore, more in depth studies must be conducted to ensure that the increase in energy output can offset the external energy required for load control as well as the increase in turbine capital and O&M costs. Some traditional methods of active control are rotor yaw, blade pitch, and variable-speed rotors. Examples of advanced active flow control devices are trailing-edge flaps, microtabs, and synthetic jets. These and other devices are discussed in detail in *Chapter 3* of this report. A flow chart showing the avenues of turbine control and some examples is shown in Fig. 1-1.

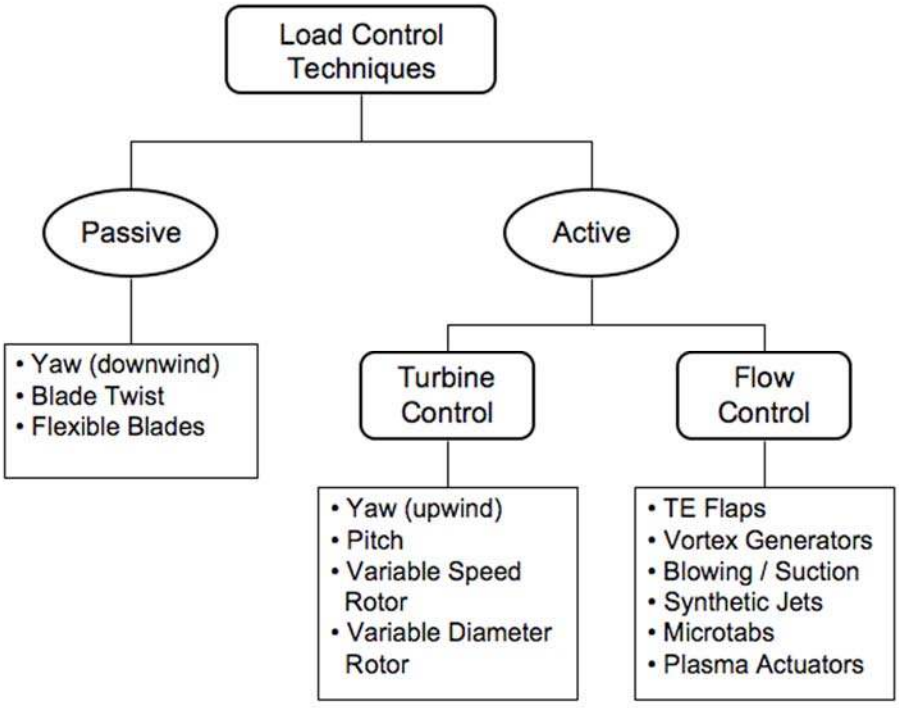

Fig. 1-1 Flow chart showing wind turbine load control techniques.

In general, the goal of wind turbine control is to balance the following requirements:[3]

1. Setting upper bounds on and limiting the torque and power experienced by the drive train, principally the low-speed shaft.
2. Minimizing the fatigue life extraction from the rotor drive train and other structural components due to changes in wind direction, speed (including gusts), and turbulence, as well as start-stop cycles of the wind turbine.
3. Maximizing energy production.

Requirement #2 is directly related to the loads experienced by the turbine during operation. The loads can be divided into two main categories: aerodynamic and structural.[4] These loads are related by the aeroelastic coupling. The relative velocities around the blade sections influence the aerodynamic loads on the rotor. Most of these loads occur in a periodic nature (appearing in multiples of the rotor frequency) but some stochastic components also exist. The contributing factors to these loads are horizontal or vertical wind shear, tower shadowing, turbulence, and yaw and tilt misalignment.[4] In addition to the two main categories of loads, gravitational forces can also have an impact by producing periodic structural loading on the rotor blades. To minimize these loads, control systems should be able to reduce the fluctuations of the aerodynamic loads or add damping to the structural modes.[5]

The immediate goal of the control strategy depends on the operating region of the turbine, which is determined by the wind speed. Fig. 1-2 illustrates the four distinct operating regions.

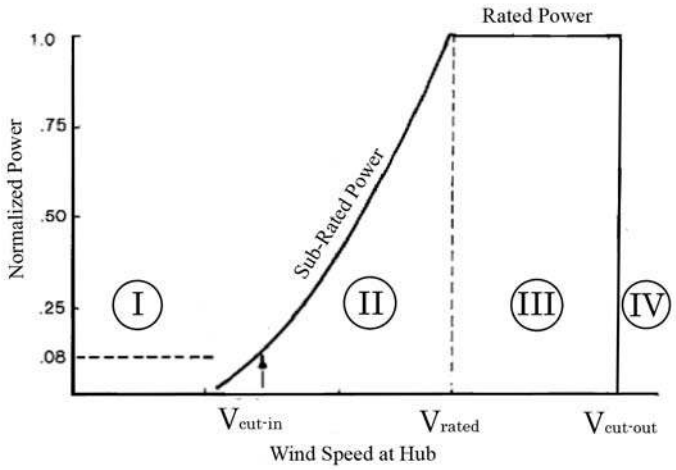

Fig. 1-2 Typical power curve of a commercial wind turbine, showing the four operating regions.

In Region I, the wind speed is too low for the turbine to generate power. Region II, also called the sub-rated power region, lies between the cut-in speed and rated speed. Here the generator operates at below rated power. The theoretical shape of this curve reflects the basic law of power production, where power is proportional to the cube of the wind speed. In Region III, the power output is limited by the turbine; this occurs when the wind is sufficient for the turbine to reach its rated output power. Region IV is the period of stronger winds, where the power in the wind is so great that it could be detrimental to the turbine, so the turbine shuts down.

1.3 Developments in Wind Turbine Operation for Load Control

At the beginning of the commercial wind energy industry, turbine operation was simple. The turbines were small (tens or hundreds of kWs in rated power), operated at a constant speed and used passive methods (stall control) to regulate power. The turbines were equipped with rotor blades that were designed to intrinsically regulate the power using fixed-pitch designed to operate near optimal tip-speed in Region II. As the wind

speed increased, the angle of attack increased and the flow about the blade would begin to stall, thereby increasing drag and limiting the amount of absorbed power. The simplicity of this control concept contributed to wind energy's rapid success; however, the evolution towards larger rotor blades soon made this control concept uneconomical.

Nowadays, most large turbines (one to several MWs in rated power) use variable-speed rotors combined with active collective blade pitch to optimize energy yield and control loads. In Region II, turbines tend to operate at fixed pitch using variable rotor speed to maintain an optimal tip-speed ratio and maximize energy capture. In Region III, the rotor operates at near constant speed and the blades are pitched to maintain the torque within acceptable limits. The control of the blade pitch and rotor speed has not only led to greater power regulation, but also to lighter blade construction due to a lower load spectrum and a lighter gear box due to reduced torque peaks.[4] Difficulties arise in turbulent winds when excessive loading (both extreme and fatigue loads) occurs, which leads to premature wear on turbine components. Using current technology, it is difficult to mitigate these loads; pitching of the entire blade is too slow and variable rotor speed allows shedding for some of the high loads, but not all. The need to mitigate excessive loads has led to investigations of new methods of control.

1.4 Investigations into New Control Methods

Variable-speed rotors and collective pitch are not capable of handling oscillatory or fatigue loads. These loads occur as a result of rotor yaw errors, wind shear, wind upflow, shaft tilt, wind gusts, and turbulence in the wind flow.[6] More sophisticated control methods are needed to account for these loads. Some methods that will be presented in

this report are advanced blade pitch control, blade twist control, variable diameter rotors, and any number of flow control devices.

1.4.1 Advanced Blade Pitch Control

1.4.1.1 Description

Pitching is the act of rotating each blade around its spanwise axis in order to change the effective angle of attack to the wind. It is used to limit the peak power, optimize rotor efficiency, and slow down the rotor. The traditional method of pitch control uses a collective mode, in which all blades are adjusted simultaneously. Advanced methods of pitch control (cyclic pitch and individual pitch) are being investigated. These innovative concepts were first developed for the rotorcraft field and have been adapted to the wind industry.[7]

Cyclic pitch control varies the blade pitch angles with a phase shift of 120° to alleviate the load variations caused by rotor tilt and yaw errors, whereas individual pitch control adjusts the pitch angle of each individual blade independently. This method requires the measurement of the local inflow angle and relative flow velocity for each blade. The goal is to create two load-reducing systems (collective pitch and individual pitch) that are independent, where collective pitch is used to keep the power at a desired level by adjusting pitch based on the mean wind speed and the individual pitch regulator is to minimize loads without affecting the power output.[8]

Cyclic and individual pitch control can reduce fatigue loads due to yaw errors, wind shear, up flow and shaft tilt. Not only do the blades benefit from this control strategy, but reductions in loads on the drive train, nacelle structure, and tower are also seen. However

these control techniques are less capable of reducing the loads due to wind gusts and turbulence.[9]

1.4.1.2 Background

Research by Larsen, Madsen, and Thomsen[8] and by Bossanyi[9] has shown that load reductions are possible using advanced pitch control. They conducted aeroelastic numerical simulations to analyze both cyclic and individual pitch control and compared it to collective pitch methods. The turbine used in the simulations had a nominal rated power of 2 MW and a rotor diameter of 76 m. The results indicated that advanced pitch control could lead to a reduction of up to 30% in both 20 year fatigue loads and extreme loads on many major turbine components. A separate simulation by Bossanyi[9] showed that individual pitch control could reduce the fatigue loads at the hub by 30-40% and at the blade roots by 20-30%.

A more recent control approach suggested using feed forward control based on the incoming wind field instead of or in addition to using local flow measurements at the blade. Van der Hooft and van Engelen[10] suggested the estimation of incoming wind speed based on energy balance and Hand, Wright, Fingersh, and Harris[11] proposed the use of a LIDAR system to directly measure the upwind incoming flow field. These methods may further improve the performance of individual pitch control.

1.4.1.3 Wind Turbine Control

There are three major concerns when considering individual pitch control.[6] First, the entire blade still must be pitched. The flow conditions along a long blade are not uniform and therefore pitching the entire blade may not be ideal. Second, the pitching mechanism may be unable to act fast enough to relieve the oscillating loads due to wind gusts. These

gusts have rise times on the order of a couple of seconds and last for 5 to 10 seconds; the International Electrotechnical Commission (IEC) wind turbine design standard calls for consideration of an extreme gust that lasts for 10 seconds where the wind speed increases by 35% from the mean wind in a period of just over two seconds.[12] Third, there is a concern that individual blade pitch will result in over-use of the pitching mechanism. It is important to design turbines to use individual pitch from the start; retrofitting current turbines with individual pitch control will lead to premature failure of the pitch mechanism due to the resulting high duty cycle. Challenges with implementation include response time requirements to counter load perturbations, the need larger pitch motors, and the power required to operate the system under a new control strategy.[6]

1.4.2 Blade Twist Control

1.4.2.1 Description

One concept for controlling fatigue loads on a wind turbine blade is to use passive blade bend-twist coupling[13-18]. The aeroelastic tailored blade is designed so that the twist distribution changes as the blade bends due to aerodynamic loads. This is now possible through the advent of composite materials, which can be implemented in a deliberate fashion to control flap-twist coupling. For example, an off-axis (e.g. 20°) orientation of reinforcement fibers (e.g. glass, carbon, Kevlar, etc.) along a supporting spar will cause the spar to twist under sufficient bending strain.[18] The transient loads due to wind gusts theoretically could be reduced because the blade would twist towards lower angles of attack, thereby mitigating the loads and potentially reducing pitch activity as well.

1.4.2.2 Background

According to Lobitz and Veers[14], bend-twist coupling can lead to a 20 - 70% decrease in fatigue damage to the turbine, corresponding to a 20 - 30% decrease in fatigue loads. An economic analysis by General Electric showed that reductions in COE of around 6% could be expected from a moderately aeroelastic tailored blade.[18]

1.4.2.3 Wind Turbine Control

Some of the challenges with this concept include reduced energy capture, higher costs, and blade integrity issues.[18] First, reduced energy capture may occur due to altering a blade that is designed for optimum energy capture at rated speed by causing it to twist. Basically, energy as well as loads will be shed. Second, higher costs associated with materials and manufacturing techniques may make the concept uneconomical. Third, the fabrication technique may lead to decreased stiffness and additional material may be required to counteract additional blade deflection.

Active blade twist control can be conceptually achieved by embedding active laminates such as piezoelectric material in the spar caps of the blade. There are several challenges that face this concept, including blade structural integrity, cost of active materials, and actuation power requirements.[6]

1.4.3 Variable Diameter Rotor

1.4.3.1 Description

This concept[18,19] is capable of improving energy capture in low wind speeds and reducing loads on the rotor in high wind conditions. Variable diameter rotors operate by extending/retracting a *tip* blade out of a *root* blade (Fig. 1-3) to increase/decrease the diameter (Fig. 1-4). During low-wind speed, a large rotor diameter provides more

capture area, which results in larger aerodynamic loads and an increase in energy capture. However, this operation generates larger blade root and tower base bending loads. In higher wind speeds, the rotor diameter can be decreased to avoid excessive loads. The tip blade would extend and retract independently of the pitching mechanism and it would respond to gross changes in the wind speed; the pitch control would still be used to regulate power.

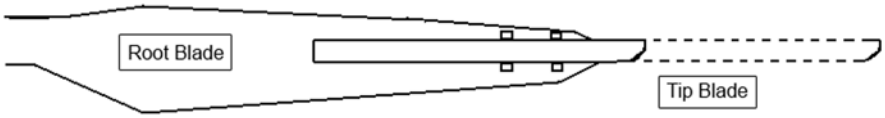

Fig. 1-3 Illustration of extendable blade.

1.4.3.2 Background

A collaboration of DOE, Energy Unlimited, and Knight and Carver[19] manufactured and tested turbine blades with this design on a 120 kW turbine. The prototype blade (Fig. 1-4b) was created using Kenetech 56-100 tips mounted within Aerostar 9-meter blades. The blades were capable of adjusting length from 8 m to 12 m. Additional changes were

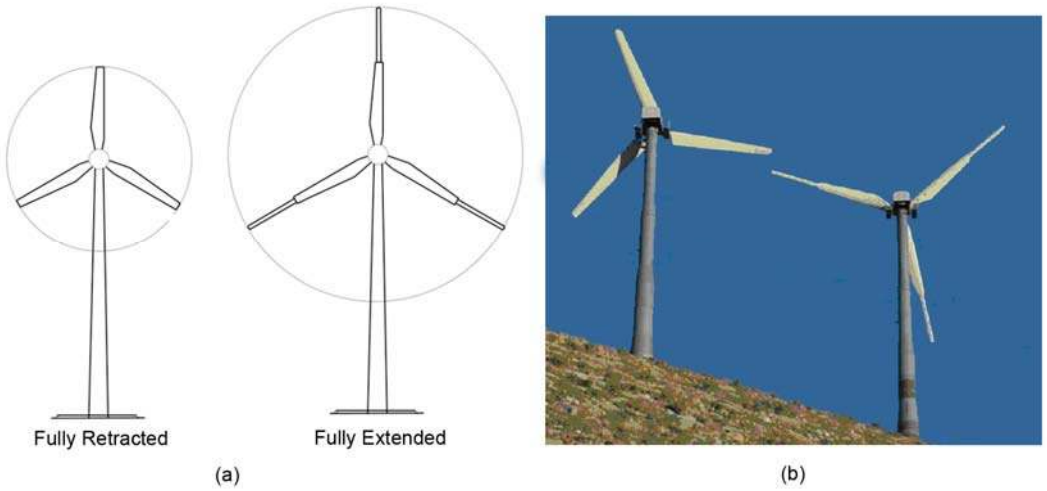

Fig. 1-4 a) Illustration of the variable diameter rotor system, b) Photograph of test blades, fully extended prototype next to a standard 9 m blades. (Source: DOE[19])

made to the turbine and more sophisticated controls were developed for proper control of blade length. Results from this prototype showed that a potential increase in power production in low winds is possible, about 20-50% above that of a standard blade in wind speeds from 7-9 m/s. A decrease in performance was found to occur at rated speed; this was most likely due to the poor aerodynamics of the prototype. The measured power curves for different blade lengths are shown in Fig. 1-5. Computational experiments showed improved aerodynamic performance at all wind speeds, accompanied by an increase in peak and fatigue loads during low wind speeds.

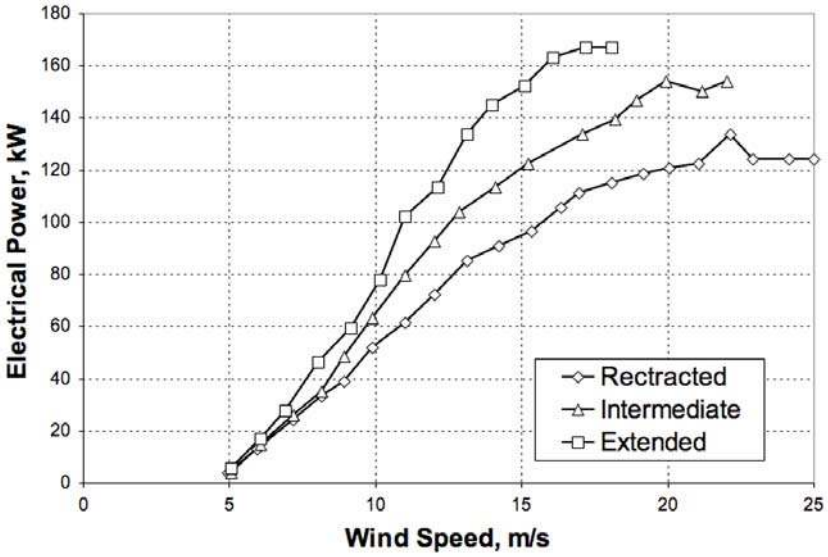

Fig. 1-5 Measured power curves of the prototype blades. (Source: DOE[19])

This design is now being developed by Frontier Wind (formerly Energy Unlimited), who is continuing to test the prototype turbine, making advances in blade design and developing more sophisticated control algorithms. GE Wind[18] also has researched this concept and has reported that a reduction in COE of approximately 18% could occur with a properly designed and operating full-size turbine equipped with a variable blade system.[18]

1.4.3.3 Wind Turbine Control

The variable diameter rotor has potential for increasing energy production for a given load spectrum. The initial results from the small prototype turbine show that the concept works; the next step is to develop a full-scale prototype turbine. There are several engineering challenges that must be resolved in order to make a successful and marketable turbine. The challenges include complex control strategies, the need to maintain a high aerodynamic efficiency, increased blade weight, and general issues with durability and reliability of the system as a whole.

1.4.4 Active Flow Control

Active flow control (AFC) is the control of the local airflow surrounding the blade. The purpose of flow control is often to improve the aerodynamic performance of an airfoil or lifting surface. However, for utility-scale wind turbines the main focus is to reduce extreme loads, which occur during high wind activity, and to mitigate fatigue loads, which vary along a blade and can occur randomly. To do this, active load control devices or "smart" devices must include actuators and sensors located along the span of the blade. The system must be able to sense changes in the local flow conditions and respond quickly to counter any negative impact on blade loading. This arrangement provides active "smart" control over the rotor. By definition, a smart structure involves distributed actuators and sensors and one or more microprocessors that analyze the responses from the sensors and use integrated control theory to command the actuators to apply localized strains/displacements to alter system response.[20] Numerous investigations on the use of AFC devices show that significant load reduction is possible.

2 ACTIVE FLOW CONTROL

Flow control is being researched for a number of fields other than wind energy. Researchers in fields such as manned and unmanned airplanes, rotorcraft, and gas turbines are all interested in and investigating the potential benefits of active load and flow control.

In general, the intent of flow control devices is to delay/advance transition, to suppress/enhance turbulence, or to prevent/promote separation. The ensuing effects include drag reduction, lift enhancement, mixing augmentation, heat transfer enhancement, and flow-induced noise reduction.[21] However, these effects are not necessarily mutually exclusive. Improving one objective may have adverse effects on other areas. The goal is to choose a flow control scheme that achieves an overall beneficial goal with minimal tradeoffs.

2.1 Flow Control Methodology

Flow control methods are categorized similarly to the load control techniques explained earlier; either passive or active. Some passive techniques include geometric shaping to manipulate the pressure gradient, the use of fixed mechanical vortex generators for separation control, the addition of a Gurney flap at the trailing edge, and the placement of longitudinal grooves or riblets on a surface to reduce drag.[22]

Active control methods can be broken into two categories: predetermined and interactive (open- or closed-loop). A flow chart displaying flow control methodologies is shown in Fig. 2-1. To demonstrate the difference between the methods, the case of constant blowing to enhance post-stall lift will be used.

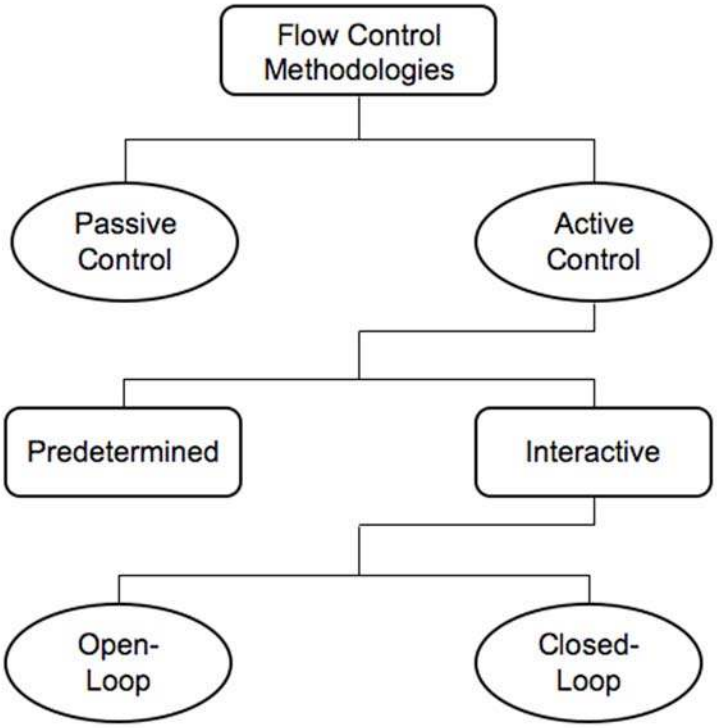

Fig. 2-1 Flow control methodologies diagram. (Source: Kral[22])

Predetermined control introduces steady or unsteady energy inputs without concern for the state of flow. Therefore, there are no sensors required for this method and the control loop is open. In this situation, the constant blowing device would operate continuously with no regard for the wind speed or pitch angle.

In contrast, an interactive control system contains an actuator, a controller, and a sensor. The system can either operate in open- or closed-loop form. Open-loop control does not observe the output process that it is controlling; therefore, it cannot determine if its input has achieved the desired goal. In the example, the constant blowing device would be programmed to turn on once a set angle of attack is exceeded.

Closed-loop control utilizes feedback to compare the actual output with the desired output. A feedback control law is used to drive the actuator or device in order to

minimize the error between the reference value and the feedback signal. In the example, the blowing device would have an additional sensor to detect the onset of flow separation. It would be programmed to turn on once flow separation is detected.

Closed-loop systems would be the most beneficial for wind turbine control. The main advantages are energy consumption and safety. Predetermined systems operate continuously even when the device is not needed, thereby using excess energy. Open-loop systems would be more efficient, but at times would still operate unnecessarily. In addition with using excess energy, both of these systems could also be detrimental to the system since they do not observe the output. Improper control of active devices has been shown to have serious negative impacts on turbine operation and overall safety. By using feedback, the control system can be configured to turn on and shut down the AFC system as needed.

2.2 Flow Control Categories

Flow control can be broken down into the three separate categories: control/sensors, actuators/devices, and flow phenomena. The communication starts with the controls and sensors, which continuously update the system controller on the flow properties and the overall operation. When adjustments are required, the controller commands the actuators to activate the flow control devices. The devices then change their method of operation, altering the local flow phenomena. The sensors track this change and the cycle repeats. Fig. 2-2 displays the flow control categories and lists some examples related to wind turbine control. The figure shows that tackling a flow control problem requires a multi-disciplinary approach and research in many areas.

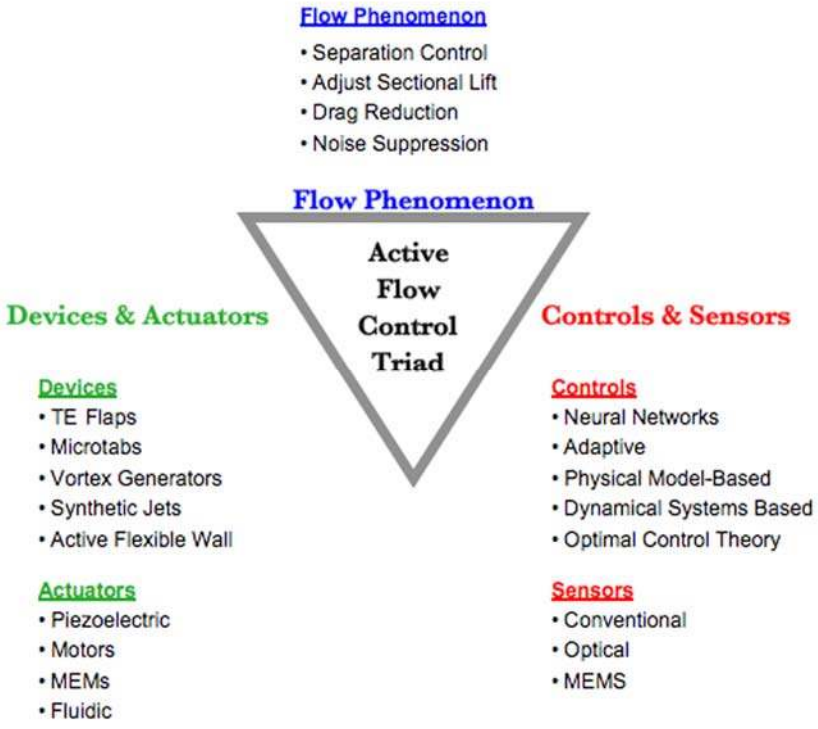

Fig. 2-2 Feedback flow control triad. (Source: Kral[22])

2.3 Flow Control on Wind Turbines

This report focuses on different AFC devices and actuators, including their associated flow phenomena. It does not go into detail about the necessary sensors and controls, which are critical components of a complete system. Although research is being conducted in these areas, it is beyond the scope of this report. However, as one investigates possible devices it is important to keep the complete system in mind.

Fig. 2-3 presents one possible layout of a control strategy for a complete system. This layout includes two types of controllers, a master controller and individual blade controllers. The master controller would have similar duties to those found in traditional wind turbine controls (manage pitch angle, tip-speed ratio, etc), but would also communicate with the blade controllers. The blade controller would receive input from the sensors (local flow conditions and/or strain in the blades), communicate with the

master controller, and then output commands to the AFC devices located on the blade. Fig. 2-3 illustrates trailing-edge devices coupled with leading-edge sensors. However, as detailed later in *Chapter 3*, there are several different types and locations of AFC devices.

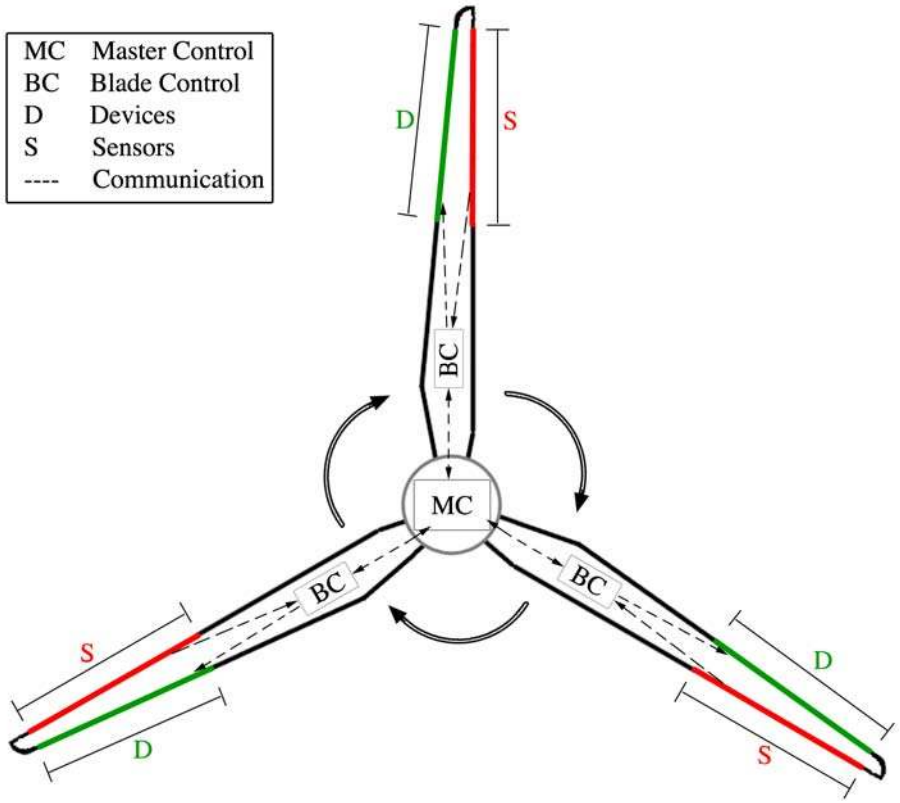

Fig. 2-3 Control strategy diagram of a complete system.

It is important to remember that the primary purpose of active flow control (AFC) systems on wind turbines is the following:

- *To mitigate excessive loads (extreme, fatigue, cyclic, etc.) caused by variations in the wind.*

One foreseeable way to counter excessive loads is to supplement current full-span pitch control with AFC devices. Pitching would still be used to optimize energy yield and control aerodynamic torque, while AFC devices would be able to react quickly to reduce

the oscillatory, high-frequency loads caused by turbulent winds. The operation of AFC devices also has some potential secondary benefits:

1) Devices may be deployed to increase lift of the blade at low wind speeds, allowing the turbine to cut-in earlier and capture additional energy.
2) On downwind machines, these devices could deploy every revolution to counteract the tower wake effect.
3) Active devices could aid in energy capture and load mitigation on turbines that experience high array effects.
4) Devices could be used to prevent tower strikes, allowing for larger diameter rotors to be used and thereby increasing energy capture.[6]
5) Aerodynamic performance enhancement and noise reduction could be realized by maintaining laminar flow over the blade.
6) The blade could operate higher on the lift curve with the devices protecting the blade from getting into stall.

3 FLOW CONTROL DEVICES

Overall, there are fifteen (15) devices that will be discussed in this report. While these devices have shown potential for wind turbine control and merit future research, none of them have matured to a point of being tested on full-scale turbines. Also, several of the techniques have not yet been investigated for wind turbine control. Instead, many of the techniques have focused on other fields such as rotorcraft or unmanned aerial vehicles (UAVs). Since all of the devices function differently, both mechanically and aerodynamically, and are at varying stages of maturity, it is difficult to make direct comparisons. The first step in discussing the numerous AFC devices is to define a labeling scheme that can be used to classify each concept. A proposed four (4) layer scheme utilized in the present report is presented in Table 1. The labeling scheme was derived from a paper on AFC for UAVs by Wood[23].

1st Layer

The first layer identifies the technique as a geometric device (G) or a fluidic device (F). Geometric devices (G) move a portion of the external surface, thereby changing the section shape and attaching the airflow about the airfoil. Fluidic devices (F) actively change the flow about the blade section by either adding air into or subtracting air from the external flow. There are two devices that do not fall into one of these two categories. One device, synthetic jets, is classified as a combination of geometric and fluidic (G / F) devices as it uses mechanical motion, which is not in contact with the external airflow, to oscillate a membrane in a cavity inside the airfoil and this, in turn, generates air motion in the external flow. The other device, plasma actuators (P), uses an electric field to generate a body force on the surrounding fluid, thus modifying its behavior.

2nd Layer

The second layer describes the location of the device, such as near the leading edge (LE), near the trailing edge (TE), or mid-chord (MC).

3rd Layer

The third layer describes how the device adjusts the lift curve. Investigations of the AFC devices show that the lift curve of an airfoil is affected in one of two ways. First, the device shifts the entire lift curve up or down, which is done by effectively changing the camber of the airfoil. This is labeled as increasing lift (I) or decreasing lift (D). Many devices are capable of shifting the lift curve both up and down; those are labeled (I/D). Second, the device extends the lift curve of the airfoil to stall at a higher angle of attack, this is labeled delay stall (DS). Fig. 3-1 displays the two different ways that the lift curve can be adjusted.

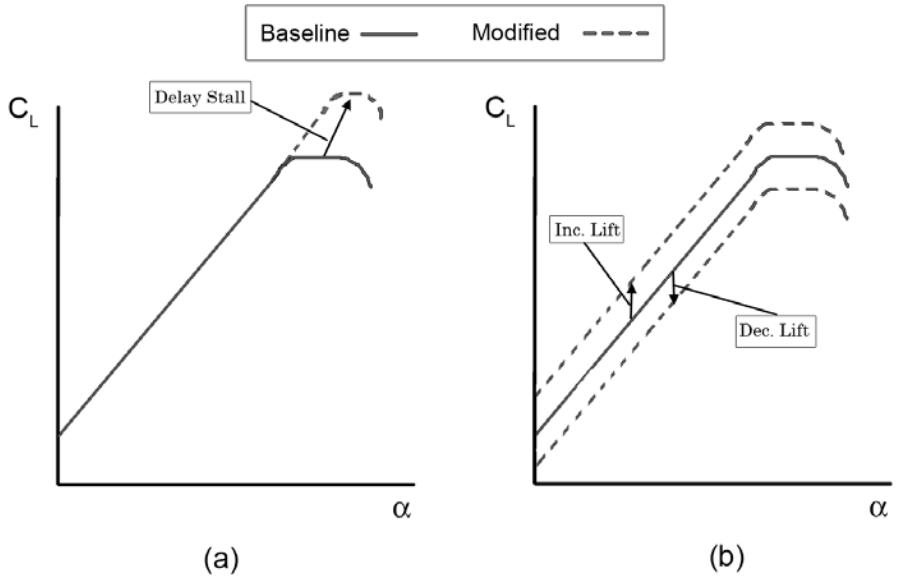

Fig. 3-1 Adjustments in lift curve due to flow control techniques, a) DS devices, b) I / D devices (Source: Berg et al.[6])

Description of modified blades with DS devices

To successfully mitigate loads, the device must be able to decrease the generated lift. At first observation, delaying stall (DS) only increases lift at high angles of attack as shown in Fig. 3-1a. This does not decrease lift; therefore, DS devices would not be considered as an option for load alleviation. Although they could contribute to some of the secondary benefits listed in *Section 2.3*. However, an idea presented by Corten[24] provides an alternative method of using DS devices to reduce turbine loads.

The common application of DS devices (in this example, passive vortex generators) is to add them onto an existing design to increase C_{Lmax} and delay stall. Corten's idea is to redesign blade so that the maximum sectional lift of a blade *with* a DS device equals that of the original blade *without* a DS device. Fig. 3-2 demonstrates the difference in chord length between the redesigned, or modified, blade and the original blade. The idea can be more easily explained by analyzing the lift equation:

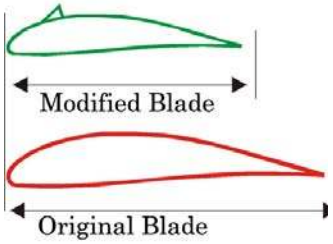

Fig. 3-2 Airfoils with comparable lift generation. (Source: Corten[24])

$$L_{\max} = C_{L\max} \cdot \frac{1}{2} \cdot \rho \cdot V^2 \cdot c \qquad \textbf{(Eqn. 3)}$$

where ρ is the air density, V is the air velocity over the blade, c is the chord length, and C_{Lmax} is the maximum lift coefficient. If C_{Lmax} is increased by a DS device, then the chord, *c*, could be reduced a comparable amount so that the generated lift still equals that of the original blade. The outcome of this redesign is illustrated in Fig. 3-3. The maximum sectional lift, L_{max}, of the original blade and the modified blade are equal;

however, the slope ($\Delta L/\Delta\alpha$) has been decreased. The benefits of reducing the slope are explained below and illustrated in Fig. 3-4.

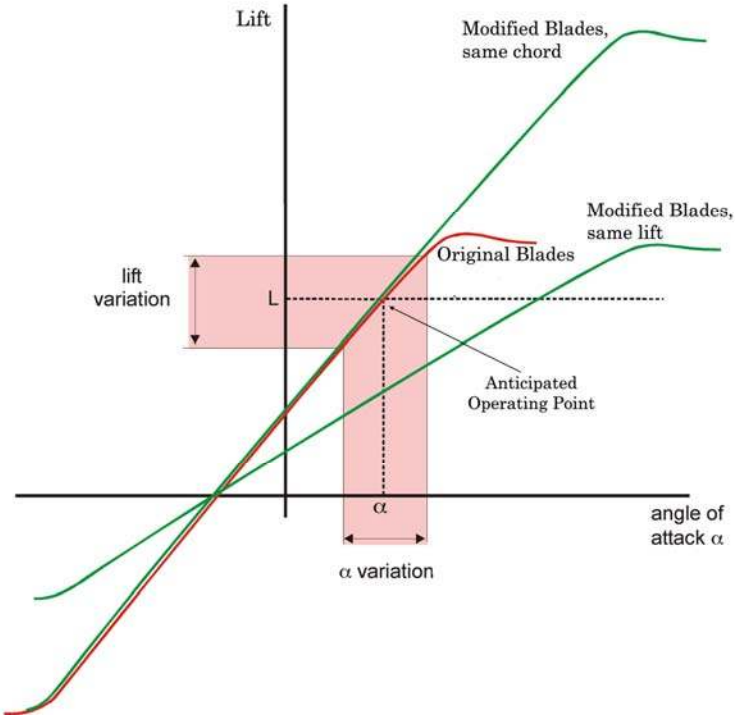

Fig. 3-3 Comparison of modified blades with the same chord and same lift. (Source: Corten[24])

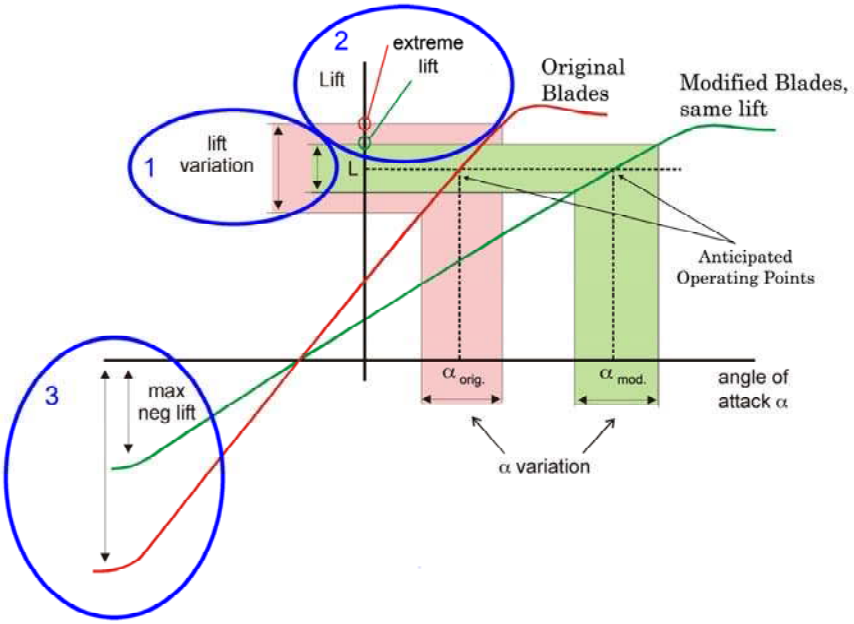

Fig. 3-4 Diagram of benefits using modified blades with DS devices. (Source: Corten[24])

The oscillating loads on a turbine are caused by sudden changes in lift seen by the blade. These changes in lift can be caused by a number of events, one of them being turbulence. Turbulence can increase/decrease the wind velocity, V, increase/decrease the angle of attack, α, seen by a rotating turbine blade, or it can do both. Therefore, to reduce these oscillating loads, the sudden changes in lift have to be mitigated. This can be accomplished by reducing the lift curve slope ($\Delta L/\Delta\alpha$). The reduced slope does three things that help to reduce the loads. One, the lift variation (ΔL) for a given $\Delta\alpha$ is reduced. Two, the maximum lift for a given $\Delta\alpha$ is lowered. Three, the magnitude of the maximum negative lift is reduced. This reduction is important during emergency shutdown for pitch-to-feather machines. As the blades pitch rapidly, they pass into negative angles of attack during which the rotor can experience high loads. Corten's research indicated a potential reduction of 20-40% for lift variation, a potential reduction of 6-12% for extreme lift, and a potential reduction of 20-40% for maximum negative lift.

The primary benefit of modifying blades with DS devices is to decrease oscillating loads. Secondary benefits are associated with the reduced chord, allowing for smaller blades and, thus requiring less material.

4^{th} Layer

The fourth and final layer differentiates between a steady (S) and unsteady (U) device (i.e. a device whose position varies with time about a nominal setting). For example, a trailing-edge flap system, although it could be in continual motion, is simply changing position to create a series of steady state conditions and is therefore considered to be a steady device. The motion itself is not used to create an aerodynamic control force, as is the case of, i.e., pulsed vortex generating jets. Most of the devices that operate unsteadily

are also capable of steady operation; therefore, these devices are labeled (S/U). However, research into these devices has shown that unsteady, or pulsed, operation is usually more effective.

Table 1 Classification chart used to label each AFC device.

	Devices	Geometric (G) / Fluidic (F) / Plasma (P)	Leading Edge (LE) / Trailing Edge (TE) / Mid-Chord (MC)	Inc. Lift (I) / Dec. Lift (D) / Delay Stall (DS)	Steady (S) / Unsteady (U)
1	Traditional Trailing-Edge Flaps	G	TE	I / D	S / U
2	Nontraditional Trailing-Edge Flaps	G	TE	I / D	S / U
3	Microtabs	G	TE	I / D	S / U
4	Miniature Trailing-Edge Effectors	G	TE	I / D	S / U
5	Microflaps	G	TE	I / D	S / U
6	Active Stall Strips	G	LE	D	S
7	Vortex Generators	G	LE	DS	S
8	Blowing and Suction	F	LE / TE	DS	S / U
9	Circulation Control	F	TE	I / D	S
10	Plasma Actuators	P	LE	DS	S
11	Vortex Generator Jets	F	LE	DS	S / U
12	High-Frequency Micro Vortex Generators	G	LE	DS	U
13	Synthetic Jets	G / F	LE	DS	U
14	Active Flexible Wall	G	LE	DS	U
15	Shape Change Airfoil	G	MC	I	S / U

Table 1 shows all fifteen devices that will be discussed. To more easily present the various AFC devices, the discussions on each device are broken into four sections. The sections are as follows:

1) *Description* - introduces the device and describes how it works, both mechanically and aerodynamically.
2) *Classification* – explains the classification for the device.
3) *Background* – presents a history of the research, including some results and the present state of the device.
4) *Wind Turbine Control* –discusses the potential each device has for the wind energy industry, including its advantages and disadvantages and the hurdles that the technology faces.

Commonalities of AFC devices

The purpose and potential benefits of AFC devices have been explained, but how they operate has not. Although each device operates differently, there are certain characteristics that are required for a device to be successful.

- It must be small in size so that a number of devices can be distributed along a portion of the span to provide sectional flow control at different locations of the turbine blade. This also means the device should be scalable, meaning it can be effective across a range of chord lengths.
- The device must have a fast activation speed. This is necessary to counter the high frequency oscillatory loads and to provide proper aeroelastic control.
- The activation forces and power requirements must be low so that the energy to operate the AFC system is lower than or equal to the additional energy gain from the turbine. This allows for the secondary benefit of improved energy capture.
- The AFC system needs to be reliable and dependable. The turbine should be able to maintain operation if one or more AFC devices fail.
- It is necessary for the device to be durable and robust in order to withstand the harsh environments seen by turbines. Basically, the addition of a flow control system should not drastically increase maintenance costs. The lifetime of the system also should be similar to the lifetime of the turbine and its components.
- The integration of the AFC system into a turbine blade needs to be taken into consideration from both a manufacturing and maintenance point of view. Current blade manufacturing techniques should still be used; if a device fails, it should be easily replaceable in an inexpensive and straightforward manner.

- In the end, the driving factor for the success or failure of an AFC system is economics. A successful system must be able to reduce the cost of energy for wind turbines.

All of the AFC devices will face certain challenges that will have to be overcome before any degree of implementation can be reached on commercial wind turbines. Since the vast majority of actuators and sensors will have to be placed on or within the turbine blade, substantial modifications to the blades will be required. This will add complexity to the entire system and require a more sophisticated control system that would be capable of properly operating the AFC devices. Research on several devices has indicated that improper control of AFC devices could have a detrimental effect on the performance and safety of a wind turbine.

3.1 Traditional Trailing-Edge Flaps

3.1.1 Description

Traditional trailing-edge flaps, or ailerons, have been utilized in the past on wind turbine blades for aerodynamic braking and load control. Fig. 3-5 shows a wind turbine blade modified with a large trailing-edge flap being tested at the National Wind Technology Center in Boulder, Colorado. There are two different configurations (depending on torsional stiffness of the blade) in which ailerons can be used for load control.[6] On a torsionally stiff blade, deflection of the flap to the pressure surface generates an increase in aerodynamic load and a deflection to the suction side decreases the aerodynamic load. On a torsionally soft blade, a deflection of the flap towards the pressure surface will create a pitching moment that twists the nose of the blade towards the pressure surface, thereby decreasing the angle of attack and, hence, the load.

Likewise, a flap deflection in the opposing direction twists the blade toward the suction surface, thereby increasing the angle of attack and, hence, the load on the blade.

Fig. 3-5 Wind turbine blade with trailing-edge flap in test stand. (Source: NREL[6])

3.1.2 Classification

G - geometric device

TE - located at the trailing edge of the blade

I / D - capable of deploying in both directions and therefore can adjust the lift curve up and down

S - operates by changing the deflection angle in a steady-state manner

3.1.3 Background

Initial investigations of active flow control devices were performed by the National Renewable Energy Laboratory (NREL) in the 1990's. The devices, often called ailerons, were analyzed for power regulation and aerodynamic braking. Wind-tunnel experiments examined the performance of ailerons at different configurations.[25,26] Field tests also were performed using the aileron device at fixed positions (no active control), during which 3-D effects associated with variable span-wise deployment of the control devices were identified during turbine operation.[27]

Stuart, Wright, and Butterfield[28,29] discuss the possible advantages of active devices for turbine control to mitigate the effects of damaging loads. A simple numerical control case study using ailerons is presented along with simulations investigating the use of actively controlled devices for load reduction.[28] In this study, the intention was not to design an optimal controller, but rather to successfully implement a simple PI control

scheme using the aeroelastic analysis code FAST[30]. The controlling ailerons were located on the outer 30% blade span. The controlled aileron case showed a reduced response time for a step-gust wind input, with reduced root flap bending moments and improved power regulation during a simulated turbulent wind input. Additional simulations[29] were also conducted using a more advanced design approach for the controller. The FAST code, along with system identification tools, was used to generate a wind turbine dynamic model for use with the active aileron. Simulation results indicated that aileron load control could assist in power regulation and reduce root flap bending moments during a step-gust and turbulent wind situation.

3.1.4 Wind Turbine Control

The trailing-edge flap design instantly comes to mind as a potential for wind turbine control because of its success in aircraft control. However, there are several concerns with the NREL flap design including its large size, additional weight, complex linkage systems and slow response. Additional power requirements to actuate the large flap and aeroacoustic noise generated by gaps are also a concern.

3.2 Nontraditional Trailing-Edge Flaps

3.2.1 Description

Nontraditional trailing-edge flaps use newer technology, such as piezoelectrics and "smart" materials, to improve upon traditional trailing-edge flaps. Whereas traditional flaps tend to be heavy, slow, and take up a large portion of the chord, nontraditional flaps have a quick activation, are lightweight, and occupy less chord. These improvements allow nontraditional flaps to counter the extreme and fatigue loads. There are three

devices discussed in this section; the compact trailing-edge flap, the adaptive trailing edge geometry (ATEG), and the adaptive compliant wing.

Compact Trailing-Edge Flaps

A compact trailing-edge flap is being researched for rotorcraft control. The compact design, seen in Fig. 3-6, is comparable to a scaled-down NREL aileron; however it uses small piezoelectric actuators located inside the blade to quickly move a tension rod that deflects the flap. The compact design allows for the quick deployment required to reduce rotor vibrations.

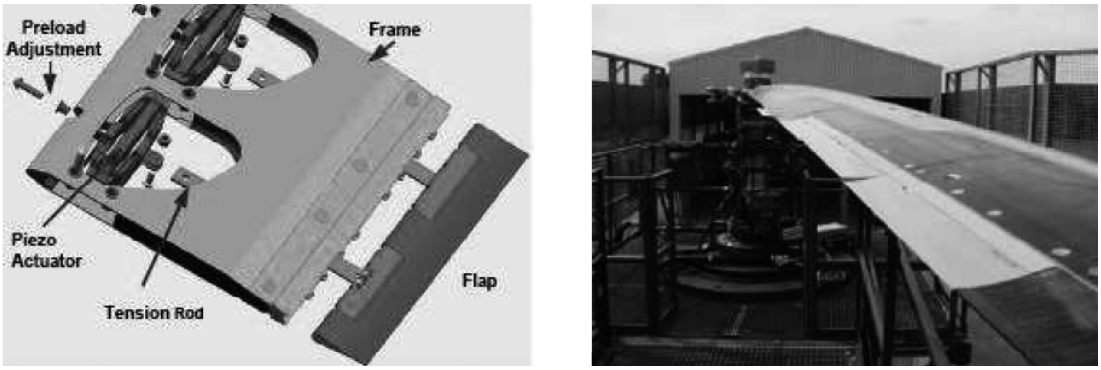

Fig. 3-6 Left: CAD model showing the layout of the piezoelectric actuated flaps. (Source: Enenkl et al.[33]), Right: Photo of actively controlled piezoelectric flaps on the BK117 blade. (Source: Roth et al.[34])

Adaptive Trailing Edge Geometry (ATEG)

The Adaptive Trailing Edge Geometry (ATEG) [35-39] is a trailing-edge flap that has no seems or hinges. The deformable flap is made of piezoelectric actuators that are attached to the main airfoil. It has the ability to deflect quickly and independently along the span of the blade. The ATEG is capable of rotating through a flap angle range, $ß_{flap}$, of 3.0 to +1.8 degrees. Fig. 3-7 illustrates the approximate size (relative to the airfoil chord) and deflection angles of the ATEG. Deflecting the ATEG towards the suction side (negative $ß_{flap}$) shows a downward translation in the lift curve, whereas a deflection to the pressure side (positive $ß_{flap}$) moves the lift curve upward, increasing aerodynamic load.

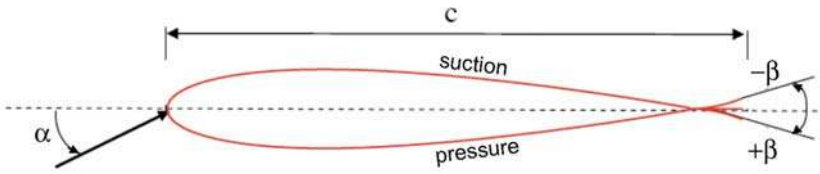

Fig. 3-7 Illustration of main airfoil and the ATEG trailing-edge flap. Three different positions of the ATEG are shown. (Source: Bak et al.[39])

Adaptive Compliant Wing

The third device considered to be a nontraditional flap is the adaptive compliant wing developed by FlexSys, Inc.[31] and the U.S. Air Force Research Laboratories. A compliant mechanism is defined as a mechanism that relies on elastic deformation of its constituent elements to transmit motion and/or force.[32] The concept and the aerodynamics are similar to those of the ATEG; however, the internal actuation mechanism is different. This design (Fig. 3-8) uses conventional electromechanical actuators to deform a compliant structure that takes the shape of the trailing edge. The flap can deflect over a range of +10 to -10 degrees at speeds up to 20 deg/sec and it can also twist differentially up to one degree per foot over the span of the model.[32]

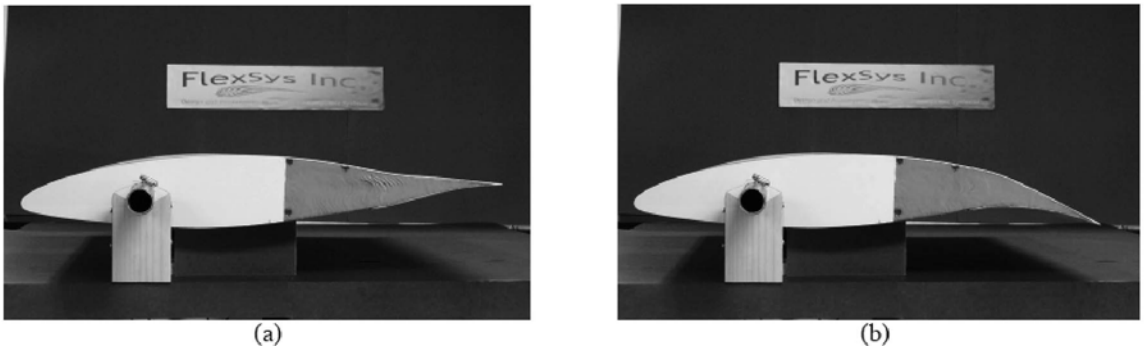

Fig. 3-8 Adaptive compliant wing wind tunnel model shown in a) -10° position and b) 10° position. (Source: Kota et al.[32])

3.2.2 Classification

G - geometric device

TE - located at the trailing edge of the blade

I / D - capable of deploying both directions and therefore can adjust the lift curve up and down

S / U - both steady and unsteady (oscillating) operation are being researched

3.2.3 Background

Compact Trailing-Edge Flaps

The most recent compact trailing-edge flap was developed under the ADASYS project (a collaboration of Eurocopter, EADS CRC, Daimler Chrysler Research Labs and DLR).[33,34] A functional full-scale rotor was built and tests of the system demonstrated large reductions (50-90%) in vibratory loads.

Adaptive Trailing Edge Geometry (ATEG)

Several computational experiments have been conducted for development of the ATEG to be used for wind turbine control. Analytical studies conducted at Risoe National Laboratory-DTU showed that significant reductions in the RMS of the unsteady load level (simulating fatigue loading) are possible with an actively controlled trailing-edge flap. Using a 2-D potential-flow solver, Basualdo[35] investigated the movement of an airfoil in a turbulent flow field and found that the standard deviation of the airfoil position normal to the chord could be reduced using an AFC device.[35] Troldborg[36] studied the static and dynamic aerodynamic performance of a 2-D airfoil equipped with different shaped ATEGs. Three different shapes were analyzed: rigid, soft curved, and strongly curved. The static simulations showed that the soft curved flaps performed better. These studies showed that an oscillating airfoil superimposed with an oscillating

ATEG could significantly reduce the amplitude of the lift generated over a wide range of reduced airfoil frequencies, k, of 0.09 – 0.36, where k is defined as;

$$k = \frac{\omega \ c}{2 \ U_\infty} \qquad \textbf{(Eqn. 4)}$$

where, ω is the frequency of pitch oscillation, *c* is the chord length, and U_∞ is the freestream velocity. The reduced airfoil frequency is used to quantify the speed of an airfoil's oscillations. Physically, it represents the portion of the oscillation cycle, in radians, that elapses during the time it takes the local flow to travel half a chord length. This parameter is important when analyzing performance during dynamic stall (the process of boundary-layer separation from an airfoil experiencing a dynamic increase in angle of attack).

Two-dimensional aeroelastic studies conducted by Buhl, Guanna, and Bak[37] showed that the ATEG could reduce the standard deviation of the normal force on an airfoil caused by changing wind speeds; up to 95% for a sudden step in wind speed and up to 81% for a turbulent flow (10% intensity).

A similar test was conducted using a simplified aeroelastic model of a Vestas V66 wind turbine to look at the equivalent flapwise blade root moment. Anderson, Gaunaa, Bak and Buhl[38] found that the flapwise moment was reduced 60% for inflow with a turbulent field of 10% intensity using a 7 m ATEG on a 33 m blade.

This preliminary research led to the construction of a physical model equipped with the ATEG system (Fig. 3-9). In 2006 Bak, Gaunaa, Anderson, Buhl, Hansen, Clemmensen and Moeller[39] performed wind tunnel tests on a Risoe-B1-18[40,41] airfoil with a 16.4% maximum thickness-to-chord ratio and a chord of 0.66 m (26.0 in.) equipped with 9%*c* piezoelectric actuated flaps. A total of 36 Thunder© TH-6R piezoelectric bender actuators were used to form a flap along the entire span (1.9 m).

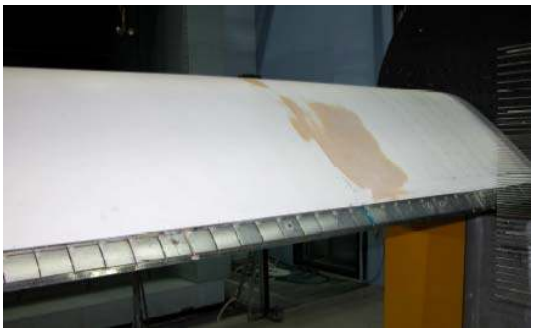

Fig. 3-9 Wind-tunnel model with trailing edge ATEG. (Photo by Risoe DTU National Laboratory for Sustainable Energy[39])

The results from the wind tunnel experiments[39] included steady and dynamic tests at 40 m/s, corresponding to a Re = 1.66×10^6. The steady state tests showed that deflecting the ATEG towards the pressure side (positive $ß_{flap}$) at an angle of $ß_{flap} = 1.5°$ resulted in a $C_L = +0.036$ and deflecting it towards the suction side (negative $ß_{flap}$) at an angle of $ß_{flap} = -2.5°$ resulted in a $C_L = -0.066$. The drag was almost unaffected by the actuation. A step change of the ATEG from $ß_{flap} = -3.0°$ to $+1.8°$ showed that, within the linear lift region of the airfoil, a $C_L = 0.10 - 0.13$ could be obtained. Steady lift results are shown in Fig. 3-10.

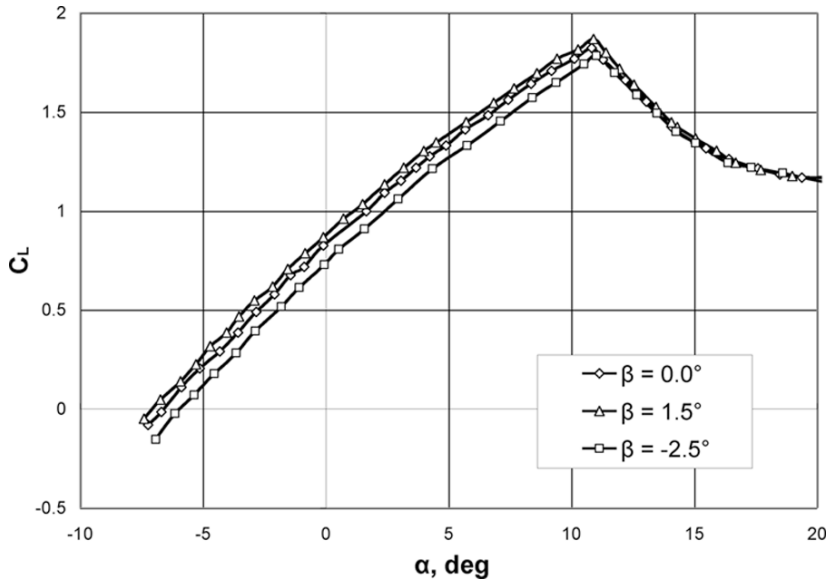

Fig. 3-10 Steady airfoil characteristics for the Risoe-B1-18 fitted with ATEG. Lift coefficient vs. *AOA* for different flap angles. (Source: Fuglsang et al.[41])

The tests also showed the ATEG's ability to cancel out the load variations of the airfoil in a sinusoidal pitch motion and that it was possible to reduce fluctuations (measured in C_L) by 80%. The phase shift between the ATEG motion and pitch motion proved to be a significant variable; large reductions were accomplished with a phase shift of 30°. Experiments simulating improper control (a 180° phase shift from the optimal shift) *increased* the C_L by 70%.

Additional experiments[42] testing the capabilities of the ATEG concept were carried out by DUWIND (Delft University Wind Energy Research Institute). The goal of these tests was to show that vibrations in a dynamically scaled blade due to randomly varying aerodynamic loads could be significantly reduced using trailing edge devices. A reduced scale wind turbine blade (span = 90 cm, chord = 12 cm) embedded with four Thunder© TH-6R piezoelectric bender actuators[43] was tested in a wind tunnel (Fig. 3-11). The actuators formed two different flaps of 50%*c* and were covered with soft foam and a latex skin. The blade was constant thickness with no twist along the span. The model was

attached to the ceiling of the tunnel with the bottom end allowed to deflect freely. The change in flapping bending strain on the blade root and the acceleration of the deflecting tip were measured. Both feed forward (open loop) and feedback (closed loop) control strategies were used in the experiments. The feedback control experiments showed reductions in root strains from 60-95%.

Fig. 3-11 DUWIND's "smart blade" experiment tested at TU Delft LSLT wind tunnel. (Source: Barlas and van Kuik[4])

Adaptive Compliant Wing

Research on the adaptive compliant wing has been conducted in a collaborative effort with FlexSys, the Air Force Research Lab's Air Vehicle Directorate, and Lockheed Martin. The concept is designed for high-endurance aircraft. Wind tunnel and in-flight tests were conducted to demonstrate the potential of this technology for effective gust load alleviation. Wind tunnel tests showed that as the flap angle was changed from -8° to +8°, C_L increased from 0.1 to 1.1 without significantly affecting drag. The in-flight test section had a 50 in. span and a 30 in. chord. The flap was capable of deforming +/- 10° at a rate up to 30 deg./sec and twisting up to one degree per foot of span.[44] The in-flight tests were carried out at high altitude and high subsonic conditions. Complete results from these tests have not been released.

3.2.4 Wind Turbine Control

Nontraditional flaps operate on the same principle as traditional flaps, to change the sectional camber by deflecting the trailing-edge portion of the airfoil. However, the use "smart" materials (in these concepts: linear and bending piezoelectric actuators, and compliant structures) make these devices aerodynamically superior to the traditional flap. This is due to minimal drag production over a wide lift range. Traditional flaps tend to produce flow separation and increase drag during deployment.

Promising results have been shown in numerical studies, wind-tunnel experiments, and also in mechanical design. Additional research to continue development of nontraditional flaps must address many criteria including the required aerodynamic shapes, the required stiffness and dynamic response, and the weight and power required to actuate the control surface.[32]

Although these "smart" materials offer many advantages, they often come with their own set of problems. Inherent drawbacks of these concepts include scalability to large models and the durability and reliability of the deployment devices (both piezoelectric and compliant structures). Long-term use is a concern because creep or degradation of these materials can occur, which would drastically limit their performance. A high-voltage electric power supply would be required to activate the piezoelectric material based actuators.

3.3 Microtabs

3.3.1 Description

Active translational microtabs have been proposed as a viable and effective device for active load control applications. The concept involves small tabs located near the trailing edge of an airfoil, similar to Gurney flaps.[45] The tabs are deployed approximately perpendicular to the airfoil surface to a height on the order of the boundary layer thickness (1-2% chord). This slight movement affects the aerodynamics of the airfoil by shifting the point of flow separation (Kutta condition), in turn, altering the trailing-edge flow conditions and effectively changing the camber. This phenomenon is illustrated in Fig. 3-12 using instantaneous streamlines from computational simulations. Lift enhancement is achieved by deploying the tab on the pressure (lower) surface and lift mitigation is achieved by deploying the tab on the suction (upper) surface.

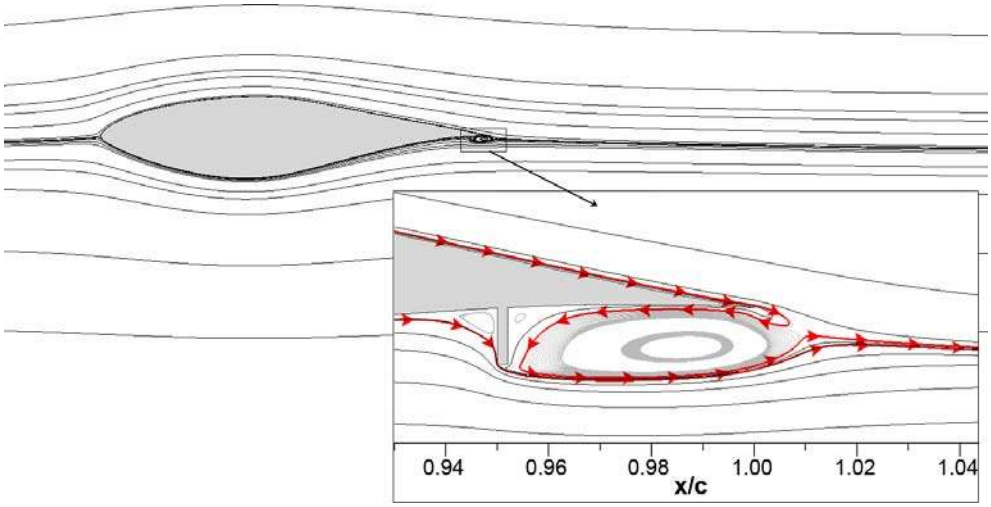

Fig. 3-12 Instantaneous streamlines of an S809 airfoil with a 1.1%*c* pressure surface tab located at 95%*c*. Inset: Tab region with critical instantaneous streamlines denoted by arrows (*Ma* = 0.25, *Re* = 1×10^6, $\alpha = 0°$). (Source: Chow and van Dam[56])

3.3.2 Classification

G - geometric device

TE - located near the trailing edge of the blade

I / D - capable of deploying both directions and therefore can adjust the lift curve up and down

S / U - steady and unsteady operation by using on/off deployment

3.3.3 Background

The initial development of the microtab concept was conducted by researchers at UC Davis in the late 1990s.[46-48] Both computational and experimental studies on lower surface microtabs on the GU25-5(11)8 airfoil[49] were performed in 2-D and 3-D operation. The effects of tab height, tab location and tab spacing were all investigated for 3-D applications. The results indicated that a tab of 1%*c* in height, located at x/*c* = 95% on the lower surface provided the best compromise for lift, drag, and volume constraints.[46] For both numerical and experimental tests, a 30-50% increase in C_L was seen in the linear lift region with 1%*c* tabs.[46]

Standish and van Dam[50] and van Dam, Standish, and Baker[51] conducted more comprehensive 2-D computational experiments further examining tab height and location on both upper and lower surface on the S809 and the GU25-5(11)8 airfoil. Pressure surface tabs demonstrated an increase in lift over all angles of attack, whereas suction surface tabs only decrease lift at angles of attack throughout the linear region. The suction surface tabs lose effectiveness at the higher angles of attack because the flow separates forward of the tab location. The optimal location for the lower surface tab in terms of lift and drag was again found to be around 95%*c* with a height on the order of the boundary layer thickness, or ~1%*c*. The computational studies were validated in the

wind tunnel on the S809 airfoil. The results[52] are shown in Fig. 3-13 and agree very well, especially in the linear region.

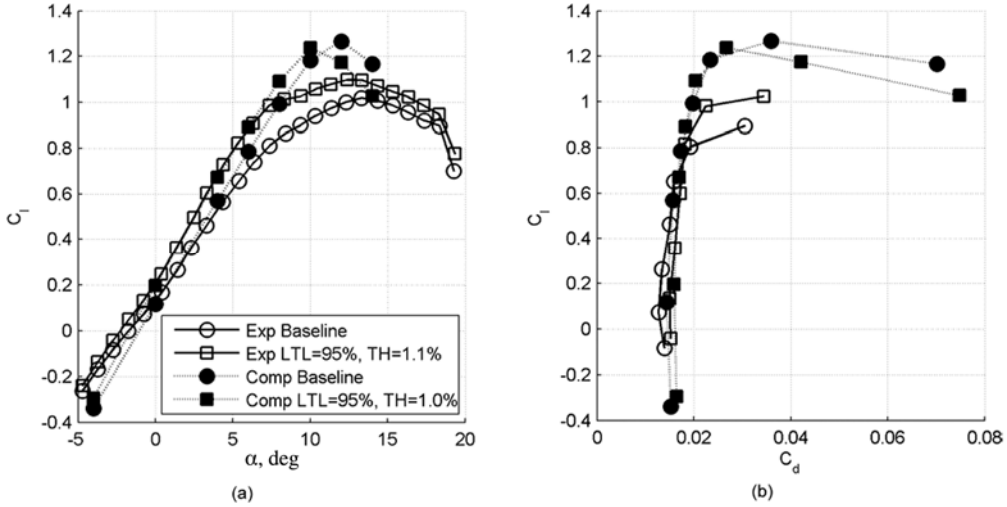

Fig. 3-13 Comparison between experimental and computational results for lower surface tabs on the baseline S809 airfoil with a *Re*=1×10^6. (Source: Baker et al.[52])

Although earlier reports on 3-D investigations indicated that solid tabs generate the best lift enhancement, gaps may be necessary for actuation purposes and for some pitching moment and drag reduction benefits.[53,54] Mayda, van Dam, and Yen-Nakafuji[55] performed more detailed computational investigations on the 3-D effects of microtabs by modeling finite width tabs on a semi-infinite wing. Studies showed that tab effectiveness reduced as the gap size was increased. The amount of gap can be identified with a solidity ratio, SR, defined as;

$$SR = \frac{span\ covered\ by\ tabs}{total\ span\ of\ model} \qquad \textbf{(Eqn. 5)}$$

Computational results indicated that a solidity ratio of 85% or higher should be maintained for proper effectiveness. A solidity ratio lower than 75% allows the flow to reattach at the trailing edge, thereby drastically reducing the tab's performance.

In order to fully understand the behavior of these devices, Chow and van Dam[56,57] conducted computational studies analyzing the unsteady behavior and potential nonlinearites during the deployment of a pressure surface microtab integrated into a S809 airfoil. For analysis purposes, a non-dimensional deployment time, $T_{deployment}$, was used to study the tab's motion.

$$T_{deployment} = \frac{U_{\infty} \cdot t_{deployment}}{c} \qquad \textbf{(Eqn. 6)}$$

where U is the free-stream velocity (m/s), $t_{deployment}$ is the actual deployment time (s), and *c* is the chord length (m).

The transient flow behavior for $T_{deployment} = 1$ can be seen in Fig. 3-14 and Fig. 3-15. As the tab deploys, a low-pressure region and a counterclockwise vortex form just aft of the tab. Up until a non-dimensional deployment time of T = 0.8 (Fig. 3-14/15f), the emergent tab-generated vortex acts like a separation bubble. As the bubble extends past the trailing edge, an interesting phenomenon occurs; the suction surface flow at the trailing edge is entrained back into the pressure surface vortex. Fig. 3-14/15g shows the suction surface flow being drawn around the trailing edge and back towards the tab. The flow continues traveling on the pressure surface, driven by the vortex, and up the aft part of the tab until it reconnects with the pressure surface flow from upstream of the tab. A new stagnation point is formed at the tip of the tab, where the two flows leave the airfoil/tab surface (Fig. 3-14/15h). The shift of the separation point from the trailing edge to the end of the tab changes the Kutta condition of the airfoil. In this situation, the effective camber is increased and C_L is increased. The results from the computational studies on the dynamic behavior of tabs show that only small transient effects are seen during deployment; therefore, these devices can be designed and operated as simple "on-

off" devices. This allows for the use of more simple control strategies and actuation mechanisms.

The latest wind-tunnel experiments investigating the microtab concept were conducted on a blade tip model.[58] The half-scale model (model span of 24.7 in.) was representative of the outboard 10% of the ERS-100 horizontal-axis turbine blade. This experiment was the first test of the microtab's performance in a fully three-dimensional flowfield. Tab heights of 1% and 1.5% chord were investigated under free and fixed transition at Reynolds numbers of 350,000 and 460,000. The tests used static, single-piece (non-segmented) tabs running the span of the model located at 95%c on the pressure surface and at 90%c on the suction surface. The microtabs showed similar effectiveness as seen in the two-dimensional tests.[58] Nearly constant lift increases of 9% and 22% were achieved with lower (pressure) surface 1%c and 1.5%c tabs, respectively. Lift reductions in the linear lift regime of 20% and 30% were seen for upper (suction) surface 1%c and 1.5%c tabs, respectively. These results confirm that tabs are effective in fully three-dimensional flowfields, a crucial step towards potential full-scale applications.

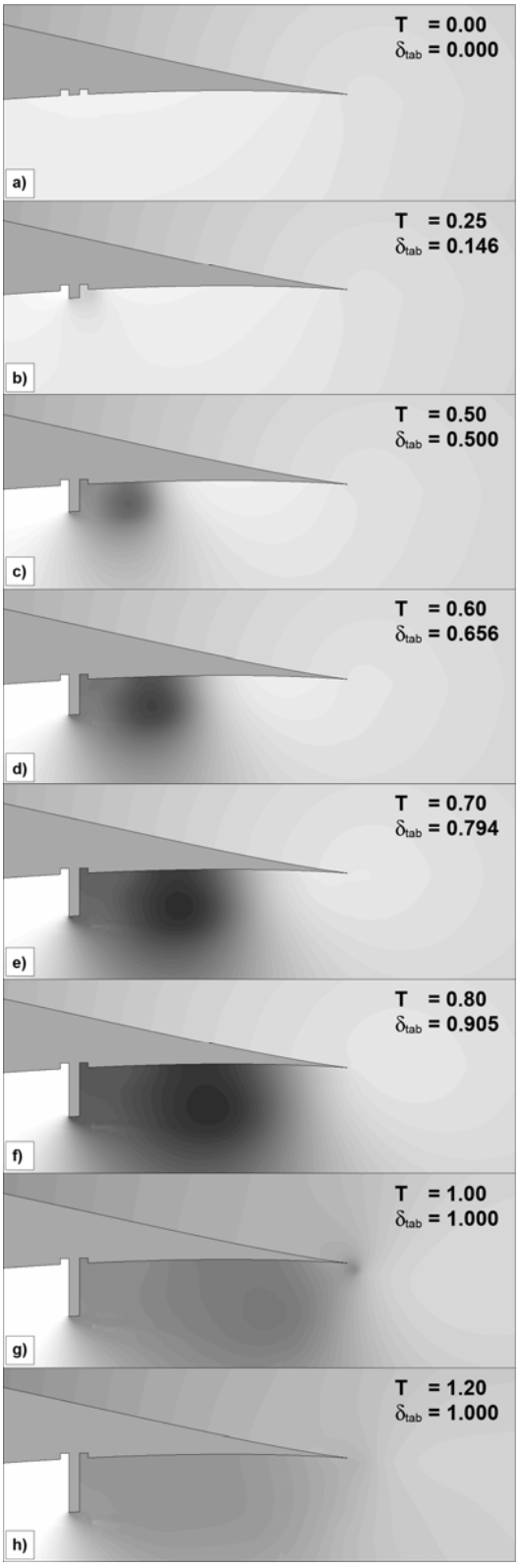

Fig. 3-14 Cp contours in tab region during deployment, ($T_{deployment}$ = 1). Darker regions indicate lower pressure. (Source: Chow and van Dam[57])

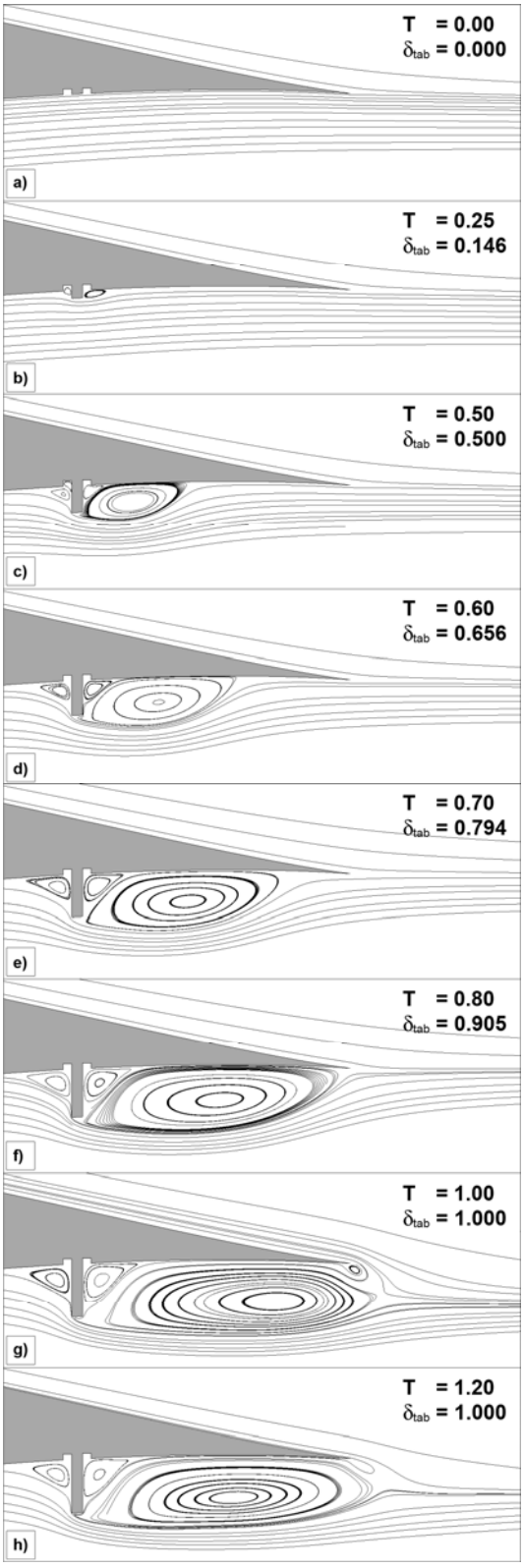

Fig. 3-15 Instantaneous streamlines in trailing-edge region of S809 airfoil during tab deployment, ($T_{deployment}$ = 1). (Source: Chow and van Dam[57])

Further research has been conducted on the effectiveness of tabs using aeroelastic simulation in conjunction with a simple control program. For this analysis, FAST/AeroDyn software[30,59] was used along with MATLAB's Simulink[60]. The NREL-developed Simulink/FAST interface was modified to simulate independent control of several radial sections of microtabs on each blade and also to allow for inputs that model the time dependence of the section lift and drag changes as the microtabs are deployed and retracted. The NREL Controls Advanced Research Turbine (CART), a 600 kW two-bladed upwind turbine, was modeled to demonstrate the impact of microtabs on blade loading. Since earlier simulations showed that the control effectiveness of the microtabs is optimized if they are located on the outer 25% of the blade span,[61] the model was equipped with a microtab system in this configuration on the suction surface of the blade. A simple control-system simulation was designed to deploy the section of microtabs on one blade every time it passed in front of the tower. The loads on only that one blade were attenuated. As the blade passed the tower, the tabs were retraced and the load attenuation diminished. This simulation was meant to provide only a graphic demonstration of the impact of microtabs; this is not a situation that would actually be implemented for actual turbine operation. The results for a 15 m/s steady wind (no turbulence- or gust-induced loading) and an 18.2 m/s turbulent wind are shown in Fig. 3-16 and Fig. 3-17, respectively. In both cases, a positive tip displacement indicates movement toward the tower; a smaller displacement means more tower clearance. The microtab-equipped blade passed upwind of the tower at an azimuth angle of 180°. Under both situations, the deployment of the tabs reduced the blade tip displacement, thus increasing the tower clearance of the tip by about 0.25 m. Analysis of the loads revealed

that the blade root fatigue damage was increased as a result of tab deployment. Deployment of the microtab system at other times was also simulated and showed an increase in loads and deflections. Improper control is a concern for all AFC devices.

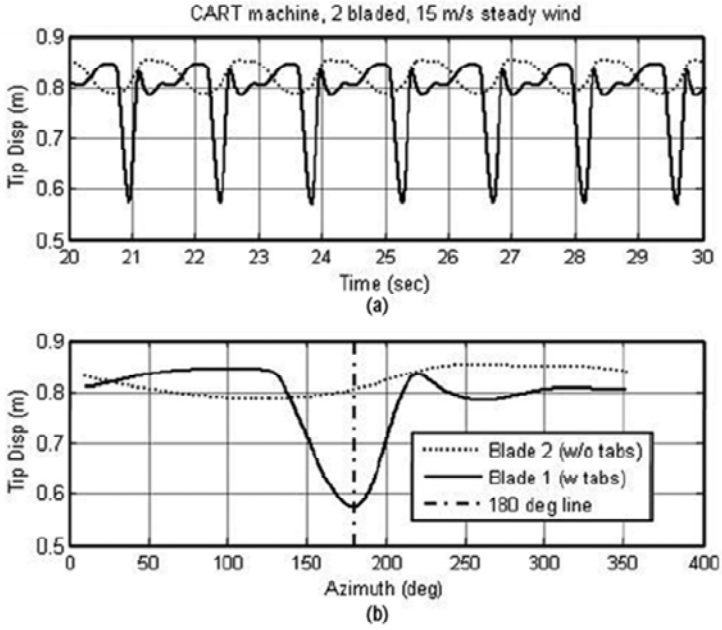

Fig. 3-16 Effect of microtabs on tip displacement of CART turbine. (a) Time series of tip displacements, (b) Tip displacements as a function of rotor azimuth angle (Source: Berg et al.[6])

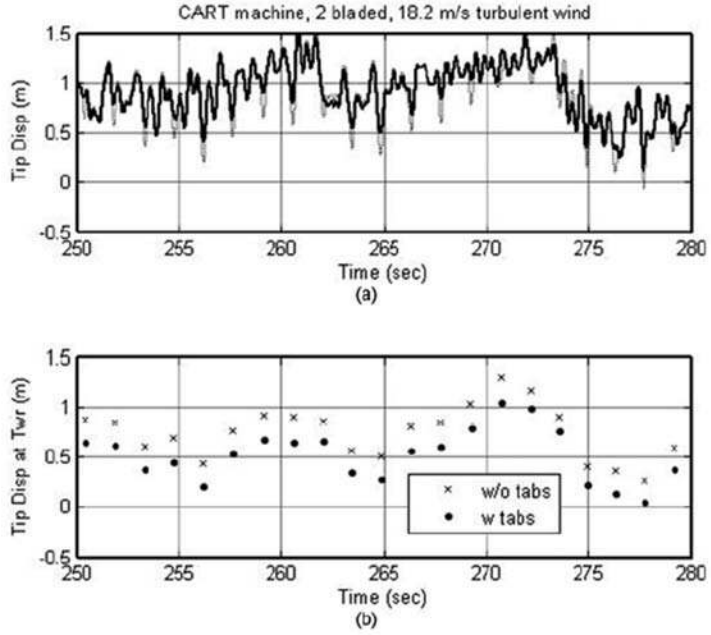

Fig. 3-17 Effect of microtabs on tip displacement of CART turbine. (a) Time series of tip displacements, (b) Tip displacements as blade passes in front of tower (Source: Berg et al. [6])

3.3.4 Wind Turbine Control

The microtab system consists of small devices that are capable of creating changes in lift comparable to the changes created by much larger flaps. Appealing features include small size, fast activation, mechanical simplicity of the design, low power requirements and a short linear deployment distance. The perpendicular motion of the tab relative to the flow requires significantly smaller forces for a given change in sectional lift compared to a traditional trailing-edge flap. The major hurdle facing this concept is minimizing air leakage between the tab and the blade. Substantial leakage would generate aeroacoustic noise and negatively affect the turbine's performance. The far aft location of the tabs makes it challenging to install an actuator near the tabs. For this reason, an appropriate design would include a lever arm connecting the tab to an electromechanical actuator placed near 70%*c*. If a motor and lever arm configuration were to be implemented, measures to reduce possible misalignment would have to be taken.

3.4 Miniature Trailing-Edge Effectors (MiTEs)

3.4.1 Description

Miniature trailing-edge effectors (MiTEs) are small translational flaps, approximately 1-5% chord in height, located at the trailing edge. The MiTE concept was inspired from the Gurney flap[45] and is similar to the microtab in many ways. The aerodynamic force alteration is produced by a small region of separated flow directly upstream of the flap, with two counter-rotating vortices downstream of the flap

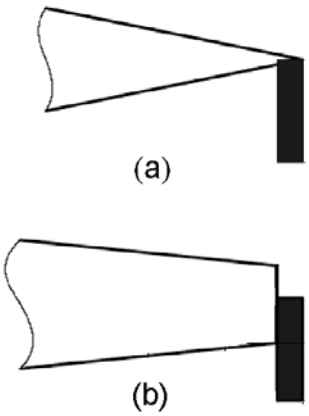

Fig. 3-18 Geometry of (a) Gurney flap and (b) MiTE attached to a sharp and blunt trailing edge airfoil. (Source: Lee and Kroo[63])

effectively modifying the trailing-edge Kutta condition. The difference between the microtabs and the MiTEs is the location. The MiTEs are located at the trailing edge, therefore a blunt trailing edge with a thickness at least the same as the flap height is required to provide a space for storing the flap when retracted (Fig. 3-18). The flap has three possible positions; up, down, and neutral. Lift enhancement occurs when the flap is in the down position and lift mitigation is realized when the flap is in the up position.

3.4.2 Classification

G - geometric device

TE - located at the trailing edge

I / D - capable of deploying both directions and therefore can adjust the lift curve up and down

S / U - steady and unsteady operation

3.4.3 Background

The MiTE concept[62] has been researched since 1998 at Stanford University where numerous computational and experimental studies have been conducted. A CAD model of a wing equipped with a MiTE system is shown in Fig. 3-19.

Fig. 3-19 Concept wing with MiTEs. (Source: Bieniawski et al.[65])

One study performed by Lee and Kroo[63] analyzed the three dimensional aerodynamics of the MiTEs using an incompressible Navier-Stokes flow solver. The study looked at the impact of flap aspect ratio, A_f, on the lift distribution and overall performance. The flap aspect ratio is defined as;

$$A_f = \frac{L_f}{L_g} \qquad \textbf{(Eqn. 7)}$$

where L_f is the length of the flap and L_g is the length of the gap between two flaps. The flap height was kept constant at 1%*c* and L_f was equal to L_g, meaning that in all cases 50% of the wing was covered by tabs. Results indicated a linear relationship between C_L and the spanwise length of the flap, L_f. The knowledge of this relationship could provide designers with more freedom when selecting the spanwise flap length to fit their specific needs.

Another computational study by Lee and Kroo[64] investigated the steady and unsteady aerodynamics of MiTEs. The focus was on the change in lift, drag, and pitching moments with fully deployed MiTEs as compared to a clean configuration. The steady state simulations looked at different trailing edge thicknesses, flap sizes, Reynolds numbers, and angles of attack. One result showed that a larger ΔC_L occurred for larger flap heights. A flap height of 3.0%c had a maximum ΔC_L of approximately 0.45 for both the sharp and blunt trailing edge configurations. Some of the results are shown in Fig. 3-20. Several other steady state results can be found in the publication[64]. The unsteady effects were analyzed using time

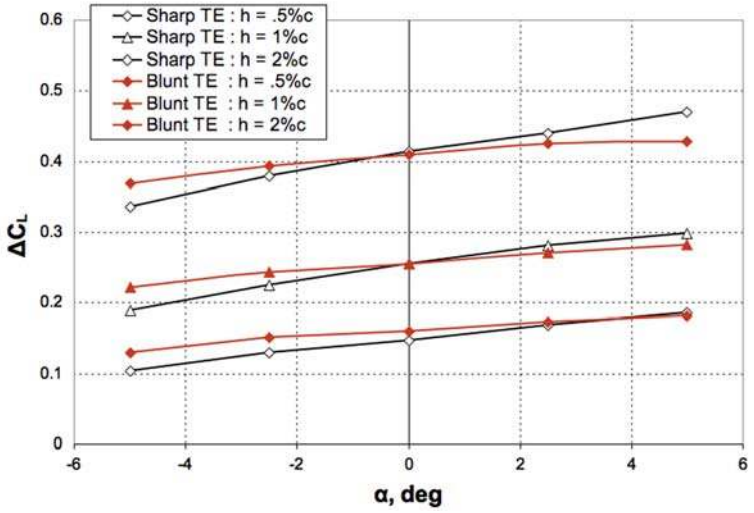

Fig. 3-20 Change in lift coefficient with respect to angle of attack for varying flap heights (Source: Lee and Kroo[64])

accurate computations. The studies looked at the vortex shedding phenomenon and the frequency response of a deploying flap. Fig. 3-21 displays CFD images of streamlines and a stagnation pressure map of a deploying MiTE.

Stanford researchers[65] also looked into novel approaches for control of MiTE systems. A flight vehicle equipped with MiTEs and a distributed flight control system with remote control was developed and tested. The vehicle had a six foot span flying wing with a 12 in. chord and a 30° sweep. The flaps had a maximum deployment of 2%*c*. The experiments demonstrated that the MiTE system was capable of providing adequate rates in pitch, roll, and yaw.

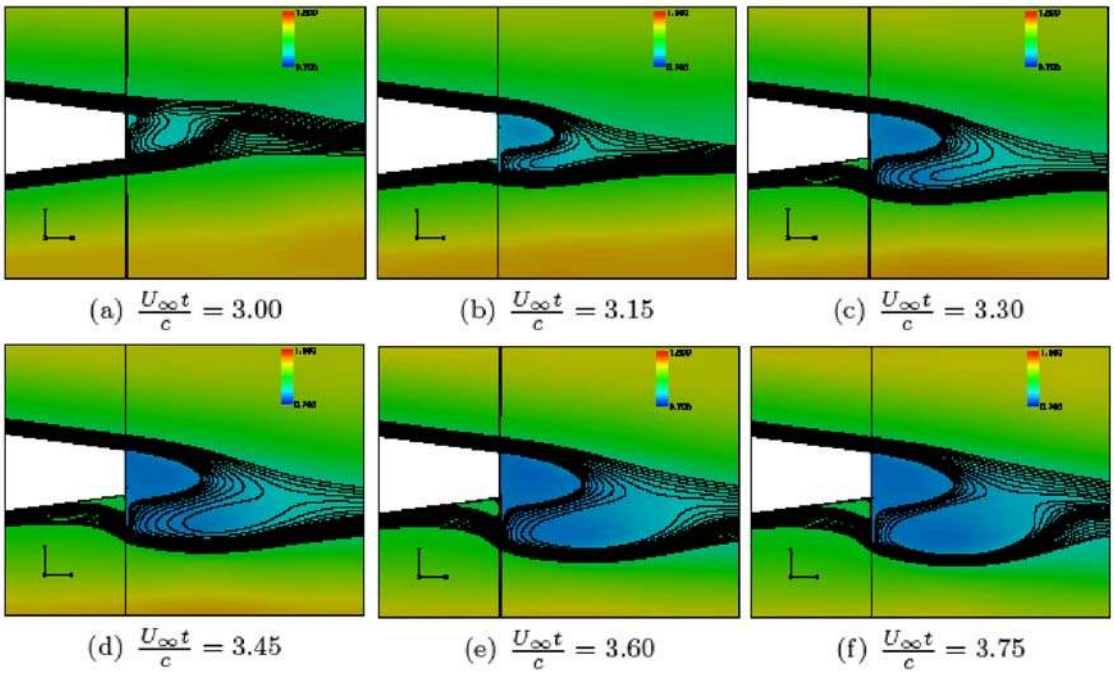

Fig. 3-21 Streamlines and stagnation pressure map of a moving flap from neutral to down position. (Source: Lee and Kroo[64])

3.4.4 Wind Turbine Control

The MiTES have similar advantages to the microtabs; they are small, require little activation force, and can respond quickly. The upside to this type of flap is that the far aft location provides more effective lift control and there is no need for slots in the blade construction, which reduces the modifications to the blade. However, the tradeoff is that a blunt trailing edge is mandatory. This will decrease performance of the turbine when the device is not active and research has shown blunt trailing edges generate noise in the tip region.[66]

3.5 Microflaps

3.5.1 Description

Microflaps are also derived from the Gurney flap[45] and are similar to both the microtab and MiTE concept. Instead of a translational device like the microtab and MiTE, the microflap is a rotating device. It takes the position of the trailing edge and is able to rotate 90° in both directions. The optimum height is similar to that of the microtabs, which is on the order of the boundary layer thickness (1-2% chord). A CFD model of a microflap is shown in Fig. 3-22. Rotating the flap up towards the suction surface reduces lift and rotating it down towards the pressure surface increases lift.

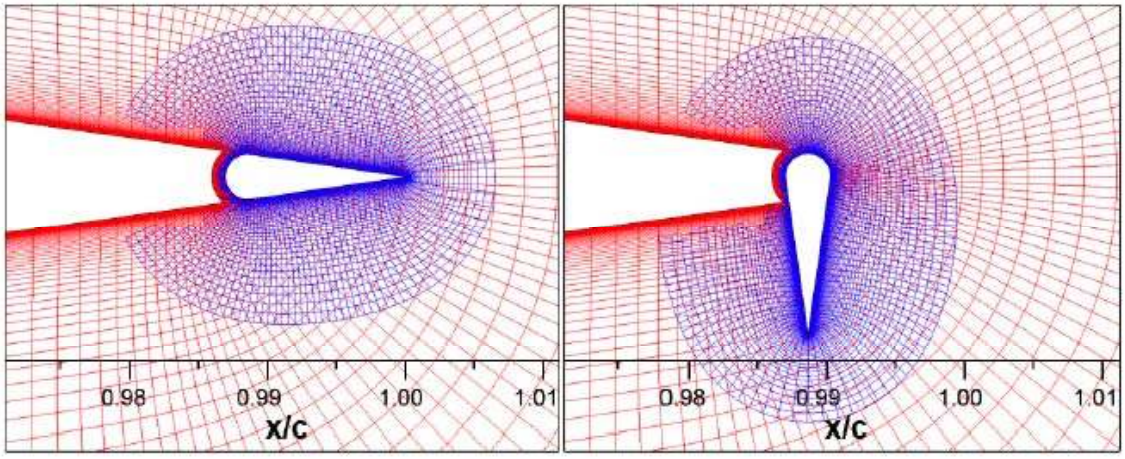

Fig. 3-22 Microflap with body-fitted O-grid in retracted and fully deployed (down) positions. (Source: van Dam et al.[67])

3.5.2 Classification

G - geometric device

TE - located at the trailing edge of the blade

I / D - capable of deploying both directions and therefore can adjust the lift curve up and down

S / U - steady and unsteady operation

3.5.3 Background

Computational studies conducted by van Dam, Chow, Zayas, and Berg[67] used a modified NACA 0012 airfoil with a semi-circular cove truncating the trailing edge. The flap was constructed within the cove and extended out, forming the trailing edge. The flap had a semi-circular arc leading edge with a diameter of 0.330%c and a chord length of 1.495%c. The goal of this computational study was to analyze the flap's time-dependent effect on sectional lift, drag, and pitching moment and its effectiveness in mitigating high frequency loads on a wind turbine. The flow conditions used were Re = 1.0 million and M = 0.25. Several studies with varying non-characteristic flap deployment times (Eqn. 6) were carried out and the results are shown in Fig. 3-23.

The overall transient behavior of the microflap was found to be similar to that of the microtabs. The flaps had a slightly faster initial response time and larger lift effectiveness due to the placement at the trailing edge. The flap placement also increased bluff-body vortex shedding.

3.5.4 Wind Turbine Control

This concept is appealing because the trailing-edge location provides more effective lift enhancement than the microtabs and the design does not require a blunt trailing edge as does the MiTEs. Limited studies have been conducted on this concept, which makes it difficult to define all of the benefits and drawbacks. Some anticipated hurdles are minimizing air leakage and designing a simple, effective actuation system that is capable of rotating the flap bi-directionally to an angle of 90°.

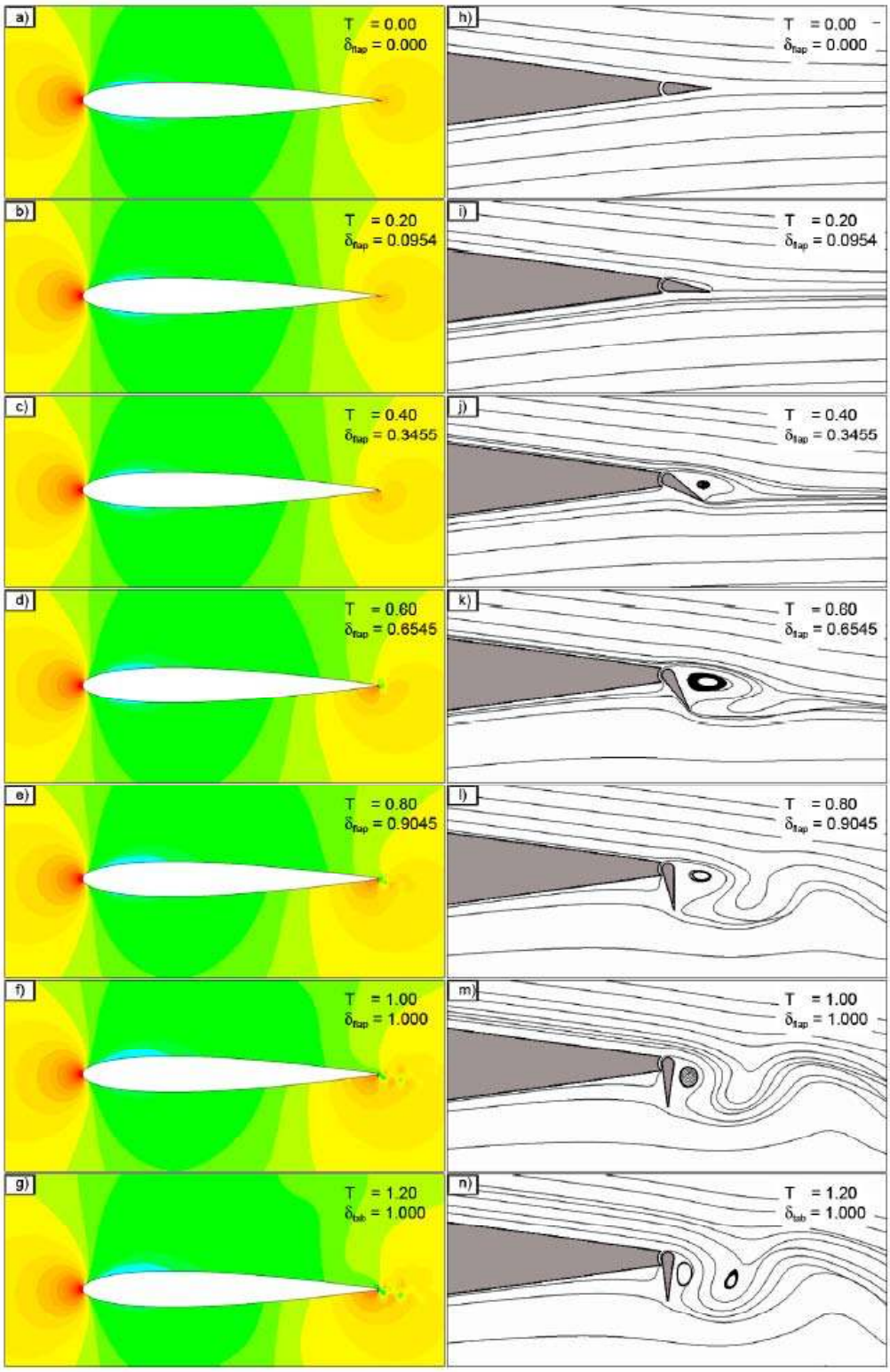

Fig. 3-23 Airfoil pressure contours (left) and instantaneous streamlines (right) due to deployment of microflap. (Source: van Dam et al.[67])

3.6 Active Stall Strips

3.6.1 Description

Small stall strips, or spoilers, are placed parallel to and near to the leading edge ($x/c < 0.1$) to provide control over the stalling characteristics of an airfoil.[68] The strips operate by separating the flow near the leading edge. Studies have been conducted for both passive and active control. Passive strips were designed to be implemented on stall-regulated wind turbines, but with modern variable-pitch turbines they do not provide any advantages. Active strips, on the other hand, could provide some benefits for turbine control. Active stall strips would be capable of deploying and retracting in response to changes in local flow conditions. Instead of increasing C_L with deployment, as many of the other AFC devices do, active stall strips decrease C_L and increase C_D as a means of control. Although, nearly all stall strips in use today are static except for the actively controlled stall strips on the Lockheed-Martin U-2 airplane.

3.6.2 Classification

G - geometric device
LE - located near the leading edge of the blade
D - used only to decrease lift
S - deploys in a steady operation

3.6.3 Background

There has not been much recent research regarding this device. A 1991 paper by Lewis, Potts, and Arain[68] summarized experiments looking at optimal location and size of a spoiler on a NASA LS (1)-0417 MOD airfoil. This airfoil was selected because of its use on the Orkney 3 MW wind turbine. Three spoiler heights (3 mm (0.767%*c*), 6 mm (1.535%*c*), and 9 mm (2.302%*c*)) at five different chordwise locations (one on the lower

surface, one on the leading edge, and three on the upper surface) were tested at different angles of attack. The locations and heights of the tested spoilers, along with predicted streamlines, are shown in Fig. 3-24.

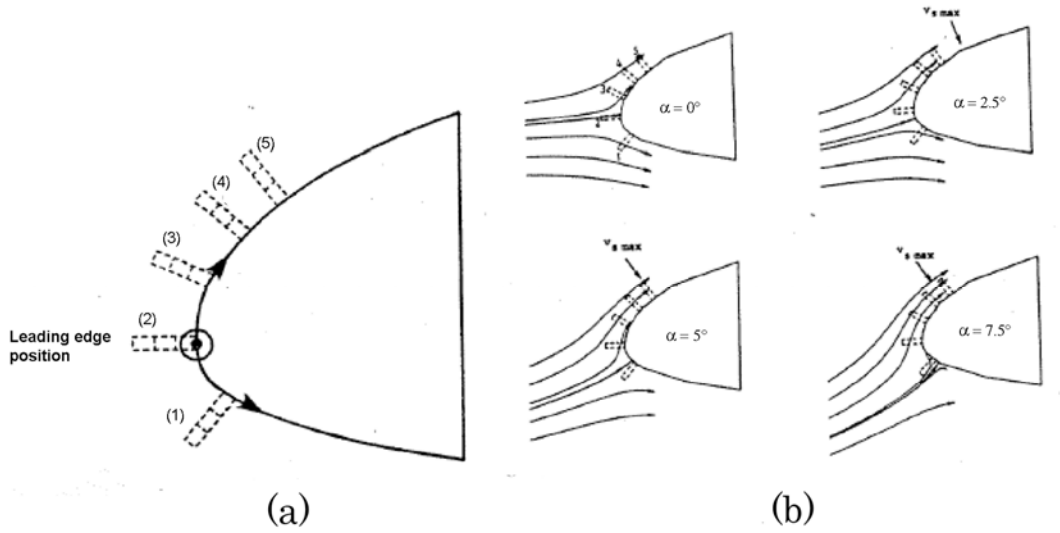

Fig. 3-24 a) Location of leading edge spoilers showing the first 10% of chord, b) Prediction of leading edge streamlines for varying angles of attack. (Source: Lewis et al.[68])

Active strips were found to be most effective at location No. 5 (x = 2.9%*c*). At this location, small spoiler heights (h < 0.77%*c*) provided drag control without inducing major stall and associated buffeting. The height of the strip could be adjusted depending on what type of control was needed. For stable (unstalled) control, the stall strip could be deployed only a short distance to provide adequate control. Results showed that a height of 0.77%*c* could decrease C_L/C_D decreased from 70 to 18. In this configuration, the strip acted as a turbulence promoter, inhibiting boundary layer separation. Greater deployment distances (0.77%*c* < h < 1.53%*c*) provided control by inducing upper surface stall and was found to be more suitable for braking. At these heights, the strip acts as a flow separation trip resulting in a C_L/C_D reduction from 18 to 3.4. The differences in the

lift curves for spoilers located at position No. 2 and position No. 5 on Fig. 3-24 can be seen in Fig. 3-25.

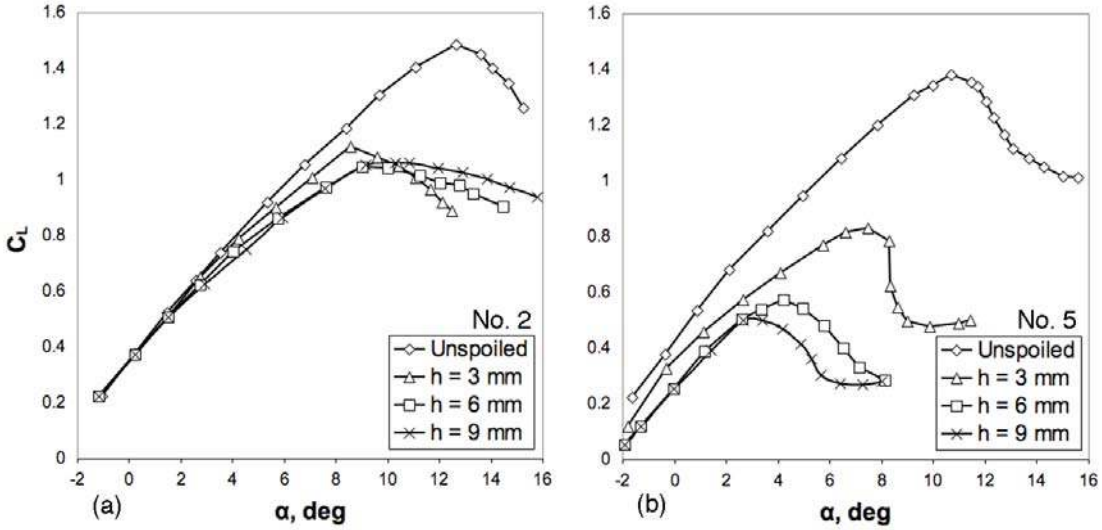

Fig. 3-25 Lift curve results for spoiler positions, a) position 2 – leading edge, b) position 5 – active spoiler position. (Source: Lewis et al.[68])

3.6.4 Wind Turbine Control

There has not been any recent research investigating this control approach. The past research was conducted for wind turbine control, but additional numerical computations and experiments should be conducted to further understand the aerodynamics and to find an optimal location and size. A control limitation of this device is that it is not possible to increase C_L. Stall strips operate in a similar manner to the microtabs and share some of the same concerns, mainly maintaining tight tolerances between the strip and the many body of the blade. Although, air leakage isn't a concern since the strips are only location on the suction surface. The forward location is beneficial from an implementation standpoint since there is plenty of space inside the blade to house an actuator; however, major concerns arise from an aerodynamic perspective because slight modifications near the leading edge of the blade could have detrimental effects on the overall performance.

3.7 Vortex Generators

3.7.1 Description

Vortex generators (VGs) are simply solid tabs mounted on the airfoil surface that promote mixing and mitigate boundary layer separation. VGs that are appropriately sized and correctly oriented produce coherent helical vortex structures that cause mixing between the air in the freestream and boundary layer.[69] They are commonly used to reduce flow separation and increase C_{Lmax}. However, at attached flow conditions conventional VGs significantly increase drag. Examples of different VG types, including geometric parameters, are shown in Fig. 3-26a; a simple arrangement of ramp-style VGs on a wing section is displayed in Fig. 3-26b.

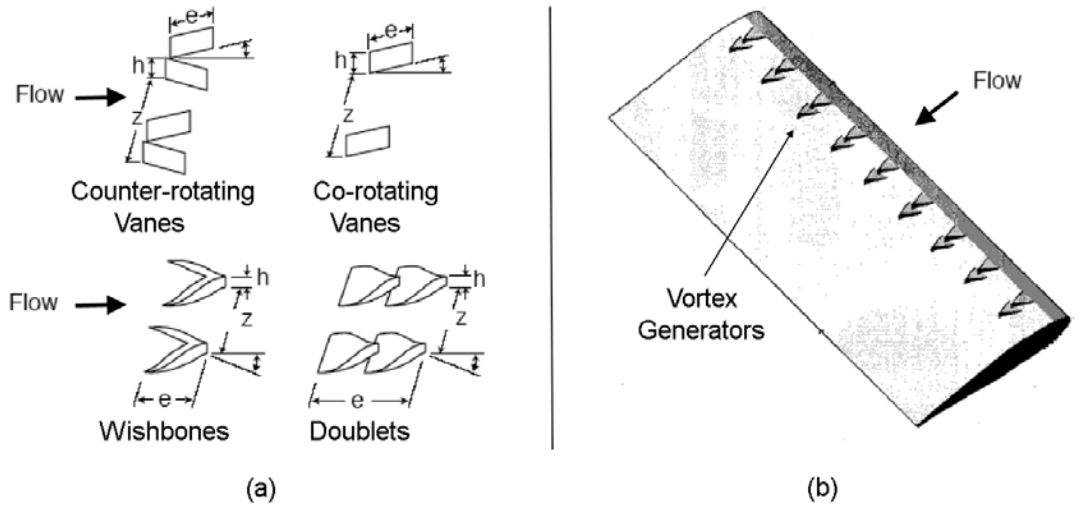

Fig. 3-26 a) VG types and geometric parameters. (Source: Lin et al.[69]), b) Illusration of VG arrangement on a wing section. (Source: Barrett and Farokhi[70])

Investigations in reducing the height of VGs found that under certain aerodynamic conditions, a properly designed "micro vortex generator" (MVG) can be just as effective in delaying separation in low speeds as a traditional VG.[69] MVGs are defined as having a height between 10% and 50% of the boundary-layer thickness. The smaller size has the

advantage of incurring less drag compared to traditional VGs; however, the generated vortices are not as strong and the placement of the MVG with respect to the flow separation region is much more critical. For these reasons, conventional VGs tend to be more effective. The MVGs are best for applications where the flow-separation location is relatively fixed; in this situation they can be placed just upstream of the separation point.

3.7.2 Classification

G - geometric device
LE - located near the leading edge of the blade
DS - used to delay stall
S - steady operation by deploying to different heights

3.7.3 Background

Although passive VGs are useful under certain conditions, active VGs have a greater potential for wind turbine control. Experiments were conducted by Barrett and Farokhi[70] to demonstrate the potential benefits of active VGs, or smart VGs. The experiments used a ramp-style VG configuration with shape-memory-alloy (SMA) actuators along with a shear-flow separation sensor and an optimal controller to form a smart vortex generator (SVG) system to optimize lift-to-drag ratio (L/D) and C_{Lmax} as a function of angle of attack.

Investigations and experiments were conducted to determine the optimum shape, type, size, and placement of the ramp-style VGs on a NACA 4415 airfoil section with an 8 in. chord at a chord Reynolds number, Re = 4.27×10^4. The VGs were placed 8-15%*c* from the leading edge. The smart ramp VGs triggered by a leading-edge shear-flow sensor and controller, was capable of deploying the VGs to an operational height of 0.22 in. in 0.8 s while consuming 9.2 W of power. Wind-tunnel results showed that C_{Lmax} and $_{stall}$ increased from C_{Lmax} = 1.26 at = 12.5° to C_{Lmax} = 1.42 at = 14.3° (Fig. 3-27a). The SVG was able to adjust its height to maximize the lift-to-drag ratio; the height (in inches) is also displayed in Fig. 3-27a. The tests showed that the L/D ratio increased up to 42% above = 12.5° (Fig. 3-27b), while displaying a minimal change (less than 0.1%) in drag. Performance tests indicated that the active vortex generators were capable of both delaying stall and unstalling the airfoil. Unstalling is achieved by activating the VGs during post-stall operation, when the flow is separated, to reattach the flow.

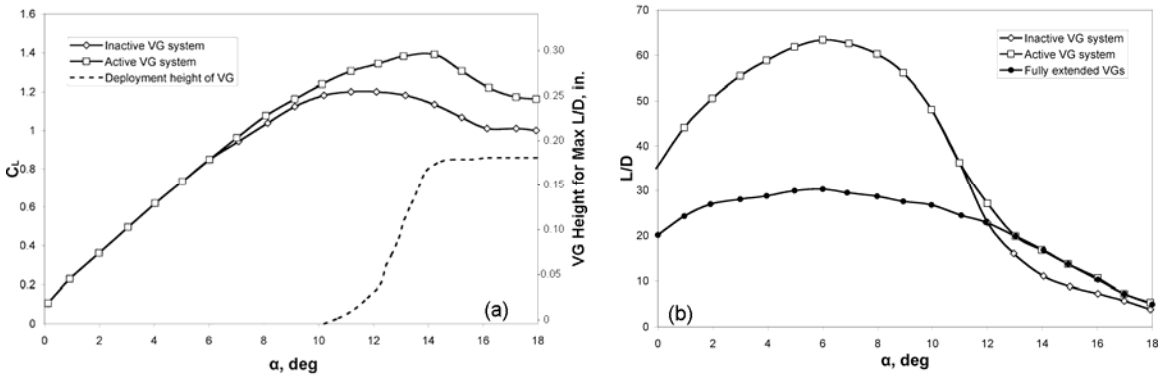

Fig. 3-27 a) Lift curve and deflection height for SVG system, b) L/D vs. alpha for the SVG system. (Source: Barrett and Farokhi[70])

Research on micro vortex generators (MVGs) as a means of flow-separation control has shown that properly designed devices can be just as effective in delaying separation as conventional VGs. Lin[71] evaluated conventional and micro VGs by comparing oil-flow visualization experiments conducted over a 2-D, 25°-sloped, backward-facing curved ramp in a shear flow tunnel. He studied several different types and sizes of MVGs and VGs and concluded that even though MVGs produce weaker vortices, properly designed MVGs would produce strong enough streamwise vortices to overcome separation and tended to be more efficient. The MVGs successfully reduced the extent of separation by almost 90%.

Using VGs and MVGs as a means to suppress separation bubbles on a low Reynolds-number aircraft was first investigated in the early 1990s. Many low-Reynolds number airfoils (Re < 1 million) experience a laminar separation bubble for angles of attack below stall. The separation bubble is formed just downstream of the maximum suction pressure; the laminar boundary layer separates and produces an unstable shear layer that rapidly transitions to a reattached turbulent boundary layer that continues to the trailing edge.[69] Small separation bubbles have little effect on lift but can create a significant increase in drag. An experimental investigation[72] was conducted on a Liebeck LA2573A airfoil using various MVG configurations to eliminate separation bubbles and reduce airfoil drag. Results showed that significant drag reduction, over a range of lift coefficients, occurred for all three types of generators (wishbone MVG with $h/\delta \sim 0.3$, ramp cone MVG with $h/\delta \sim 0.4$, wishbone VG with $h/\delta \sim 0.8$) at the design condition. The MVGs showed a larger decrease in drag (38% for a wishbone MVG) compared to the traditional VGs (30% reduction for wishbone VG).

3.7.4 Wind Turbine Control

Fixed vortex generators have been extensively researched and implemented on wind turbines, but not for active load control applications, rather they are typically installed near the root of the blade to mitigate inboard flow separation. However, active VGs could be placed in the outboard region of the blades and be used for control purposes by increasing C_{Lmax} and $_{stall}$ only when necessary. The implementation of active VGs would require actuators and slots in the blade. Similar to other AFC devices, the requirement for slots in the surface of the turbine blade raises concerns about possible reduced performance and noise generation. The forward placement of the VGs is advantageous because there is plenty of space to house an actuation system within a turbine blade.

The main disadvantage of active VGs and the other DS devices is that they only are capable of delaying stall. Delaying stall is not as desirable for control purposes as adjusting the entire lift curve as the I/D devices are able to do. One possible solution is to take Corten's[24] idea (described in the introduction of *Chapter 3*) of passively applying VGs to wind turbine blades one step further and utilize actively controlled VGs, similar to the research conducted by Barrett and Farokhi[70]. However, in this configuration the VGs would be normally deployed instead of normally retracted. The VGs could then retract in certain situations to reduce C_{Lmax} and minimize loads; the downside of using normally deployed VGs is that they increase drag at attached flow conditions. One advantage of this is to use design blades with shorter chords, this could save weight and cost on materials. This idea could possibly be applied to other DS devices discussed throughout this report.

3.8 Blowing and Suction

3.8.1 Description

Conventional blowing and suction techniques delay stall by adding high-momentum air into the boundary layer. Blowing devices add stored high-momentum air through slots in the aerodynamic surface. Suction devices remove low-momentum fluid near the surface, which deflects high-momentum free-stream fluid towards the surface, thus reenergizing the boundary layer.[73]

The introduction of high-momentum air, from either blowing or suction, into the boundary layer assists in overcoming adverse pressure gradients, postponing separation. The blowing/suction slots can be located near the leading edge and/or near the trailing edge as shown in Fig. 3-28. The slots are normally positioned in a near uniform fashion along the span of the blade and the blowing/suction can occur steadily or unsteadily. The presence of the slots can change the effective shape of the airfoil at higher angles of attack, causing an increase in drag; however, at low angles of attack this is generally not an issue.

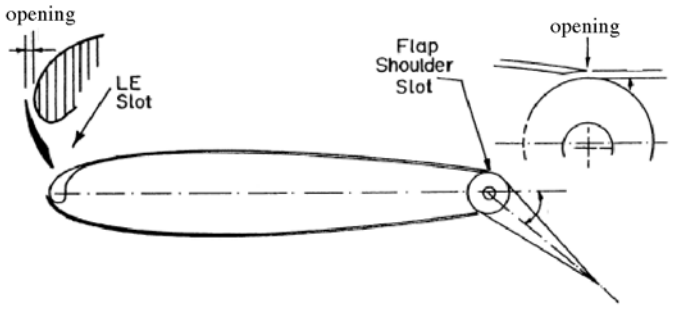

Fig. 3-28 Illustration of possible blowing/suction configuration showing slot locations and deflectable flap. (Source: Greenblatt and Wygnanski[73])

The *slot, or jet, momentum coefficient* defines the relative strength of blowing ($C_\mu > 0$) and suction ($C_\mu < 0$).

$$C_\mu = \frac{\dot{m}_{jet} V_{jet}}{\frac{1}{2}\rho_\infty V_{ref}^2 A_{ref}} \qquad \textbf{(Eqn. 8)}$$

where $\dot{m}_{jet} = \rho_{jet} V_{jet} A_{jet}$ is the mass flow rate of air through the slot, V_{ref} is the reference freestream velocity, and A_{ref} is the planform area. Physically, this coefficient represents the ratio of slot momentum to free-stream momentum.

Pulsed operation is also possible. Pulsed blowing sends short pulses rather than a continuous jet of fluid into the boundary layer and has been found to be more effective. The improved effectiveness is believed to come from the production of vorticity inside the boundary layer. This additional vorticity transports additional free-stream momentum into the boundary layer, therefore requiring less momentum to be injected through the slot itself. The *reduced forcing frequency*, F^+, is commonly used to characterize the ratio between the actuator forcing frequency and the frequency at which fluid events will be convected down the blade surface by the freestream flow.[74]

$$F^+ = \frac{f \cdot X}{V} \qquad \textbf{(Eqn. 9)}$$

where f is the pulsing frequency of the blowing/suction device, X is the representative length scale of the separation zone where eddies or unsteady waves are present (normally the distance from the actuator to the trailing edge), and V is the velocity of the flow past the actuators (normally the freestream velocity, U_∞).

3.8.2 Classification

F - fluidic device

LE/TE - located either near the leading edge or trailing edge

DS - used to delay stall

S / U - can be configured to operate in both modes

3.8.3 Background

The application of blowing for flow control on rotors has a long history with the first flight test occurring in 1955 on a Cessna CH-1 helicopter.[75] Recent experiments by Seifert, Daraby, Nishri, and Wygnanski[76] comparing steady and pulsed blowing leading-edge slots showed that pulsed blowing was more effective. A NACA 0015 airfoil equipped with a leading-edge slot was tested for Reynolds numbers between 150,000 and 750,000. The experiments showed that pure pulsed blowing from the leading edge at a very low momentum coefficient, $C_\mu = 0.0008$, and at a reduced forcing frequency, $F^+ = 0.8$, increased the lift coefficient at $\alpha = 16°$ by 30% relative to the non-blowing case. The steady blowing case with the same momentum coefficient did not show any effect.

Research conducted by Weaver, McAlister, and Tso[77] looked at the benefits of using steady and pulsed blowing to improve the dynamic stall characteristics of the airfoil. The Boeing-Vertol VR-7 airfoil (used on helicopter rotors) equipped with an upper surface blowing slot was used. The airfoil had a chord of 4.0 in., a slot span of 7.9 in., and a slot height of 0.003 in. The airfoil was tested in a water tunnel with a Reynolds number of 100,000 and underwent sinusoidal pitching oscillations described by

$$\alpha = \alpha_m + 10° \sin(\omega t) \qquad \textbf{(Eqn. 10)}$$

where α is the angle of attack, α_m is the mean angle of attack, ω is the frequency of pitch oscillation, and t is time.

The experiments investigated α_m values of 10° and 15° at reduced airfoil frequencies, k, from 0.005 to 0.15 (ω is related to the reduced airfoil frequency through Eqn. 4). The reduced forcing frequency, F^+, ranged from 0 to 3 and the momentum coefficient, C_μ, ranged from 0.03 to 0.66. Unsteady lift, drag, and pitching-moment loads were measured, and fluorescent dye was used to visualize the flow. The results showed that steady, upper-surface blowing trapped a separation bubble near the leading edge during a portion of the airfoil's upward rotation. The presence of the separation bubble was attributed to significantly enhancing the lift. The largest changes in C_L were obtained at the lowest reduced airfoil frequencies, the lowest mean angle of attack, and the highest value of C_μ. The performance decreased as the reduced frequency and mean angle of oscillation increased. Pulsed blowing showed similar effectiveness and offered the largest improvement at $F^+ = 0.9$. Under certain conditions, both blowing types increased the C_{Lmax}; pulsed blowing increased it by 20% and steady blowing by 12%.

3.8.4 Wind Turbine Control

Although these techniques have been successfully implemented on aircraft, there are many concerns related to wind turbine applications. The conventional design, using slots and stored high-momentum air, would be difficult to implement on turbine blades. Main concerns would be added weight and complexity of spanwise slots and the need for compressed air storage. Much of the research regarding conventional blowing and suction is now outdated; however, past studies have paved the way for the development of other unconventional devices that use the same fundamental approach. These devices would be more appealing for turbine control and many of them are discussed later.

3.9 Circulation Control

3.9.1 Description

Circulation control is one concept derived from conventional blowing and suction research. The circulation control wing (CCW) was developed to increase the circulation, which increases the sectional lift coefficient of an airfoil.[78] The device is comprised of a series of thin high-velocity jets that blow high-momentum air tangentially over the rounded trailing-edge surface of an airfoil. Under the influence of this jet, the boundary layer remains attached along the curved surface longer than usual and moves the rear stagnation point towards the pressure (lower) side of the airfoil thereby increasing the circulation around the entire airfoil. This flow phenomenon is called the Coanda effect[79], a balance of the pressure and centrifugal forces.

3.9.2 Classification

F - fluidic device

TE - located at the trailing-edge of the blade

I / D - most research has been involved with increasing lift, however it is realistic to use this technique to decrease lift also

S - steady blowing has been researched

3.9.3 Background

The CCW has been researched extensively both numerically[78,80-84] and experimentally[85-88]. To make earlier CCW designs more effective, the trailing edge of the airfoil was modified to have a rounded edge with a larger radius. The disadvantage of this modification was a high drag penalty while the jet was off.[85] One solution to this was to make the lower surface of the trailing edge a flat surface, while keeping a highly curved upper surface.[85]

Recent studies have focused on the potential benefits of CCW on wind turbine blades. Tongchitpakdee, Benjanirat, and Sankar[78] performed computational studies evaluating the performance of circulation control on the NREL Phase VI rotor, which has S809 blade profiles. The NREL Phase VI rotor, a stall-controlled HAWT, has been successfully tested in the wind tunnel and used in the past as a validation tool for a number of numerical studies. Prior to modeling circulation control, the flow solver was validated for the baseline case with the NREL rotor experimental database[89-92]. Calculations were performed for the NREL Phase VI rotor at two wind speeds, 7 and 15 m/s, and three yaw angles, 0°, 10°, and 30°. The jet momentum coefficients (Eqn. 8) ranged from 0 to 0.10.

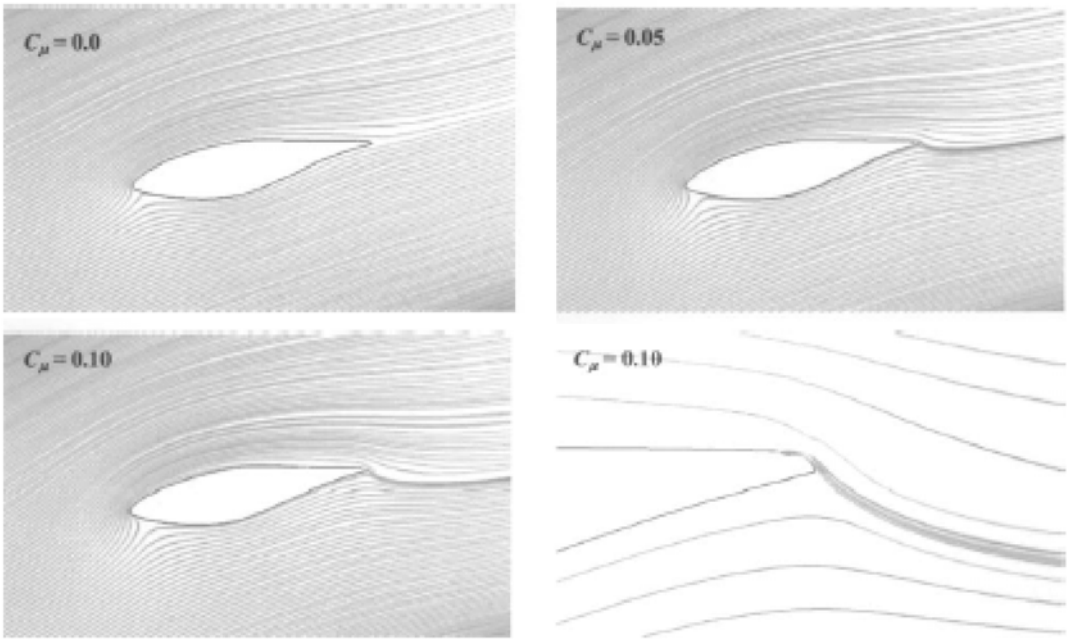

Fig. 3-29 Computed streamlines over the airfoil at 7 m/s, 0° yaw. (Source: Tongchitpakdee et al. [78])

Fig. 3-29 displays the change in the flow field, at a low wind speed of 7 m/s, as the jet momentum coefficient is increased, thus increasing circulation about the airfoil. The resulting deflection of the streamlines near the trailing edge can be observed in the figure.

The jet remains attached to the curved trailing edge, thereby improving the suction on the trailing-edge suction surface. The front stagnation point also is affected; as C_μ increases, the stagnation point moves further back on the pressure surface, and substantial turning of the flow outside of the boundary layer is observed.

At 7 m/s, the flow was well behaved and fully attached over the blade, allowing the CCW to be effective. Tests at the higher wind speed of 15 m/s did not prove as effective due to flow separation forward of the jet. Liu[84] evaluated the possibility of installing a second jet near the leading edge to prevent leading edge stall. He found that the combination of a blowing jet and a CCW could suppress 2-D airfoil stall and improve the effectiveness of the CCW at high angles of attack.

3.9.4 Wind Turbine Control

Much of the research on CCW is being conducted to produce large values of lift and therefore induce a larger loading to create more power. This strategy is not beneficial for load reduction. However, circulation control may potentially mitigate excessive loads if controlled properly or the device could be installed on the pressure surface of the airfoil. One major drawback of this system is the need to install air ducts running the length of the turbine blade to supply the jets with high-pressure air. A second drawback is the required rounded shape of the trailing edge, which results in increased drag and aeroacoustic noise due to vorticity shedding.

3.10 Plasma Actuators

3.10.1 Description

Surface non-thermal plasma actuators operate by creating an electric field between two electrodes, an anode (+) and a cathode (-). By applying a large voltage difference between the electrodes, an electric field is formed and induces an "electric wind", or "ionic wind", close to the surface. The electric wind is formed by collisions between drifting ions and the neutral particles in the electrode gap region[93]. The induced wind acts as a body force and drives the nearby fluid, creating a zero-net mass flux (ZNMF) jet, modifying the boundary-layer airflow profile and postponing separation. The behavior of the actuators is dependent on geometrical parameters (electrode shape and size, gap distances, etc), electrical parameters (voltage, waveform and frequency if AC, etc), ambient air properties (temperature, pressure, humidity, wind speed, etc), and the nature of the dielectric wall.[91-93]

Today, there are many different configurations that are classified as plasma actuators. New devices or different configurations are researched and developed every year. Four configurations will briefly be discussed to develop a conceptual understanding of plasma actuator dynamics. The devices are 1) DC surface corona discharge, 2) AC surface dielectric barrier discharge, 3) sliding discharge, and 4) wall jet. The descriptions of these devices are discussed in further detail by Moreau, Benard, Jolibois, and Touchard[95].

The DC surface corona discharge actuator consists of two wire electrodes mounted flush on the surface of a dielectric profile (Fig. 3-30a). When a high DC voltage (>10 kV) is applied, a corona is formed around the smaller diameter wire (usually the anode) and an electric wind is created tangential to the surface between the two electrodes. The

electric wind is capable of modifying the boundary-layer airflow profile. Fig. 3-30b displays a visualization of a low velocity airflow along a flat plate. If the actuator is off, the smoke remains horizontal. When the actuator is active, flow above the anode is entrained towards the surface from the outer layer, causing the smoke to be drawn to the surface and then accelerated in the discharge region. The advantage of this device is that it requires a simple power supply, however the design is limited to an electric wind velocity of only a few m/s.

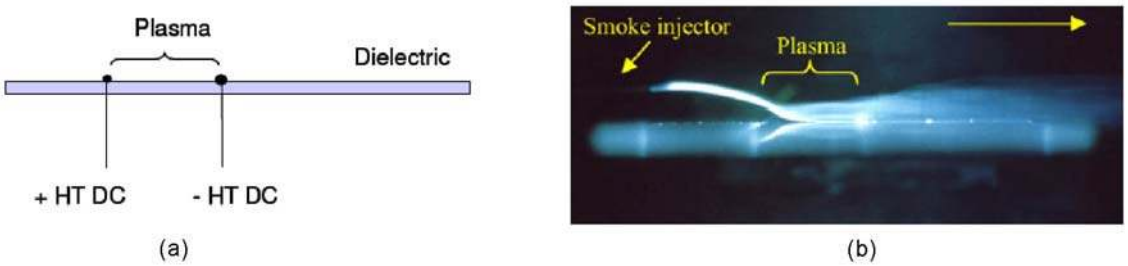

Fig. 3-30 a) Schematic side view of the DC corona discharge actuator, b) 2D visualization of manipulated airflow along a flat plate. (Source: Moreau et al.[93])

The AC dielectric barrier discharge (DBD) is composed of two flat electrodes mounted on both sides of a dielectric material. One is grounded and the other is connected to a high AC voltage (several kV) with a frequency between 100 Hz and several kHz. A plasma sheet of blue ionized air is visible on the upper side of the dielectric as it extends between the two electrodes as shown in Fig. 3-31. It looks like a quasi-uniform glow, but in fact it is constituted of micro discharges distributed uniformly in time and space along the electrode length. The electrical power consumption is slightly more than the DC surface coronas, but a higher electric wind velocity is generated and this can exert stronger effects on the local flow conditions.

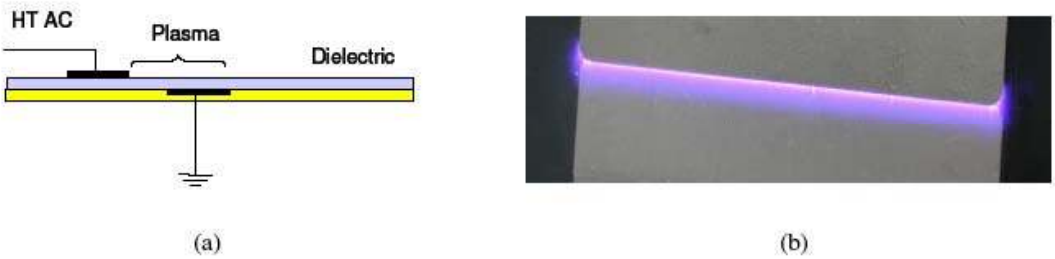

Fig. 3-31 a) Schematic side view of the AC Barrier discharge actuator, b) top view of produced discharge. (Source: Moreau et al.[93])

The sliding discharge actuator is capable of generating a stable plasma sheet. It was first used for airflow applications by Roth and Sherman[96]. As shown in Fig. 3-32a, it uses three plane electrodes; two are flush mounted on the wall surface of a dielectric and exposed to the air (#1 and #3) and the other (#2) is on the opposite side of the dielectric. Electrodes #2 and #3 are connected together and usually grounded while electrode #1 is excited. If a voltage with appropriate AC and DC components is applied to electrode #1, a plasma sheet is formed as shown in Fig. 3-32.

Fig. 3-32 a) Schematic side view of three-electrode discharge actuator, b) top view of produced discharge. (Source: Moreau et al. [93])

The plasma wall jet or plasma synthetic jet was introduced by Jukes, Choi, Johnson, and Scott[97] in 2004 and is illustrated in Fig. 3-33a. This device uses two air exposed surface electrodes and one covered electrode to create two separate surface dielectric barrier discharges. If electrodes #1 and #3 are excited by the same high voltage, a plasma jet perpendicular to the surface is created. If the electrodes are excited by two different voltages, the angle of the jet is modified. For example, if $V_{AC1} > V_{AC2}$, the jet is deflected to the right (Fig. 3-33). This configuration is different from to the other plasma

actuation devices; instead of generating a plasma region parallel to the wall it creates a vertical wall jet that penetrates into the boundary layer. The wall jet is able to generate vortices in the boundary layer, which improves the effectiveness of the device by increasing the mixing between the free-stream flow and boundary layer flow. Another important feature of the plasma synthetic jet actuator is that it can easily be reversed to act as a suction or blowing device. Recent studies have analyzed the performance of different electrode configurations, including pulsed operation.[98,99]

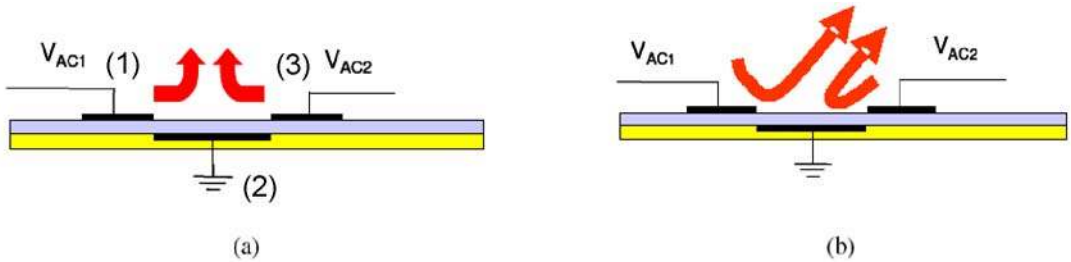

Fig. 3-33 Schematic side view of the wall jet device, a) $V_{AC1} = V_{AC2}$, b) $V_{AC1} > V_{AC2}$. (Source: Moreau et al.[93])

3.10.2 Classification

P	-	plasma device applies a body force to surrounding flow
LE	-	located near the leading edge of the blade
DS	-	used to delay stall
S / U	-	can be configured to operate in both modes

3.10.3 Background

The use of plasma actuators as a means of aerodynamic flow control is a relatively new concept. Before 2000, there were few published works on the topic. The first significant scientific papers were published in 1968 by Velkoff and Ketchman[100] and in 1978 by Yabe, Mori, and Hijikata[101]. It was not until the mid 1990's that research began to take off and a few research groups analyzed airflow control using the most basic plasma actuator device, DC surface corona discharge.[102,103] In 1998, Roth, Sherman, and Wilkinson[96] published their first results pertaining to a surface dielectric barrier discharge

(DBD). The initial research on surface plasma and the development of these simple devices allowed many researchers in aerodynamics to study the effects of plasma actuators without being a specialist in plasma generation. This has led to considerable growth in the field since 2000. Now more than 30 groups are working in the field and over 150 papers have been published to date. A more detailed background on the development of plasma actuators can be found in Moreau[91].

Corke and his fellow researchers have been researching separation control over airfoils with plasma actuators for the past 5 years[104-110]. Their first publication[104] looked at using a single DBD actuator for flow control; results showed that a measurable lift increase occurred over a range of angles of attack accompanied by an increase in drag. The plasma effect was compared to a slight increase in camber. Another study[105] compared the use of passive mechanical vortex generators with a plasma-based active method. The airfoil used was a NACA 66_3-018 with a chord of c = 12.7 cm. Different actuator locations were tested, one at the leading edge (x/c = 0) and the second at x/c = 0.5. Reynolds numbers ranged from 79,000 < Re < 158,000. The primary result was that the actuators delayed stall by 8° with up to a 400% improvement in lift-to-drag ratio. Results indicate that the optimum location for plasma actuators is close to the leading edge.

Since 2003, Corke et al. [105-107] have conducted numerous experiments on flow control on the NACA 0015 airfoil and have shown that stall can be successfully delayed. One study obtained the lift curve of an airfoil with a DBD actuator powered on and off (Fig. 3-34). The results showed that the plasma actuator successfully delayed stall and increased C_L for > 15°. Moreau et al.[91] brought up the concern that past experiments could not explain if the delayed stall was due to the plasma actuators adding momentum into the boundary layer or was due to the laminar to turbulent transition induced by the presence of the actuators causing the boundary layer to trip. They showed that the plasma actuators were, in fact, capable of preventing flow separation and promoting flow reattachment. This work also showed that actuators were most effective when placed near the separation point, similar to vortex generators and other flow separation mitigation devices.

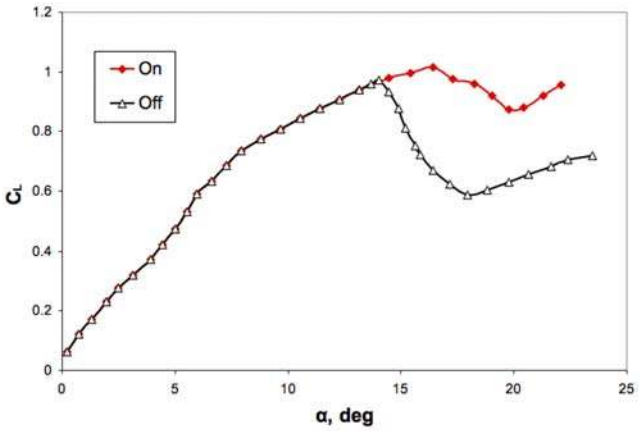

Fig. 3-34 Comparison of computed lift coefficient with plasma on and off, Re = 158,000. (Source: Post and Corke[106])

Jolibois, Forte, and Moreau[111] also investigated the optimal location for plasma actuators. The study involved seven independent DBD plasma actuators mounted on the suction side of a 1 m chord NACA 0015 airfoil. To prevent uncertainty about the flow transitioning due to the physical presence of the actuator, the researchers tripped the flow at the leading edge with a turbulator. Flow visualizations and PIV measurements were recorded to further understand the physical effect of each actuator. This study concluded

that the optimum location for effectiveness and efficiency was at the separation point. However, this is difficult to achieve, as the natural separation point of an airfoil will change as a function of the angle of attack and Reynolds number.

Fig. 3-35 illustrates the streamlines of the time-averaged airflow over an airfoil at $\alpha = 15°$. In the absence of plasma acutation, the airflow naturally separates at $x/c = 0.45$. When a downstream actuator ($x/c = 0.70$) is activated, the airflow partially reattaches and the separation point is shifted to $x/c = 0.55$, demonstrating that these actuators retain their effectiveness even when not optimally placed.

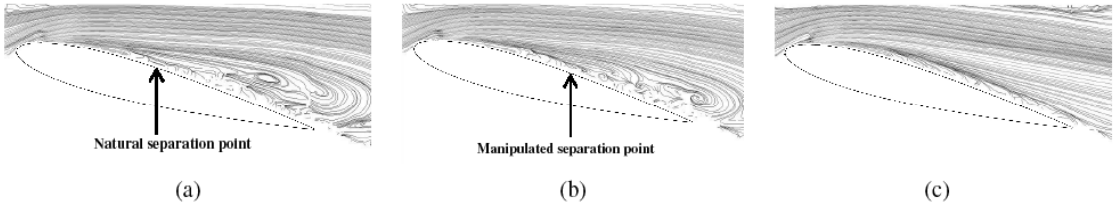

Fig. 3-35 Streamlines of the time-average airflow above the suction side of a NACA 0015 airfoil at $\alpha = 15°$, a) no actuation, b) actuation at $x/c = 0.70$, c) actuation at the natural separation point at $x/c = 0.45$. (Source: Moreau et al.[93])

Fig. 3-36 presents the velocity profiles on a flat plate at a free-stream velocity of 5 m/s for both numerical and experimental studies. The experimental study compared the velocity profiles of different plasma electric current values. Increasing the current generates a more powerful electric wind and has a greater effect on local velocity. The numerical study illustrated the change in the velocity profile due to a DC actuator that acted in both co-flow and counter-flow directions. The results showed that the plasma actuators are capable of increasing or decreasing the localized velocity near the flat plate. The free-stream velocity used in these studies was relatively low. Fig. 3-37 shows that plasma actuators do not have such an impact on the velocity profile when the free-stream velocity is increased.

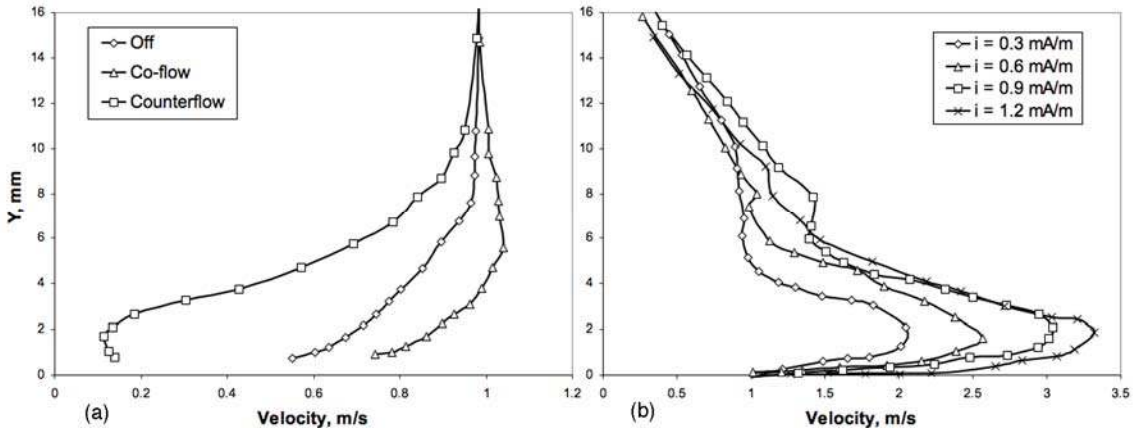

Fig. 3-36 a) Numerical velocity profiles in the boundary layer of a 5 m/s free airflow along a flat plate, with co- and counter-flows, b) Measured jet velocity profiles for time-averaged current values. (Source: Moreau[91])

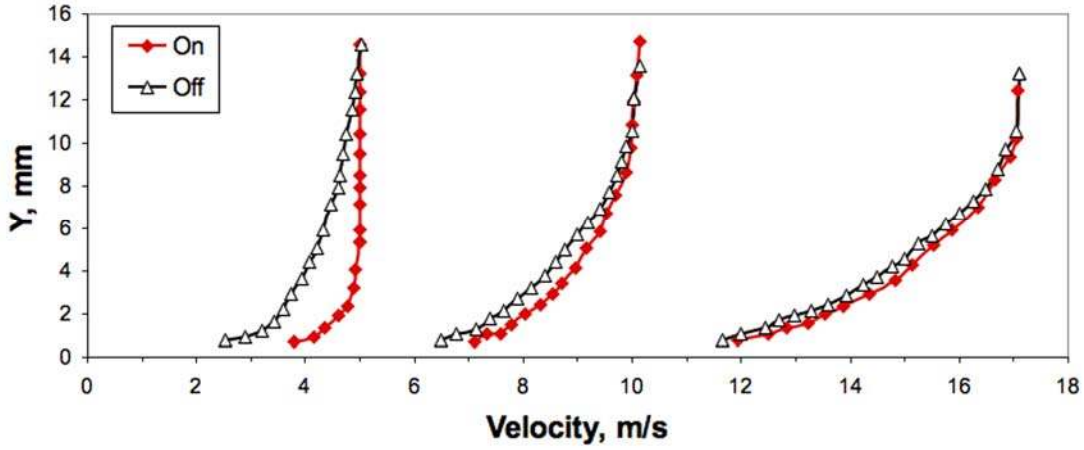

Fig. 3-37 Velocity profiles, with and without corona discharge, in the boundary layer at 5,10, and 17 m/s. (Source: Moreau[91])

3.10.4 Wind Turbine Control

Plasma actuators have received considerable attention over the recent years as a practical flow control device due to their advantages over fluidic and mechanical devices. They are able to directly convert electrical energy into kinetic energy, which is used to modify the airflow. They have advantages over mechanical devices; the device is simple, lightweight and uses no moving parts; therefore, it is likely not be a source of vibration or noise. Unlike fluidic devices, plasma actuators do not require a source of high-

momentum air. Therefore, compressed air storage and plumbing running the length of a turbine blade is not needed. Research has also shown that the presence of the electrodes does not interfere with the surrounding airflow when inactive and major modifications to the turbine blade are not required for installation. Another feature is that plasma actuators can be designed to operate in co-flow and counter-flow conditions, which allows for more options when controlling localized flow.

The primary disadvantages are maintaining a stable plasma region, low efficiency and the requirement of high voltage lines running inside the turbine blades. Under certain conditions and configurations, maintaining a stable electric wind can be difficult. Plasma devices have reduced performance in higher wind speeds. In fact, studies[91] indicate that the performance is quite low at a wind speed of 17 m/s, whereas other AFC devices have proved effective at wind speeds above 30 m/s. This is one area that advancements in plasma actuators need to be made. Another area for improvement is the energy conversion efficiency. The energy conversion from electrical to kinetic energy has a low efficiency (a few percent[91]); a large part of the electrical power goes into gas heating rather than direct gas motion.

3.11 Vortex Generator Jets

3.11.1 Description

Vortex generator jets (VGJs) are jets of air that pass through a wall (the skin of an airfoil) and into a crossflow to create a dominant streamwise vortex.[112-115] The vortex remains embedded in the boundary layer over the airfoil and entrains high-momentum air from the undisturbed flow into the boundary layer. This process helps mitigate boundary-layer separation and leads to an increase in C_{Lmax} and $_{stall}$. The vortex created by the VGJ and the traditional VG is very similar; however, the VGJ is more controllable and less intrusive. A schematic of a simple VGJ is shown in Fig. 3-38.

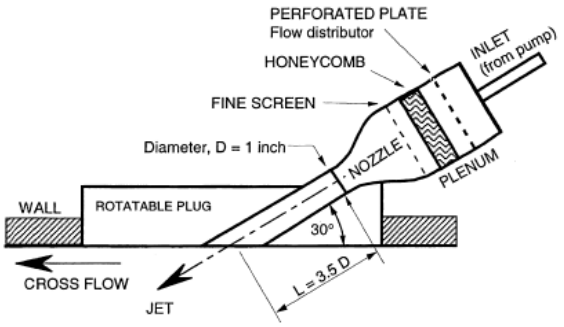

Fig. 3-38 Schematic of a VGJ actuator shown with a pitch angle of 30° and a rotatable plug to vary the skew angle. (Source: Khan and Johnston[116])

3.11.2 Classification

F - fluidic device

LE - located near the leading edge of the blade

DS - used to delay stall

S / U - both steady (conventional) and unsteady (pulsed) operation have been researched

3.11.3 Background

In 1990, Lin, Howard, and Bushnell[117] studied various passive and active methods for controlling two-dimensional turbulent separated flows. The VGJs were found to be the most effective method investigated at that time. The VGJ was compared to the traditional solid vortex generator and found to produce similar benefits but without any additional

drag penalty. Johnston and Nishi[113] researched spanwise arrays of VGJs and showed that arrays were effective in reducing the size of the separated regions of the flow. In 1992, Compton and Johnston[115] determined that a vortex produced from a single VGJ resembled the vortex produced by a traditional solid vortex generator, but the VGJ vortex tended to decay at a slightly faster rate downstream.

Additional research focused on the development of a pulsed vortex generator jet (PVGJ), which has been found to be more effective and efficient in delaying stall.[118-122] This is due to both the enhanced vorticity production associated with the impulsively started jet flow and to the reduction in mass flow due to a reduced duty cycle, or pulse cycle (typically 10% to 50%). The pulsing system can be designed to readily adjust three parameters; the pulsing frequency, the jet velocity ratio, and the duty cycle. These parameters can be optimized to produce coherent structures that maximize energy addition into the boundary layer to prevent separation.

The advantages of PVGJs are actively being investigated for application in several fields, including aircraft, low-pressure gas turbines (LPT) and unmanned aerial vehicles (UAVs). Magill and McManus[123] showed that this flow control method can enhance the lift, and hence the maneuverability, of advanced military fighters in post-stall flight. The PVGJs increased lift (C_{Lmax} increased by 7%) and L/D ratio, while minimizing additional drag. Other research conducted by Magill and McManus[124] demonstrated separation control in a subsonic flow over a NACA 4412 airfoil equipped with a simple leading-edge flap. The maximum lift coefficient was increased by more than 20% under optimum conditions. However, this increase was severely degraded if the pulsing frequency and amplitude were not properly tuned.

Bons, Sondergaard, and Rivir[74,125,126] performed studies with both steady and pulsed jets on a LPT model. These studies showed that VGJs could reduce wake losses up to 50-65%. Other learned items were that the key mechanism to properly control PVGJs is the starting and stopping of the pulses rather than the injection itself and that pulsing may play a reduced role at higher Reynolds number.

Heinzen, Hall, and Chokani[127] investigated the effectiveness of both VGJ and PVGJ systems on an Unmanned Air Vehicle (UAV) wing. The effectiveness of delaying stall was measured by pressure distribution changes on the top surface of the wing. Experiments in both the wind tunnel and in flight were carried out. The PVGJs were placed on the leading edge of the flap and were activated to test their ability to delay the onset of stall. The results showed that PVGJs were effective at delaying stall and the best results occurred when the reduced frequencies (Eqn. 9), F^+, were near unity. When implemented in a test flight, the PVGJs increased lift and enhanced control at high angles of attack.

Tensi, Bourgois, Bonnet, Breux, and Siauw[128] recently investigated stall delay on a NACA 0015 airfoil equipped with VGJs jets mounted on the upper side of the model at a chord location, x/*c*, of 30%. The jets were found to introduce strong streamwise vortices into the flow. The test setup had VGJ pitch and skew angles of 30° and 60°, respectively, and flow conditions of V = 40 m/s and Re = 0.93 × 10^6. The angle of attack, , ranged from 9° to 16° and jet momentum coefficient, C_μ, (Eqn. 8) from 0 to 0.9%. Several tests were carried out analyzing the change in C_L and C_D and the amount of separation delay. Results (Fig. 3-39) indicated that the VGJs were effective in increasing C_{Lmax} (5-10%) and decreasing C_D (up to 50%). A greater effectiveness was seen as C_μ was increased. Laser tomoscopy observations were conducted at higher incidences (= 16° and 17°) to visually show the effect of vortex generating jets (Fig. 3-40). Laser tomoscopy utilizes special equipment to display and characterize aerodynamic speed fields and it can provide airflow images and identify the time-accurate size and position of the vorticity structure.

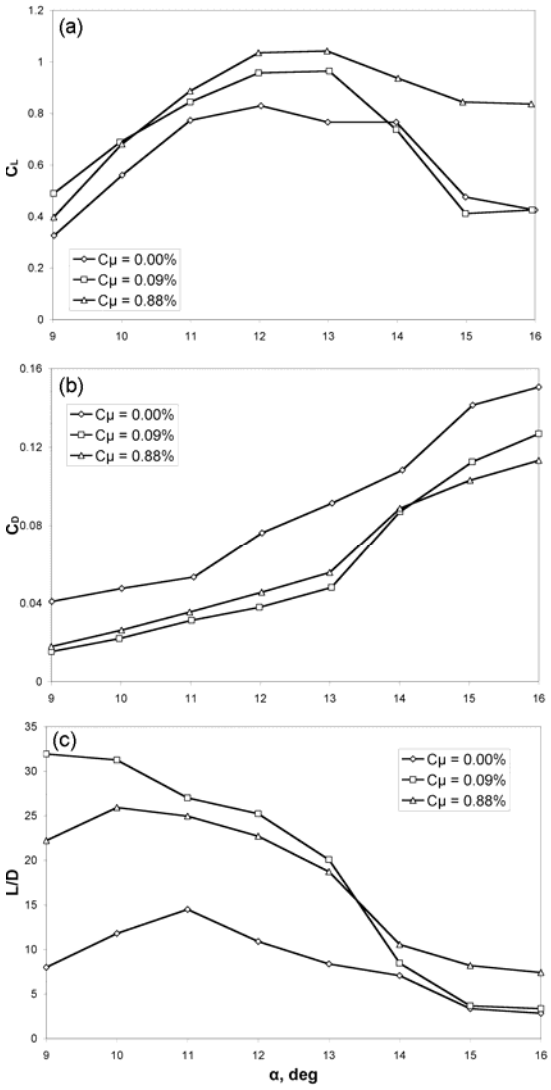

Fig. 3-39 Effect of VGJ jet momentum coefficient, C_μ, on C_L, C_D, and L/D. (Source: Tensi et al.[128])

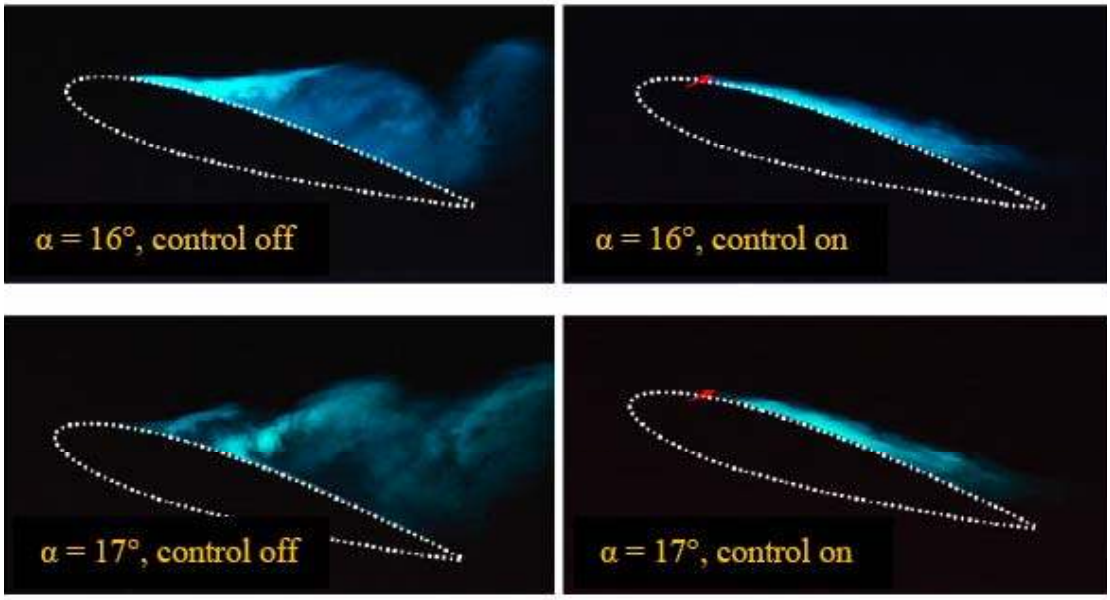

Fig. 3-40 Laser sheet visualization of VGJ effects. (Source: Tensi et al.[128])

3.11.4 Wind Turbine Control

Steady and pulsed vortex generator jets have shown promise in both numerical and experimental studies. Additional studies should be conducted using wind turbine airfoils and flow conditions.

Overall, this device has many appealing features for turbine implementation. The forward location of the jets is beneficial for installation purposes. Another advantageous feature is the wide controllability of the device. The strength, penetration distance, and angle of the vortex can be adjusted allowing for many options of flow modification. The device has no complicated mechanical system and does not interfere with the flow when inactive. The system does, however, require compressed air lines. Further research is needed to determine the air requirement and power consumption. Measures may also need to be taken to ensure the exit ports remain free of dirt, insects, or ice.

3.12 High-Frequency Micro Vortex Generators

3.12.1 Description

Another design concept that has been derived from the traditional vortex generator is the High-Frequency Micro Vortex Generator (HiMVG). Similar in operation to the PVGJs, the HiMVG uses mechanical motion to generate periodic vortices. These vortices cause high-momentum streamwise air to be driven towards the surface, thus energizing the boundary layer and mitigating separation. The vortices are created by a mechanical element (or micro vortex generator) that oscillates rapidly within the boundary layer at a certain frequency. Fig. 3-41 displays one design of a HiMVG system that uses a piezoelectric actuator and a compliant structure to rapidly oscillate the vortex generator blade.

3.12.2 Classification

G - uses an oscillating geometric device to produce vortices in the fluid that affect the aerodynamics

LE - located near the leading-edge of the blade

DS - used to delay stall

U - only used in the unsteady configuration

3.12.3 Background

As mentioned earlier, the development of the HiMGV can be traced back to the traditional VG, but more specifically to the micro vortex generator (MVG), a compact version of the traditional VG. Lin[69,71] conducted research on reducing the size of vortex generators to sub-boundary layer heights (0.2 to 0.4 times the boundary-layer height), while still maintaining their effectiveness. Lin's optimized MVG shapes were used for the HiMGV design because of their small size and light weight, which allowed the

HiMVG to rapidly oscillate at high frequencies. Other studies that were critical in the development of the HiMVG include the research conducted on PVGJs and the periodic excitation control studies by Seifert, Darabi, and Wygnanski[129]. The fundamental difference between the HiMVGs and the PVGJs is that the latter uses high-momentum air as the working medium to produce the unsteady excitation, whereas the physical presence and mechanical motion of the HiMVGs creates the unsteady excitation.

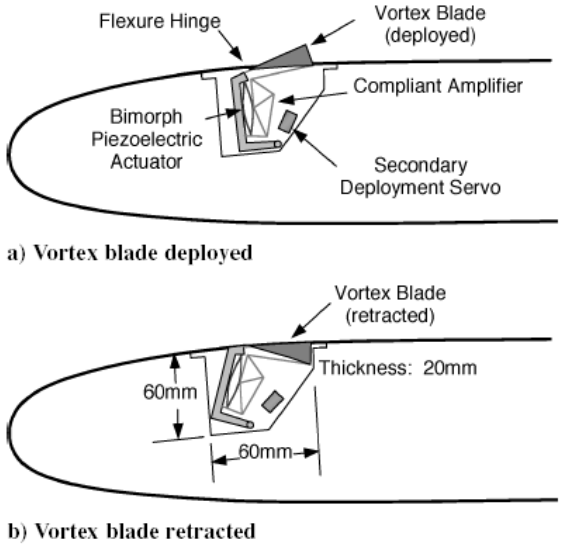

Fig. 3-41 Schematic of a HiMVG system. (Source: Osborn et al.[131])

In 1995, the Air Force Research Laboratory developed a first generation HiMVG[130] with limited oscillation frequency of 10-20 Hz. This frequency range was found to lie well below the requirement for optimum separation control; however it was adequate to confirm that separation control was feasible and was used for static testing of the vortex generator array.

In 2004, a second generation HiMVG was built and tested by a collaboration of FlexSys, Inc.[31], the University of Michigan, and the U.S. Air Force Research Laboratory.[131] The system design used displacement amplification compliant structures, coupled with an appropriate actuator, to increase the deployment frequency. The design was capable of oscillating MVGs at the optimum frequencies and amplitudes needed for separation control for different flow fields. The compliant structure had a displacement

amplification of 20:1, which enabled a deployment height of 5 mm (0.4 times the boundary layer height) to be reached. The system, consisting of two voice-coil actuators and seven blades, was capable of operating between 0 and 90 Hz. The model consisted of a flat plate with a rounded leading edge and a variable angle trailing-edge flap at 65%*c*. The flap was used to separate the flow while the HiMVG system, mounted on the flat plate portion of the model, attempted to keep the flow attached even when it passed the deployed flap. A surface-mounted static pressure array measured pressures during the experiments. A higher pressure measurement indicated a strongly attached flow and a lower pressure measurement indicated flow detachment. The system was tested in the wind tunnel at wind speeds of 55 ft/s and 70 ft/s in the University of Michigan subsonic wind tunnel.

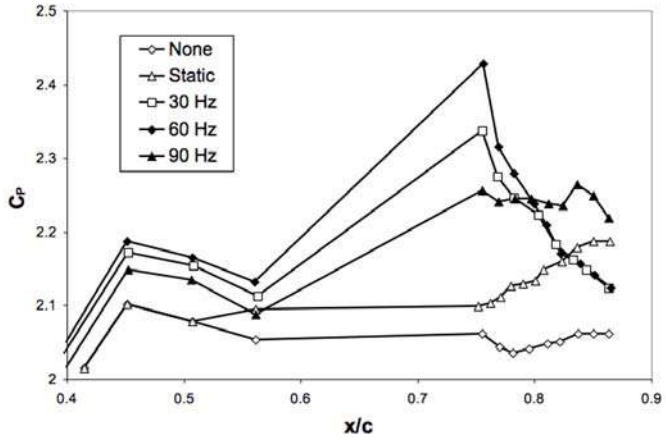

Fig. 3-42 HiMVG dynamic test results for U_∞ = 70 ft/s. (Source: Osborn et al.[131])

Results of the 70 ft/s test case can be seen in Fig. 3-42. The figure shows that maximum C_P (indicating a strongly attached flow) was achieved at a deployment frequency of 60 Hz. Similar to the results from the PVGJ study[127], the HiMVG system performed optimally (large improvement in pressure recovery) when the reduced forcing frequency (Eqn. 9), F^+, was near unity. The dynamic operation of the system was more effective at avoiding boundary layer separation than was conventional static deployment, reinforcing the concept that the addition of periodic excitation into a separating turbulent-

boundary layer increases the momentum transfer across the shear layer, enhancing its resistance to separation under adverse pressure gradients.[131] Periodic excitation improved the lift, even when it did not fully eliminate separated flow.[132] Future work identified by the researchers[131] includes replacing the voice-coil actuators with suitable piezoelectric actuators to allow for a maximum frequency of 240 Hz.

3.12.4 Wind Turbine Control

The results show promise for HiMVGs as a means of active flow control. As a first step towards turbine control applications, computational and experimental studies should be conducted on wind turbine airfoils and flow conditions to ensure the technology will be effective.

The advantage of using these devices rather than fluidic devices is that there is no need for a compressed air system. This simplifies the overall design, eases implementation, and reduces system weight. The location of the device is advantageous because there is plenty of space inside the blade to house the actuation system. The total system would require minimal power since the compliant structure allows for a small force and a short actuation distance.

Concerns with this design are similar to those for the microtab, in that tight tolerances are required. When the device is inactive, gaps between the blade and the HiMVG could create noise and reduced performance, especially since the device is located nearer to the leading edge. Degradation of the compliant structure over time may also be of concern.

3.13 Synthetic Jets

3.13.1 Description

Synthetic jets create streamwise vortices that are similar to those generated by pulsed vortex generator jets. The primary difference is that synthetic jets are zero net-mass flux (ZNMF) devices, i.e. they do not require a high-momentum air source. The jets are commonly generated by using an oscillating diaphragm that is located in a cavity embedded flush with the aerodynamic surface. They are formed from the working fluid flowing over the airfoil. Fig. 3-43 shows an illustration of a typical device used to create a synthetic jet. The diaphragm is operated so that fluid is alternatively sucked into the cavity and then ejected in a periodic manner, creating discrete vortical structures that flow from the surface. The jet is created by the advection and interaction of these vortices. The jets interact with the flow over the surface by displacing the local steamlines and inducing an apparent or virtual change in the shape of the surface. Jets are typically located at 10-20%*c* and can be installed at any angle to the aerodynamic surface.

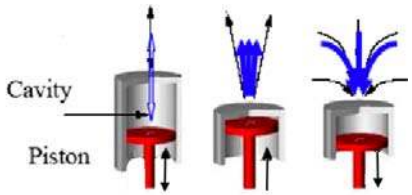

Fig. 3-43 Synthetic jet production principle. (Source: Tensi et al.[128])

3.13.2 Classification

G / F - geometric device generates fluidic motion
LE - located near the leading edge of the blade
DS - used to delay stall
U - unsteady device

3.13.3 Background

The first synthetic jet that was integrated into an aerodynamic surface was developed by James, Jacobs, and Glezer[133] in 1996. The researchers investigated the formation of synthetic jets using an oscillating diaphragm mounted flush on a flat plate submerged in water. These experiments showed that the jets are produced entirely from radially entrained fluid. The jets were observed as small clusters of cavitation bubbles appearing and subsequently collapsing near the center of the diaphragm during each oscillation cycle. Numerous researchers have since investigated the aerodynamic qualities of synthetic jets and integration of synthetic jets into flow control systems. A number of publications have been written on synthetic jets in both experimental[134-137] and numerical studies[138-140].

Experiments by Seifert, Bachar, Koss, Shepshelovich, and Wygnanski[141] investigated a NACA 0015 airfoil equipped with unsteady suction and blowing near the leading edge tangential to the surface. The study consisted of wind-tunnel tests at high angles of attack, where the airfoil would reach maximum lift and eventually stall, creating a wake region above the aft region of the airfoil. The test showed a significant increase in maximum lift when using a relatively low momentum input. Observations also showed synthetic jets caused reattachment of the flow in the trailing-edge region.

Numerical simulations have supported some of the experimental findings. Donovan, Kral, and Cary[142] simulated the experiments of Seifert et al[141]. Using an unsteady Reynolds Averaged Navier-Stokes (RANS) incompressible flow solver with a turbulence model, they found that a significant lift increase, about 29%, in the post-stall regime could be obtained using synthetic jets. Performance was improved when the actuator was placed close to the airfoil leading edge. Further studies by Ravindran[143] confirmed that

unsteady tangential suction and blowing could be used for separation control and that the lift increased as the blowing coefficient, C_μ, increased.

Recent experiments by Tensi et al.[128] showed the positive effect of synthetic jets on the reattachment of a separated boundary layer. The low-speed wind tunnel tests were conducted on a NACA 0015 airfoil equipped with synthetic jets located at x/*c* = 20%. In total, 61 injectors with a pitch of 30° relative to the wall and diameters of d = 3 mm were installed into the model. Three non-dimensional frequencies, F^+ = 3.2, 4.5, and 6.7, were tested over a range of angles of attack with an air velocity of U = 6 m/s (Re = 0.4×10^6). Qualitative observations were made using tomoscopy observations and PIV (Particle Imaging Velocimetry) measurements; some results can be seen in Fig. 3-44 and Fig. 3-45. PIV technology is an optical method used to take accurate, quantitative measurements of the speed fields of the seeded airflow from the data on vortex trajectories. The efficiency of the jet system was also quantified by comparing the extent of separation shown in PIV measurements.

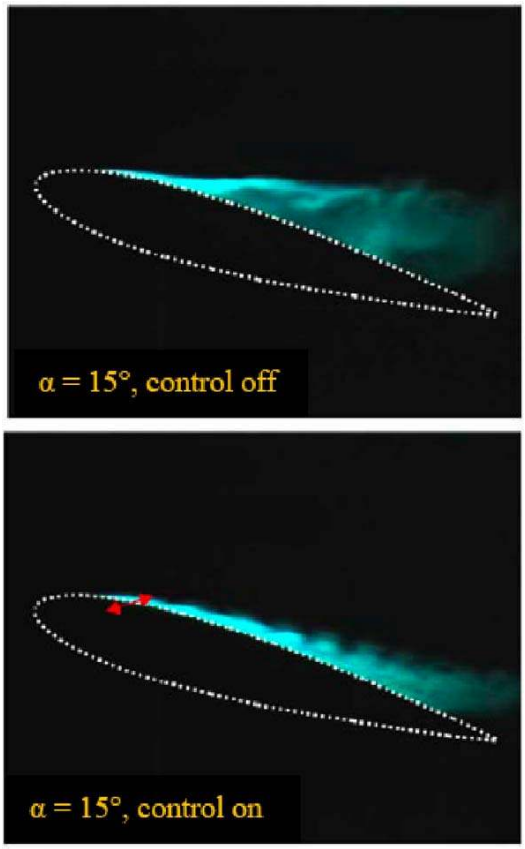

Fig. 3-44 Tomoscopy flow visualization of synthetic jet operation (C_u = 1.94%, F^+ = 6.7). (Source: Tensi et al.[128])

3.13.4 Wind Turbine Control

The unique attributes of synthetic jets, coupled with the development of actuators that are easily integrated into the aerodynamic surface, make synthetic jets attractive for active flow control. The system consists of small actuators that require minimal power. No compressed air lines are needed; this simplifies the system and reduces the weight. The location (~20%*c*) of the actuators is advantageous for installation and actuator housing and is not too close to the leading edge where problems may arise from slight airfoil modifications.

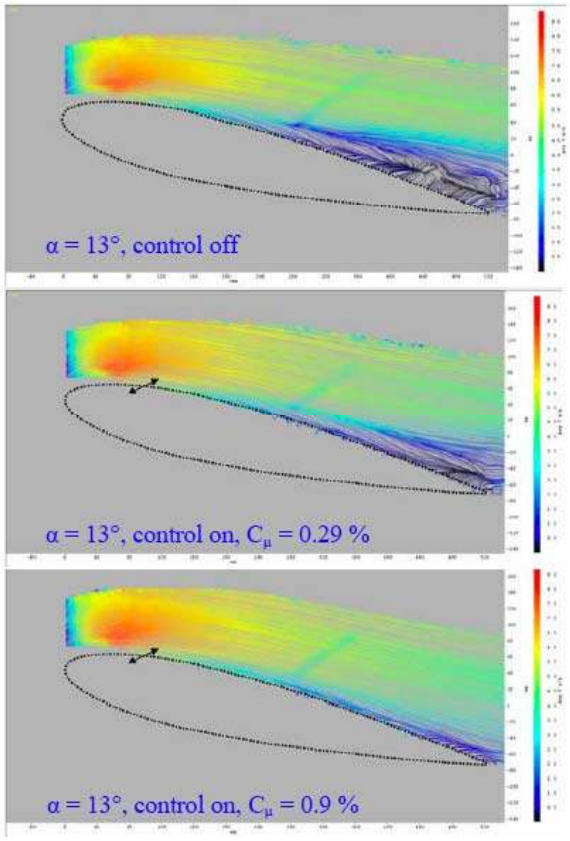

Fig. 3-45 PIV measurements of synthetic jet operation. (Source: Tensi et al .[128])

Investigations on wind turbine airfoils and flow conditions should be conducted to study the effectiveness of synthetic jets for load control. The presence of the cavities may interfere with the flow patterns while the device is inactive, thereby generating noise and decreasing performance. Tight tolerances would be necessary to limit the interference. Other concerns are decreased performance due to soiling and icing of the blades.

3.14 Active Flexible Wall

3.14.1 Description

The micro-flexural active flexible wall (AFW)[144] is a device that detects the onset of boundary layer separation and introduces small disturbances into the boundary layer near the leading edge of the airfoil to counteract the growth of flow separation. The device consists of an array of transducers that are mounted inside a flexible housing, made of an inner wall and an outer wall. The entire system is thin (50-100 microns) and the flexible housing is affixed to the leading edge of an aerodynamic surface in such a way that it is virtually non-intrusive to the flow when not actuated.

The device provides an active flow separation control system that locally interacts with the boundary-layer flow and is capable of operating in two modes: a sensor mode and an actuator mode.[144] In sensor mode, the system is able to detect small disturbances in the flow that occur when the flow begins to separate from the trailing edge. In actuator mode, the transducers are activated and begin to vibrate the outer surface of the housing, causing small perturbations in the flow. The controller is capable of using spatial location and frequency content of the input signals to determine which transducers to excite and at what frequency in order to prevent or delay flow separation. The transducers selected for activation are typically immediately upstream of the separation point.

3.14.2 Classification

G - small mechanical vibrations create perturbations on the airfoil surface, generating vortices
LE - located near the leading edge of the blade
DS - used to delay stall
U - unsteady operation

3.14.3 Background

The physical model (Fig. 3-46) consisted of a flexible housing with an outer layer made of 6 m thick Mylar sheet with an aluminum coating and an inner layer of 0.02 mm thick polyamide sheet. The transducers were made of copper strips of two different sizes (high and low) to provide upper and lower limits for the vibrating Mylar sheet. The high and low strips were alternatively spaced about 1 mm apart. The AFW was attached to the leading edge of a NACA 0012 airfoil. The system was capable of operating in both sensor mode and actuator mode. In the sensing mode, a DC bias (90V) is applied between the Mylar and high copper strips; flow induced vibrations of the membrane can be detected as an induced AC signal picked up from the Mylar and the copper strip of interest. In the actuation mode, an AC signal (8-48 kHz, ~150 V_{rms}) is applied to copper strips located near the separation point; this induces micro-flexural vibrations of the flexible Mylar membrane at the two points of actuation. The displacement amplitudes of the membrane were typically on the order of 0.1 μms, about three orders of magnitude smaller than the boundary layer thickness. The power consumption for this setup was about 30 W for a 30 cm span.

Investigations looked at using the AFW device to delay stall during static[145] and dynamic situations[146]. Wind tunnel experiments were conducted using a NACA 0012 airfoil equipped with distributed pressure tabs. The model had a chord of 291 mm and a span of 450 mm. Static stall experiments found that the optimum excitation location was just forward of the separation location. This location corresponded to $x/c = 0.03$ for test conditions of Re = 57,800 and = 15.5°. The optimum excitation frequency was found to be 3.4 kHz, twice the frequency of the AC actuation signal. At optimum conditions,

the separation was delayed, causing a 4% increase in the section lift coefficient, C_L. The dynamic stall experiments used the same airfoil with flow conditions of Re = 6.13×10^5 and a reduced airfoil frequency, k, (Eqn. 4) of 0.105. Two strips were excited at frequencies of 8, 20, 24, and 48 kHz. Results showed the AFW system could delay airfoil stall by 9% (from = 19.6° to 21.4°).

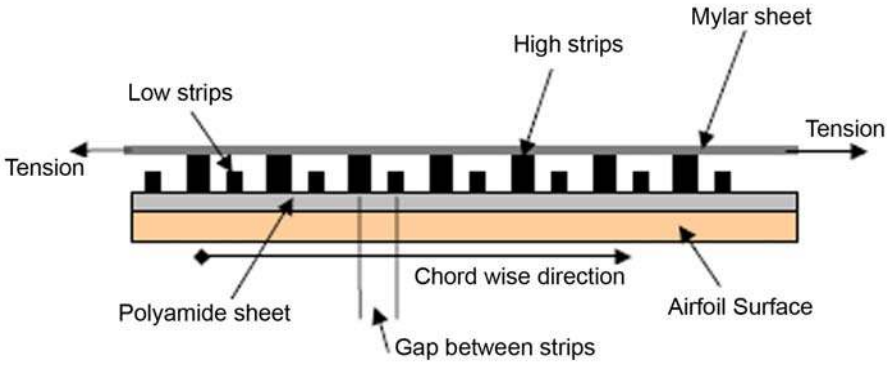

Fig. 3-46 Schematic of the AFW. (Source: Sinha[146])

3.14.4 Wind Turbine Control

The main advantages of this device are that it can be applied to a turbine blade without major modifications, has low power requirements, does not affect the flow when inactive and can operate in both sensor and actuation mode. Further investigations on the ability to control wind turbine loads using both the sensor and actuation mode of this device should be conducted. The AFW is located very near the leading edge and at that location potential problems may arise if the device becomes soiled or damaged.

3.15 Shape Change Airfoil

3.15.1 Description

The shape change airfoil, or adaptive airfoil, operates by physically changing the shape of an airfoil. Piezoelectric material is used to form part of the upper surface of the airfoil and, as it deforms, the camber changes. The design by Munday and Jacob[147-149] is shown in Fig. 3-47. This particular design has the actuators mounted within the airfoil such that the free end of the piezoelectric material lines up with the main part of the airfoil when the actuator is at its smallest effective radius (most curved). A thin plastic sheet is placed over the actuator to smooth the profile and the entire assembly is wrapped in a latex membrane to hold it together and eliminate seams. When the actuators are deployed to the greatest effective radius (close to being flat), they push against the upper cross-section and physically change the camber.

The system is designed to operate by rapidly deploying and retracting the piezoelectric actuators; this motion not only modifies the camber of the airfoil but also generates vortices in the flow about the airfoil (Fig. 3-48). The vortices convect downstream while entraining high-momentum free-stream air into the boundary layer, thereby postponing separation.

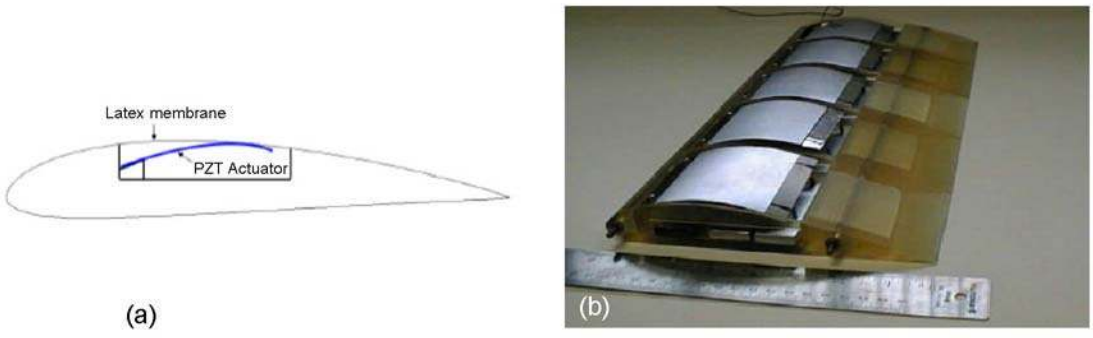

Fig. 3-47 a) Schematic (a) and model (b) of the adaptive wing. (Source: Pern et al.[152])

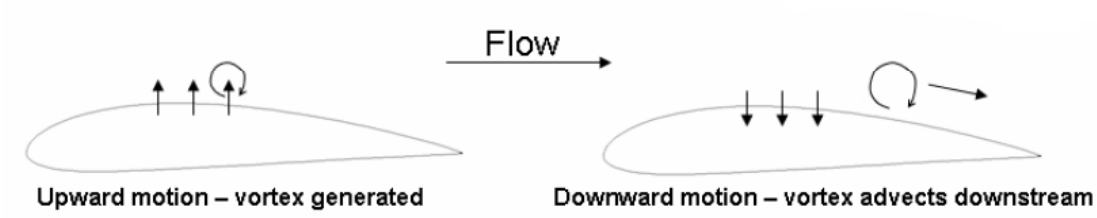

Fig. 3-48 Schematic of flow control mechanism. (Source: Pern et al.[152])

3.15.2 Classification

G - physical changes in the camber are used to generate vortices

MC - located near mid chord

I - increases lift

S / U - only modest improvements are seen in steady operation, unsteady operation is more effective

3.15.3 Background

The first experiments with the shape change airfoil were conducted by Pinkerton and Moses[150] in 1997. Their objective was to assess the ability of a new piezoelectric actuator to alter the upper surface geometry of a subscale airfoil. The piezoelectric actuator, called Thunder[43], was developed by NASA and is capable of larger bending displacements (several mm) than previous piezoelectric actuators. The goal was to use Thunder to change the airfoil's camber, which, in turn, would adjust the local flow field around the airfoil to increase maximum lift and delay stall. The study focused on the feasibility of the actuator rather than aerodynamic performance.

Research in 2002 expanded upon the concept and looked into the aerodynamics and optimal control strategies. A modular test section was built using the base profile of a NACA 4415 and the actuation system as described previously in *Section 3.15.1*. Munday and Jacob[147] analyzed the effects of static shape changes (the actuator remained stationary at a number of pre-determined positions) by collecting force and PIV measurements. They concluded that only modest improvement in L/D can be achieved

with static actuator positions. Maximum actuator displacement slightly increased both lift and drag and increased L/D by 2%.

Pern[151] investigated a circular-arc airfoil and showed that an airfoil with an oscillating, rather than a fixed, camber setting would produce higher lift coefficients. This improved performance was due to vortex generation; the oscillating motion created a series of vortices that added momentum and entrained the flow above the boundary layer towards the surface. The boundary-layer thickness downstream of the vortex source was drastically reduced because the flow was energized and remained attached, despite the adverse pressure gradient. If only one vortex was created, the flow would lose quickly momentum and separate due to the adverse pressure gradient. By oscillating the upper surface, vortices were continually generated and traveled downstream, adding to the energy of the flow and overcoming the adverse pressure gradient.[152]

Additional experiments[149] evaluated the performance of a NACA 4415 airfoil equipped with the shape change system by measuring the separated flow thickness at 70%c using smoke-wire flow visualization. Researchers conducted a series of low-speed wind tunnel tests at Re = 2.5×10^4 and 5.0×10^4, angles of attack of 0°, 3°, 6° and 9°, and at reduced frequencies F^+ (Eqn. 9) ranging from 0 to 11. Flow visualization showed that the uncontrolled airfoil experienced large separation; however, oscillating the curvature of the upper surface reduced flow separation. Oscillating the surface with a small amplitude of 0.002c reduced the size of the separated flow region by 30-60% as compared to flow over a similarly shaped static wing.

Pern, Jacob, and LeBeau[152] expanded upon the previous tests by evaluating the performance under a wider range of flow conditions, actuation frequencies and amplitudes. The angle of attack was varied between 0° and 24° at Re = 2.5×10^4, 5.0×10^4, 7.5×10^4 and 1.0×10^5. In this experiment, there were four modules, each with a chord length of 0.203 m, connected together to form a span of 0.33 m. In this configuration, the actuator could change the profile of the suction surface by about 0.01c. The maximum deflection of 3 mm peak to peak occurred at x/c = 0.45. Increasing the camber when the angle of attack, , was between 4° and 20° resulted in an increase in L/D. The measured lift and drag characteristics for F^+ = 0, 0.1, and 0.2 at Re = 1.0×10^5 are shown in Fig. 3-49. Increases in C_L were much more prominent for the lower Reynolds number test cases. Observations from flow visualization and smoke-wire visualization (Fig. 3-50) showed that the oscillating frequency was the main factor for flow control. The researchers also

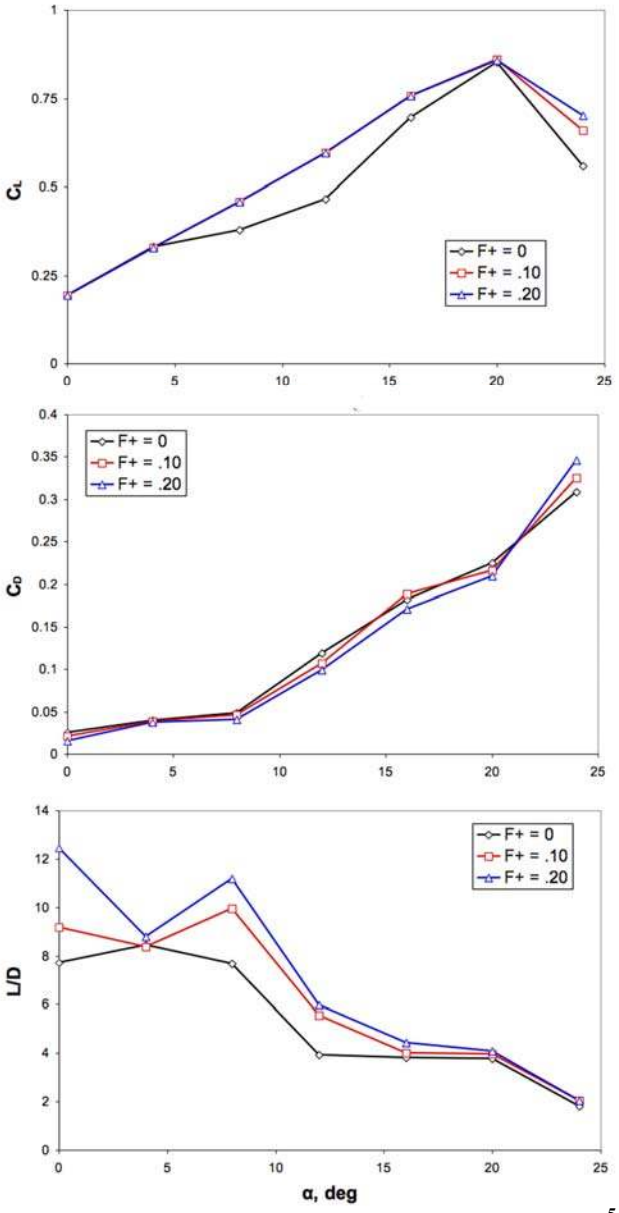

Fig. 3-49 Lift and drag characteristics at Re = 1.0 x 10^5. (Source: Pern et al.[152])

suggested that a significant reduction in separated flow occurred at frequencies $F^+ > 0.1$. CFD analysis showed good qualitative agreement in the development of the vortex with the wind-tunnel experiments. The location of vortex formations was at about $x/c = 0.5$ in both computational and experimental studies.

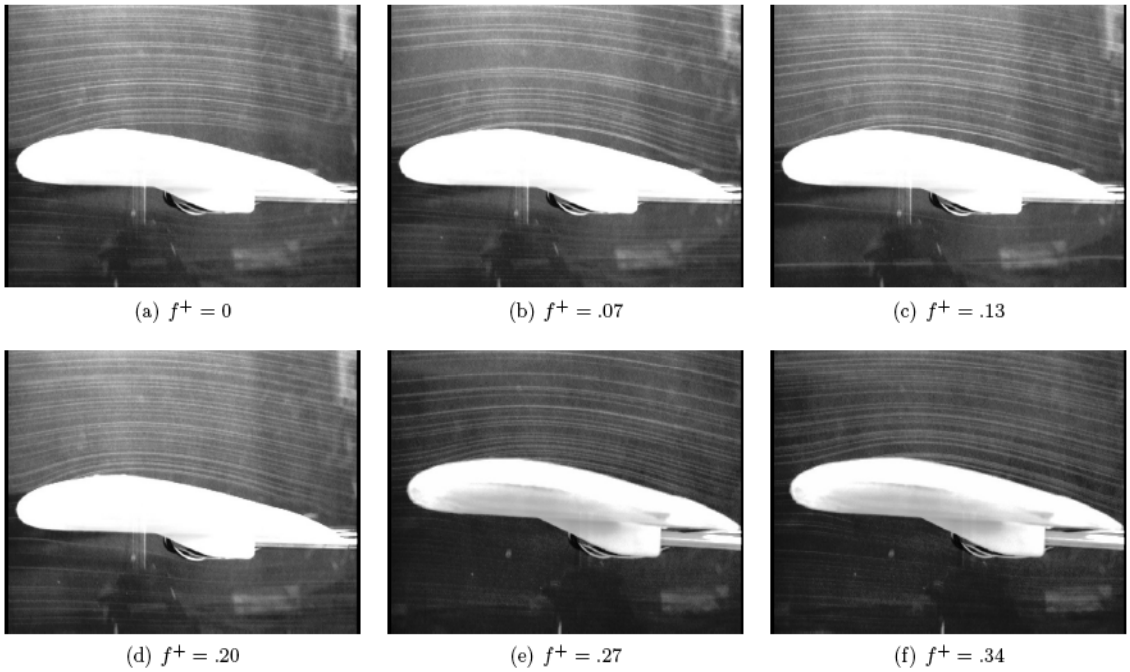

Fig. 3-50 Smoke-wire flow visualization at Re = 7.5 x 10^4, α=8°. (Source: Pern et al.[152])

3.15.4 Wind Turbine Control

This concept has shown promise in both computational and experimental studies. The shape change airfoil has a smooth deployment area, giving it an advantage over other methods which require holes or slots in the exterior skin of the airfoil. There would be minimal problems associated with noise generation and reductions in performance due to soiling. The greatest hurdle of this concept is that the piezoelectric material covers a large portion of the chord. This could be problematic with implementation on full-sized blades and could have detrimental effects on the overall structural integrity. Difficulties with

using deforming piezoelectric actuators can also arise from the requirement for a high-voltage source and reduced performance over time due to creep.

3.16 Device Summary

Active flow control is a rapidly growing field and with numerous devices being investigated. It is impossible to list all of the devices that could be used for future wind turbine control; however, this report attempted to introduce some of the most promising devices. Overall, fifteen (15) potentially useful devices were discussed. A description of how the device works, both aerodynamically and mechanically, was presented. A classification system was created to help separate the devices and a brief research background on each device was included. Comparisons between each device are difficult to make because they are all at varying stages of research and are applied to different fields. However, their advantages and disadvantages related to possible wind turbine control were discussed.

The main characteristic that separates the devices into two classes is how they adjust the lift curve; either by delaying stall (DS) or by shifting the curve up or down (I/D). Since wind turbines normally operate in the linear region of the lift curve, the devices that have the most promise for load alleviation are I/D devices. However it was shown that DS devices could still be used. Investigations into the AFC devices have shown that there is substantial potential for the improvement of wind turbine control.

The purpose of this report was not to directly compare devices or recommend the most viable device for turbine control; instead it was meant to provide the reader with a global view of today's research that could make significant contributions to wind turbine control in the future. As research progresses, specific flow control devices will begin to

stand out as viable options for load control. Of course, the true test of an AFC device will be a field demonstration on a large-scale wind turbine. At this time, field tests are many years away and more research is needed before this can be achieved.

4 CONCLUSION

The wind industry is rapidly growing and signs indicate that it will remain this way for years to come. As the industry has grown, so has the size of the turbines. Significant growth has made it impossible to control turbines passively as they were controlled in the past; therefore, modern turbines rely on sophisticated control systems to assure safe and optimal operation under a variety of atmospheric conditions. As the rotors continue to grow in size, the industry needs to make yet another shift in their approach to turbine control by considering localized flow control along the blades. Larger rotors experience more pronounced structural and fatigue loading, particularly in turbulent winds. This loading can have a detrimental effect on the rotor and surrounding components and can lead to an increase in O & M and a decrease in turbine life. Implementing new load control techniques could decrease excessive loads, which are key factors in turbine design.

The AFC devices introduced in this report are possible solutions to these issues. These devices are small, lightweight, and can actuate at speeds that can counter the loading from turbulent winds. Improved control could lead to increased turbine life, reduced required materials, improved energy capture, better overall performance, and reduced COE of wind energy. Lowering COE ensures competitive prices against traditional and other renewable energy sources and the continued maturation of the industry.

REFERENCES

[1] BTM Consult ApS, "Ten Year Review of the International Wind Power Industry 1995-2004," Sept. 2005.

[2] American Wind Energy Association, "AWEA 2007 Market Report," Jan. 2008.

[3] Committee on Assessment of Research Needs for Wind Turbine Rotor Materials Technology. *Assessment of Research Needs for Wind Turbine Rotor Materials Technology*. Washington, D.C.: National Academy of Press, 1991.

[4] Barlas, T.K., and van Kuik, G.A.M., "State of the Art and Prospectives of Smart Rotor Control for Wind Turbines," *J. of Physics: Conference Series 75 (2007) 012080, Proc. of The Science of Making Torque from Wind,* Copenhagen, Denmark, Aug. 2007.

[5] Geyler, M., "Advanced Pitch Control for Wind Turbines," Technical Report 2001.001, Delft University of Technology – DUWIND, Jan. 2001.

[6] Berg, D.E., Zayas, J.R., Lobitz, D.W., van Dam, C.P., Chow, R., and Baker, J.P., "Active Aerodynamic Load Control of Wind Turbine Blades," *Proc. of the 5th Joint ASME/JSME Fluids Engineering Conference*, San Diego, CA., 2007.

[7] Bossanyi, E.A., "The Design of Closed Loop Controllers for Wind Turbines," *Wind Energy*, Vol. 3, 2000, pp. 149-163.

[8] Larsen, T.J, Madsen, H.A., and Thomsen, K., "Active Load Reduction Using Individual Pitch, Based on Local Blade Flow Measurements," *Wind Energy*, Vol. 8, 2004, pp. 67-80.

[9] Bossanyi, E.A., "Developments in Individual Blade Pitch Control," *Proc. EWEA The Science of Making Torque From the Wind*, Delft, the Netherlands, 2004.

[10] van der Hoft, E.L., and van Engelen, T.G., "Feed Forward Control of Estimated Wind Speed," Technical Report ECN-C-03-137, Dec. 2003.

[11] Hand, N.M, Wright, A.D., Fingersh, L.J., and Harris, M., "Advanced Wind Turbine Controllers Attenuate Loads when Upwind Velocity Measurements Are Inputs," *44th AIAA/ASME*, 2007.

[12] IEC 61400-1 Ed. 3 "Wind Turbines – Part 1: Design Requirements"

[13] Lobitz, D.W., and Veers, P.S., "Aeroelastic Behavior of Twist-Coupled HAWT Blades," *Proc. of 1999 ASME Wind Energy Symposium*, Jan. 1999.

[14] Lobitz, D.W., Veers, P.S., Eisler, G.R., Laino, D.J., Migliore, P.G., and Bir, G., "The Use of Twisted-Coupled Blades to Enhance the Performance of Horizontal Axis Wind Turbines," SAND01-1303, Sandia National Laboratories, Albuquerque, NM, 2001.

[15] Veers, P., Bir, G., and Lobitz, D., "Aeroelastic Tailoring in Wind-Turbine Blade Applications," Presented at Windpower 1998, American Wind Energy Association Meeting and Exhibition, Bakersfield, CA, April 28 – May 1, 1998.

[16] Lobitz, D.W., and Laino, D.J., "Load Mitigation with Twist-Coupled HAWT Blades," *Proceeding of 1998 ASME Wind Energy Symposium*, Jan. 1998.

[17] Lobitz, D. W., Veers, P. S., and Migliore, P. G., "Enhanced Performance of HAWTs using Adaptive Blades," *Proceeding of 1996 ASME Wind Energy Symposium*, Jan. 1996.

[18] GE Wind Energy, LLC, "Advanced Wind Turbine Program Next Generation Turbine Development Project," Subcontract Report NREL/SR-5000-38752, May 2006.

[19] DOE, "Variable Length Wind Turbine Blade," DE-FG36-03GO13171, June 30, 2005.

[20] Chopra, I., "Review of State of Art of Smart Structures and Integrated Systems," AIAA Journal, 40, 2002.

[21] Gad-el-Hak, M., "Overview of Turbulence Control Research in U.S.A.," Proceedings of the Symposium on Smart Control of Turbulence, ed. N. Kasagi, pp. 1-20, University of Tokyo, 2-3 Dec. 1999, Tokyo, Japan.

[22] Kral, L. D., "Active Flow Control Technology," *ASME Fluids Engineering Division Technical Brief*, 1998.

[23] Wood, R.M., "A Discussion of Aerodynamic Control Effectors (ACEs) for Unmanned Air Vehicles (UAVs)," AIAA Paper 2002-3495, 2002.

[24] Corten, G.P., "Vortex Blades," *Proc. from WindPower 2007*, Los Angeles, CA, June 4, 2007.

[25] Migliore, P.G., Quandt, G.A., and Miller, L.S., "Wind Turbine Trailing Edge Aerodynamic Brakes," Technical Report NRETL/TP-441-6913, Feb. 1995.

[26] Miller, L.S., "Experimental Investigation of Aerodynamic Devices for Wind Turbine Rotational Speed Control," Technical Report NREL/TP-441-6913, NREL, Feb. 1995.

[27] Miller, L.S., Quandt, G.A., and Huang, S., "Atmospheric Tests of Trailing Edge Aerodynamic Devices," Technical Report NREL/SR-500-22350, NREL, Jan. 1998.

[28] Stuart, J.G., Wright, A.D., and Butterfield, C.P., "Considerations for an Integrated Wind Turbine Controls Capability at the National Wind Technology Center: An Aileron Control Case Study for Power Regulation and Load Mitigation," *Prepared for AWEA Windpower '96*, NREL/TP-440-21335, 1996.

[29] Stuart, J.G., Wright, A.D., and Butterfield, C.P., "Wind Turbine Control Systems: Dynamic Model Development using System Identification and the FAST Structural Dynamics Code," *35th AIAA/ASME*, 1997.

[30] NWTC Design Codes (FAST by Jason Jonkman). http://wind.nrel.gov/designcodes/simulators/fast/. Last modified 12-August-2005; accessed 12-August-2005

[31] "Mission Adaptive Compliant Wing (MACW)," FlexSys Inc., Nov. 28, 2006. <http://www.flxsys.com/Projects/MACW/>.

[32] Kota, S., Hetrick, J., Osborn, R., Paul, D., Pendleton, E., Flick, P., and Tilmann, C., "Design and Application of Compliant Mechanisms for Morphing Aircraft Structures," *Proc. of SPIE,* Vol. 5054, 2003.

[33] Enenkl, B., Klopper, V,. and Preibler, D., "Full Scale Rotor with Piezoelectric Actuated Blade Flaps," *28th European Rotorcraft Forum*, 2002.

[34] Roth, D., Enenkl, B., and Dieterich, O., "Active Rotor Control by Flaps for Vibration Reduction – Full Scale Demonstrator and First Flight Test Results," *32nd European Rotorcraft Forum*, 2006.

[35] Basualdo, S., "Load Alleviation of Wind Turbine Blades Using Variable Airfoil Geometry," *Wind Engineering,* Vol. 29, No. 2, 2005, pp. 169-182.

[36] Troldborg, N., "Computational Study of the Risø-B1-18 airfoil with a Hinged Flap Providing Variable Trailing Edge Geometry," *Wind Engineering,* Vol. 29, No. 2, 2005, pp. 89-113.

[37] Buhl, T., Gaunaa, M., and Bak, C., "Potential Load Reduction Using Airfoils with Variable Trailing Edge Geometry," *Journal of Solar Energy Engineering*, Vol. 127, Nov. 2005, pp. 503-516.

[38] Andersen, P.B., Gaunaa, M., Bak, C. and Buhl, T., "Load Alleviation on Wind Turbine Blades using Variable Airfoil Geometry," *Proc. of 2006 European Wind Energy Conference and Exhibition,* Athens (GR), Feb.– Mar. 2006.

[39] Bak, C., Gaunaa, M., Anderson, B.B., Buhl, T., Hansen, P., Clemmensen, K., and Moeller, R., "Wind Tunnel Test on Wind Turbine Airfoil with Adaptive Trailing Edge Geometry", AIAA Paper 2007-1016, Jan. 2007.

[40] Fuglsang, P., Bak, C., Gaunaa, M. and Antoniou, I., "Wind Tunnel Tests of Risø-B1-18 and Risø-B1-24", Tech. Report Risø-R-1375(EN), Risø National Laboratory, Roskilde, Denmark, 2003.

[41] Fuglsang, P., Bak, C., Gaunaa, M., and Antoniou, I., "Design and Verification of the Risø-B1 Airfoil Family for Wind Turbines," *J. Sol. Energy Eng.*, Vol. 126, 2004, pp. 1002–1010.

[42] Hulskamp, A.W., Beukers, A., Bersee, H., van Wingerden, J.H., and Barlas, T.K., "Design of a Wind Tunnel Scale Model of an Adaptive Wind Turbine Blade for Active Aerodynamic Load Control Experiments," *16th ICCM*, 2007.

[43] "Thunder Actuators and Sensors," FACE®, Dec. 12, 2006. <http://www.presostore.com>.

[44] Scott, W.B., "Morphing Wings," *Aviation Week & Space Technology,* Nov. 2006.

[45] Liebeck, R.H., "Design of Subsonic Airfoils for High Lift," *Journal of Aircraft*, Vol. 15, No. 9, Sept. 1978, pp. 547-561.

[46] Yen, D.T., van Dam, C.P., Bräuchle, F., Smith, R.L., and Collins, S.D., "Active Load Control and Lift Enhancement Using MEM Translational Tabs," *Fluids 2000,* AIAA-2000-2422, Denver, CO, June 2000.

[47] Yen-Nakafuji, D.T., van Dam, C.P., Smith, R.L., and Collins, S.D., "Active Load Control for Airfoils Using Microtabs," *Journal of Solar Energy Engineering*, Vol. 123, No. 4, Nov. 2001, pp. 282-289.

[48] Yen, D.T., "Active Load Control using Microtabs," *PhD Dissertation, University of California, Davis*, 2001.

[49] Kelling, F.H., "Experimental Investigation of a High-Lift Low-Drag Aerofoil," ARC CP 1187, Sept. 1968. (Also GU Aero Report 6802, Sept 1968).

[50] Standish, K.J., and van Dam, C.P., "Computational Analysis of a Microtab-Based Aerodynamic Load Control System for Rotor Blades," *J. American Helicopter Society*, Vol. 50, No. 3, Jul. 2005, pp. 249-258.

[51] van Dam, C.P, Standish, K.J., and Baker, J.P., "Computational and Experimental Investigation into the Effectiveness of a Microtab Aerodynamic Load Control System," Sandia Report AO273, Aug. 2004.

[52] Baker, J.P., Standish, K.J., and van Dam, C.P., "Two-Dimensional Wind Tunnel and Computational Investigation of a Microtab Modified S809 Airfoil," AIAA Paper 2005-1186, *43rd AIAA Aerospace Sciences Meeting and Exhibit*, Reno, NV, 2005.

[53] Vijgen, P. M. H. W., Howard, F. G., Bushnell, D. M., and Homes, B. J., "Serrated Trailing Edges for Improved Lift and Drag Characteristics," US Patent No. 5,088,665, February 18 1992, (Invention Disclosure LAR 13870-1-CU, Aug. 31, 1987).

[54] Vijgen, P. M. H. W., van Dam, C. P., Holmes, B. J., and Howard, F., "Wind Tunnel Investigations of Wings with Serrated Sharp Trailing Edges," Low Reynolds Number Aerodynamics, edited by T. J. Mueller, No. 54 in Lecture Notes in Engineering, Springer-Verlang, 1989, pp. 295-313.

[55] Mayda, E.A., van Dam, C.P., and Yen-Nakafuji, D.T., "Computational Investigation of Finite Width Microtabs for Aerodynamic Load Control," AIAA Paper 2005-1185, Jan. 2005.

[56] Chow, R., and van Dam, C.P., "Unsteady Computational Investigations of Deploying Load Control Microtabs," *Journal of Aircraft*, Vol. 43, No. 5, Sept-Oct 2006, pp. 1458-1469.

[57] Chow, R., and van Dam, C.P., "Computational Investigations of Deploying Load Control Microtabs on a Wind Turbine Airfoil," AIAA Paper 2007-1018, Jan. 2007.

[58] Baker, J.P. and van Dam, C.P., "Wind Tunnel Study of the Microtab Load Control System on a Wind Turbine Blade Tip," Unpublished Paper, 2006.

[59] Moriarty, P.J., and Hansen, A.C., "AeroDyn Theory Manual", TP-500-36881, National Renewable Energy Laboratory, Boulder, CO, 2005.

[60] MATLAB and SIMULINK. The MathWorks, Inc. April 8, 2007 <http://www.mathworks.com/products/>.

[61] Zayas, J.R., van Dam, C.P., Chow R., Baker, J.P., and Mayda, E.A., "Active Aerodynamic Load Control for Wind Turbine Blades", European Wind Energy Conference, February 2006.

[62] Kroo, I, "Aerodynamic Concepts for Future Aircraft," *30th AIAA Paper 1999-3524, AIAA Fluid Dynamics Conference*, Norfolk, Va, June-July 1999.

[63] Lee, H, and Kroo, I.M., "Computational Investigations of Wings with Miniature Trailing Edge Control Surfaces," AIAA Paper 2004-2693, 2004.

[64] Lee, H, and Kroo, I.M., "Computational Investigations of Airfoils with Miniature Trailing Edge Control Surfaces," AIAA Paper 2004-1051, 2004.

[65] Bieniawski, S.R., Kroo, I.M., and Wolpert, D.H., "Flight Control with Distributed Effectors," AIAA Paper 2005-6074, 2005.

[66] Baker, J.P., Mayda, E.A., and van Dam, C.P., "Experimental Analysis of Thick Blunt Trailing-Edge Wind Turbine Airfoils," *Journal of Solar Energy Engineering*, Nov. 2006.

[67] van Dam, C.P., Chow, R., Zayas, J.R., and Berg, D.E., "Computational Investigations of Small Deploying Tabs and Flaps for Aerodynamic Load Control," The Science of Making Torque from the Wind, Denmark, *J. Phys.: Conf. Series*, Vol. 75, No.1, August 2007.

[68] Lewis, R.I., Potts, I., and Arain, A.A., "Aerodynamic Properties of NASA LS (1)-0417 MOD with Leading Edge Microspoilers for Lift/Drag Control," *Wind Engineering*, Vol. 15, No. 1, 1991, pp. 40-67.

[69] Lin, J.C., "Review of Research on Low-Profile Vortex Generators to Control Boundary-Layer Separation," *Progress in Aerospace Sciences*, Vol. 38, 2002, pp. 389-420.

[70] Barrett, R., and Farokhi, S., "Subsonic Aerodynamics and Performance of a Smart Vortex Generator System," Journal of Aircraft, Vol. 33, No. 2, March-April 1996.

[71] Lin, J.C., "Control of Turbulent Boundary-Layer Separation using Micro-Vortex Generators," AIAA Paper 99-3404, *30th AIAA Fluid Dynamics Conference*, Norfolk, VA, June 28-July 1, 1999.

[72] Kerho, M., Hutcherson, S., Blackwelder, R.F., and Liebeck, R.H., "Vortex Generators used to Control Laminar Separation Bubbles," *J. of Aircraft*, Vol. 30, No. 3, 1993, pp. 315-9.

[73] Greenblatt, D., and Wygnanski, I., "The Control of Flow Separation by Periodic Excitation," *Progress in Aerospace Sciences*, Vol. 36, 2000, pp. 487-545.

[74] Bons, J., Sondergaard, R., and Rivir, R. "The Fluid Dynamics of LPT Blade Separation Control Using Pulsed Jets," *ASME Journal of Turbomachinery,* Vol. 124, No. 1, pp. 77-85, 2002.

[75] Hinton, S.H., "Application of Boundary Layer Control to Rotor Blades," *Journal of the American Helicopter Society*, Vol. 2, No. 2, April 1957, pp. 36-64.

[76] Seifert, A., Daraby, A., Nishri, B., and Wygnanski, I., "The Effects of Forced Oscillations on the Performance of Airfoils," AIAA Paper 93-3264, AIAA Shear Flow Conference, Orlando, Fl., July 6-9, 1993.

[77] Weaver, D., McAlister, K.W., and Tso, J., "Suppression of Dynamic Stall by Steady and Pulsed Upper-Surface Blowing," NASA Tech. Paper 3600, ATCOM Tech Report 95-A-005, 1996.

[78] Tongchitpakdee, C., Benjanirat, S., and Sankar, L.N., "Numerical Studies of the Effects of Active and Passive Circulation Enhancement Concepts on Wind Turbine Performance," *Journal of Solar Energy Engineering,* Vol. 128, Nov. 2006.

[79] Metral, A.R., "On the Phenomenon of Fluid Veins and their Application, the Coanda Effect," AF Translation, F-TS-786-RE, 1939.

[80] Englar, R.J., Smith, M.J., Kelley, S.M., and Rover, R.C. III, "Application of Circulation Control to Advanced Subsonic Transport Aircraft, Part II: Transport Application," *J. of Aircraft*, Vol. 31, No.5, Sept-Oct. 1994, pp. 1169–1177.

[81] Shrewsbury, G.D., and Sankar, L.N., "Dynamic Stall of Circulation Control Airfoils," AIAA Paper 90-0573, 1990

[82] Liu, Y., Sankar, L.N., Englar, R.J., and Ahuja, K.K., "Numerical Simulations of the Steady and Unsteady Aerodynamic Characteristics of a Circulation Control Wing," AIAA Paper 2001-0704, 2001.

[83] Liu, Y., Sankar, L.N., Englar, R.J., Ahuja, K.K., and Gaeta, R., "Computational Evaluation of the Steady and Pulsed Jet Effects on the Performance of a Circulation Control Wing Section," AIAA Paper No. 2004-0056, 2004.

[84] Liu, Y., "Numerical Simulations of the Aerodynamic Characteristics of Circulation Control Wing Sections," *Ph.D. dissertation, School of Aerospace Engineering, Georgia Institute of Technology*, Atlanta GA, 2003.

[85] Englar, R.J., and Huson, G.G., "Development of Advanced Circulation Control Wing High Lift Airfoils," AIAA Paper 83-1847, 1983

[86] Englar, R.J., "Circulation Control Pneumatic Aerodynamics: Blown Force and Moment Augmentation and Modification; Past, Present and the Future," AIAA Paper 2000-2541, 2000.

[87] Englar, R.J., Smith, M.J., Kelley, S.M., and Rover, R.C. III, "Development of Circulation Control Technology for Application to Advanced Subsonic Aircraft," *AIAA Aerospace Sciences Conference*, AIAA Paper No. 93-0644, 1993.

[88] Englar, R.J., Smith, M.J., Kelley, S.M., and Rover, R.C. III, "Application of Circulation Control to Advanced Subsonic Transport Aircraft, Part I: Airfoil Development," *J. of Aircraft*, Vol. 31, No.5, Sept-Oct. 1994, pp. 1169–1177.

[89] Giguère, P., and Selig, M.S., "Design of a Tapered and Twisted Blade for the NREL Combined Experiment Rotor," National Renewable Energy Laboratory, NREL/SR-500-26173, Golden, CO, 1999.

[90] Hand, M.M., Simms, D.A., Fingersh, L.J., Jager, D.W., Cotrell, J.R., Schreck, S., and Larwood, S.M., "Unsteady Aerodynamics Experiment Phase VI: Wind Tunnel Test Configurations and Available Data Campaigns," National Renewable Energy Laboratory, NREL/TP-500–29955, Golden, CO, 2001.

[91] Simms, D.A., Schreck, S., Hand, M.M., and Fingersh, L.J., "NREL Unsteady Aerodynamics Experiment in the NASA Ames Wind Tunnel: A Comparison of Predictions to Measurements," NICH Report No. TP-500-29494, 2001.

[92] Fingersh, L.J., Simms, D.A., Hand, M.M., Jager, D.W., Cotrell, J.R., Robinson, M., Schreck, S., and Larwood, S.M., "Wind Tunnel Testing of NREL's Unsteady Aerodynamics Experiment," AIAA Paper No. 2001-0035, 2001.

[93] Moreau, E., "Airflow Control by Non Thermal Plasma Actuators," *Journal of Phys. D,* 40: 605-636, 2007.

[94] Moreau, E., Artana, G., and Touchard, G., "Surface Corona Discharge Along an Insulating Flat Plate in Air Applied to Electrohydrodynamically Airflow Control : Electrical Properties," *Electrostatics,* 178: 285290, 2004.

[95] Moreau, E., Benard, N., Jolibois, M., and Touchard, G., "Airflow Control by Plasma Actuators : Last Significant Results at the University of Poitiers," *2nd European Conference for Aerospace Sciences,* 2007.

[96] Roth, J.R, and Sherman, D.M., "Boundary Layer Flow Control with a One Atmosphere Uniform Glow Discharge Surface Plasma," AIAA Paper 98-0328, January 1998.

[97] Jukes T.N., Choi K.S., Johnson G.A., and Scott S.J., "Turbulent Boundary Layer Control for Drag Reduction Using Surface Plasma," AIAA Paper 2004-2216, 2004.

[98] Santhanakrishnan, A., and Jacob, J.D., "Flow Control with Plasma Synthetic Jet Actuators," J. Phys. D: *Appl. Phys.* Vol. 40, 2007, pp. 637-651.

[99] Santhanakrishnan, A., Jacob, J.D., and Suzen, Y.B., "Flow Control Using Plasma Actuators and Linear/Annular Plasma Synthetic Jet Actuators," *3rd AIAA Flow Control Conference,* San Francisco, CA, June 5-8, 2006.

[100] Velkoff, H., and Ketchman, J., "Effect of an Electrostatic Field on Boundary Layer Transition," *AIAA Journal,* Vol. 16, 1968, pp. 1381–3.

[101] Yabe, A., Mori, Y., and Hijikata, K., "EHD Study of the Corona Wind Between Wire and Plate Electrodes," *AIAA Journal,* Vol. 16, 1978, pp. 340–5.

[102] El-Khabiry, S. and Colver, G.M., "Drag Reduction by a DC Corona Discharge Along an Electrically Conductive Flat Plate for Small Reynolds Number Flow," *Phys. Fluids,* Vol. 9, 1997, pp. 587–99.

[103] Vilela Mendes, R., and Dente, J.A., "Boundary Layer Control by Electric Fields: A Feasibility Study," *J. Fluid Eng.,* Vol. 120, 1998, pp. 626–9.

[104] Corke, T.C., Jumper, E.J., Post, M.L., Orlov, D., and McLaughlin, T.E., "Applications of Weakly-Ionized Plasmas as Wing Flow-Control Devices," AIAA Paper 2002–0350, 2002.

[105] Post, M.L., and Corke, T.C., "Separation Control on High Angle of Attack Airfoil Using Plasma Actuators," AIAA Paper 2003-1024, 2003.

[106] Post, M.L., and Corke, T.C., "Separation Control Using Plasma Actuators - Stationary and Oscillating Airfoils," AIAA Paper 2004-0841, 2004.

[107] Post, M.L., and Corke, T.C., "Separation Control Using Plasma Actuators - Dynamic Stall Control on an Oscillating Airfoil," AIAA Paper 2004-2517, 2004.

[108] Corke, T.C., He, C. and Patel, M.P., "Plasma Flaps and Slats: An Application of Weakly-Ionized Plasma Actuators," AIAA Paper 2004-2127, 2004.

[109] Post, M.L., and Corke, T.C., "Overview of Plasma Flow Control: Concepts, Optimization and Applications," AIAA Paper 2005-0563, 2005.

[110] Corke, T.C., Mertz, B. and Patel, M.P., "Plasma Flow Control Optimized Airfoil," AIAA Paper 2006-1208, 2006.

[111] Jolibois, J., Forte, M. and Moreau, E., "Separation Control along a NACA0015 Airfoil using a Dielectric Barrier Discharge Actuator," IUTAM Symposium on Flow Control with Mems, London, England, September 2006.

[112] Selby, G.V., Lin, J.C., and Howard, F.G., "Control of Low-Speed Turbulent Separated Flow Using Vortex Generator Jets," *Experiments in Fluids*, Vol. 12, 1992, pp. 394-400.

[113] Johnston, J.P., and Nishi, M., "Vortex Generator Jets: Means for Flow Separation Control," *AIAA Journal*, Vol. 28, 1990, pp. 989-994.

[114] Johnston, J.P., "Pitched and Skewed Vortex Generator Jets for Control of Turbulent boundary Layer Separation: A Review," SEDSM 99-6917 3rd ASME/JSME Joint Fluids Engineering Conference, San Francisco, CA, July 18-23, 1999.

[115] Compton, D.A., and Johnston, J.P., "Streamwise Vortex Production by Pitched and Skewed Jets in a Turbulent Boundary Layer," *AIAA Journal*, Vol. 30, 1992, pp. 640.

[116] Khan, Z.U., and Johnson, J.P., "On Vortex Generating Jets," *International Journal of Heat and Fluid Flow*, Vol . 21, 2000, pp. 506-511.

[117] Lin, J.C., Howard, F.G., and Bushnell, D.M., "Investigation of Several Passive and Active Methods for Turbulent Flow Separation Control," AIAA Paper 90-1598, 1990.

[118] McManus, K.R., Legner, H.H., and Davis, S.J., "Pulsed Vortex Generator Jets for Active Control of Flow Separation," AIAA Paper 94-2218, 25th AIAA Fluid Dynamics Conference, June 1994.

[119] McManus, K.R., Ducharme, A., Goldey, C., and Magill, J., "Pulsed Jet Actuators for Suppressing Flow Separation," AIAA Paper No. 96-0442, 34th AIAA Aerospace Sciences Meeting, January 1996.

[120] Seifert, A., Bachar, T., Koss, D., Shepshelovich, M., and Wygnanski, I., "Oscillatory Blowing: A Tool to Delay Boundary Layer Separation," *AIAA Journal*, Vol. 31, No. 11, 1993, pp. 2052-2060.

[121] Wygnanski, I. and Seifert, A., "Control of Separation by Periodic Oscillation," AIAA Paper 94-2608, 18th AIAA Ground Test Conference, Colorado Springs, CO, June 20-29, 1994.

[122] Johari, H. and McManus, K.R., "Visualization of Pulsed Vortex Generator Jets for Active Control of Boundary Layer Separation," AIAA Paper 97-2021, 28th AIAA Fluid Dynamics Conference, June 1997.

[123] Magill, J.C., and McManus, K.R., "Exploring the Feasibility of Pulsed Jet Separation Control for Airfcraft Configureations," *Journal of Aircraft*, Vol 38, 2001, pp. 48-56.

[124] Magill, J.C., and McManus, K., "Control of Dynamic Stall using Pulsed Vortex Generator Jets," AIAA Paper 98-0675, Jan. 1998.

[125] Bons, J., Sondergaard, R., and Rivir, R. "Control of Low-Pressure Turbine Separation Using Pulsed Vortex Generator Jets," 37th AIAA Aerospace Sciences Meeting and Exhibit, Reno, NV, AIAA 99-0367, January 1999.

[126] Bons, J., Sondergaard, R., and Rivir, R. "Turbine Separation Control Using Pulsed Vortex Generator Jets," *ASME Journal of Turbomachinery*, Vol. 123, No. 4, 2001, pp. 198-206.

[127] Heinzen, S., Hall, C. and Chokani, N. "In-Flight Application of Active Separation Control Using Pulsed Jet Blowing," AIAA 2002-0416, January 2002.

[128] Tensi, J., Bourgois, S., Bonnet, J.P., Breux, J.M., and Siauw, W.L., "Airfoil Performance Enhancement Using Fluidic Actuators," *Laboratoire d'Etudes Aérodynamiques UMR 6609,* 2007.

[129] Seifert, A., Darabi, A., and Wygnanski, I., "On the Delay of Airfoil Stall by Periodic Excitation," *Journal of Aircraft*, Vol. 33, No. 4., 1996, pp. 691–699.

[130] Lisy, F., and Schmidt, R., "Large Throw, Imbedded Microactuators for Drag Reduction," U.S. Air Force Research Lab., Contract F33615-95-C-3003, Wright–Patterson AFB, OH, Dec. 1995.

[131] Osborn, R.F., Kota, S., Hetrick, J.A., Geister, D.E., Tilmann, C.P., and Joo, J., "Active Flow Control Using High-Frequency Compliant Structures," AIAA Paper 2001-4144, 2001.

[132] Seifert, A., and Pack, L. G., "Active Control of Separated Flows on Generic Configurations at High Reynolds Numbers," AIAA Paper 99-3403, June 1999.

[133] James, R.D., Jacobs, J.W., and Glezer, A., "A Round Turbulent Jet Produced by an Oscillating Diaphragm," *Phys. Fluids* 8:2484, 1996.

[134] Smith, B.L., and Glezer. A., "The Formation and Evolution of Synthetic Jets," *Phys. Fluids* 31:2281–97, 1998.

[135] Mallinson, S.G., Hong, G., and Reizes, J.A., "Some Characteristics of Synthetic Jets," *AIAA 30th Fluid Dyn. Conf. 99-3651*, Norfolk, VA, 1999.

[136] Crook, A., Sadri, A.M., and Wood, N.J., "The Development and Implementation of Synthetic Jets for Control of Separated Flow," *AIAA 17th Appl. Aerodyn. Conf. 99-3176*, Reno, Nev., 1999.

[137] Mueller, M.O., Bernal, L.P., Miska, P.K., Washabaugh, P.D., Chou, T.K.A., Parviz, A.P., Zhang, C., and Najafi, K., "Flow Structure and Performance of Axisymmetric Synthetic Jets," AIAA Paper 2001-1008, *39th Aerosp. Sci. Meet.*, Reno, Nev., 2001.

[138] Kral, L.D., Donovan, J.F., Cain, A.B., and Cary, A.W., "Numerical Simulation of Synthetic Jet Actuators," AIAA Paper 1997-1824, 1997.

[139] Rizzetta, D.P., Visbal, M.R., and Stanek, M.J., "Numerical Investigation of Synthetic Jet Flow-Fields," AIAA Paper 1998-2910, *29th AIAA Fluid Dyn. Conf.,* Albuquerque, NM, 1998.

[140] Guo, D., and Kral, L.D., "Numerical Simulation of the Interaction of Adjacent Synthetic Jet Actuators," AIAA Paper 2000-2565, *Fluids 2000 Conference and Exhibit*, Denver, CO, 2000.

[141] Seifert, A., Bachar, T., Koss, D., Shepshelovich, M., and Wygnanski, I., "Oscillatory Blowing: A Tool to Delay Boundary-Layer Separation," *AIAA Journal*, Vol. 31, No. 11, 1993.

[142] Donovan, J.F., Kral, L.D., and Cary, A.W., "Active Control Applied to an Airfoil," AIAA Paper 98-0210, 1998.

[143] Ravindran, S.S., "Active Control of Flow Separation Over an Airfoil," NASA/TM-1999-209838, 1999.

[144] Sinha, S.K., "System for Efficient Control of Separation using a Driven Flexible Wall," U.S. Patent 5,961,080, Oct. 1999.

[145] Sinha, S.K., and Zou, J., "On Controlling Flows with Micro-Vibratory Wall Motion," AIAA Paper 2000-4413, Aug. 2000.

[146] Mangla, N.L. and Sinha, S.K., "Controlling Dynamic Stall with an Active Flexible Wall," AIAA Paper 2004-2325, June-July 2004.

[147] Munday, D., and Jacob, J. D., "Flow Control Experiments for Low-Re Adaptive Airfoils," AIAA Paper 2000-0654, Jan. 2000.

[148] Munday, D., and Jacob, J. D., “Active Control of Separation on a Wing with Conformal Camber," AIAA Paper 2001-0293, Jan. 2001.

[149] Munday, D., and Jacob, J. D., “Active Control of Separation on a Wing with Oscillating Camber," *Journal of Aircraft*, 39 No. 1, 2002.

[150] Pinkerton, T.L., and Moses, R. W., “A Feasibility Study to Control Airfoil Shape Using THUNDER," NASA TM-4767, 1997.

[151] Pern, N.J., “Vortex Mitigation Using Adaptive Airfoils,” Master’s Thesis, University of Kentucky, Lexington, Kentucky, Aug. 1999.

[152] Pern, N.J, Jacob, J.D., and LeBeau, R.P., “Characterization of Zero Flux Flow Control for Separation Control of an Adaptive Airfoil,” AIAA Paper 2006-3032, 2006.

DISTRIBUTION:

Tom Acker
Northern Arizona University
PO Box 15600
Flagstaff, AZ 86011-5600

Ian Baring-Gould
NREL/NWTC
1617 Cole Boulevard MS 3811
Golden, CO 80401

Keith Bennett
U.S. Department of Energy
Golden Field Office
1617 Cole Boulevard
Golden, CO 80401-3393

Karl Bergey
University of Oklahoma
Aerospace Engineering Dept.
Norman, OK 73069

Mike Bergey
Bergey Wind Power Company
2200 Industrial Blvd.
Norman, OK 73069

Derek Berry
TPI Composites, Inc.
373 Market Street
Warren, RI 02885-0328

Gunjit Bir
NREL/NWTC
1617 Cole Boulevard MS 3811
Golden, CO 80401

Marshall Buhl
NREL/NWTC
1617 Cole Boulevard MS 3811
Golden, CO 80401

C.P. Sandy Butterfield
NREL/NWTC
1617 Cole Boulevard MS 3811
Golden, CO 80401

Garrett Bywaters
Northern Power Systems
182 Mad River Park
Waitsfield, VT 05673

Doug Cairns
Montana State University
Dept. of Mechanical & Industrial Eng.
College of Engineering
PO Box 173800
Bozeman, MT 59717-3800

David Calley
Southwest Windpower
1801 West Route 66
Flagstaff, AZ 86001

Larry Carr
NASA Ames Research Center
24285 Summerhill Ave.
Los Altos, CA 94024

Jamie Chapman
Texas Tech University
Wind Science & Eng. Research Center
Box 41023
Lubbock, TX 79409-1023

Kip Cheney
PO Box 456
Middlebury, CT 06762

Craig Christensen
Clipper Windpower Technology, Inc.
6305 Carpinteria Ave. Suite 300
Carpinteria, CA 93013

R. Nolan Clark
USDA - Agricultural Research Service
PO Drawer 10
Bushland, TX 79012

C. Cohee
Foam Matrix, Inc.
1123 E. Redondo Blvd.
Inglewood, CA 90302

Joe Cohen
Princeton Economic Research, Inc.
1700 Rockville Pike, Suite 550
Rockville, MD 20852

C. Jito Coleman
Northern Power Systems
182 Mad River Park
Waitsfield, VT 05673

Ken J. Deering
The Wind Turbine Company
PO Box 40569
Bellevue, WA 98015-4569

James Dehlsen
Clipper Windpower Technology, Inc.
6305 Carpinteria Ave. Suite 300
Carpinteria, CA 93013

Edgar DeMeo
Renewable Energy Consulting Services
2791 Emerson St.
Palo Alto, CA 94306

S. Finn
GE Global Research
One Research Circle
Niskayuna, NY 12309

Peter Finnegan
GE Global Research
One Research Circle
Niskayuna, NY 12309

Trudy Forsyth
NREL/NWTC
1617 Cole Boulevard
Golden, CO 80401

Brian Glenn
Clipper Windpower Technology, Inc.
6305 Carpinteria Ave. Suite 300
Carpinteria, CA 93013

R. Gopalakrishnan
GE Wind Energy
GTTC, 300 Garlington Road
Greenville, SC 29602

Dayton Griffin
Global Energy Concepts, LLC
1809 7th Ave., Suite 900
Seattle, WA 98101

Maureen Hand
NREL/NWTC
1617 Cole Boulevard MS 3811
Golden, CO 80401

Thomas Hermann
Odonata Research
202 Russell Ave. S.
Minneapolis, MN 55405-1932

D. Hodges
Georgia Institute of Technology
270 Ferst Drive
Atlanta, GA 30332

William E. Holley
GE Wind Energy
GTTC, M/D 100D
300 Garlington Rd.
PO Box 648
Greenville, SC 29602-0648

Adam Holman
USDA - Agricultural Research Service
PO Drawer 10
Bushland, TX 79012-0010

D.M. Hoyt
NSE Composites
1101 N. Northlake Way, Suite 4
Seattle, WA 98103

Scott Hughes
NREL/NWTC
1617 Cole Boulevard MS 3911
Golden, CO 80401

Kevin Jackson
Dynamic Design
123 C Street
Davis, CA 95616

Eric Jacobsen
GE Wind Energy - GTTC
300 Garlington Rd.
Greenville, SC 29602

George James
Structures & Dynamics Branch Mail Code ES2
NASA Johnson Space Center
2101 NASA Rd 1
Houston, TX 77058

Jason Jonkman
NREL/NWTC
1617 Cole Boulevard
Golden, CO 80401

Gary Kanaby
Knight & Carver Yacht Center
1313 Bay Marina Drive
National City, CA 91950

Benjamin Karlson
Wind Energy Technology Department
Room 5H-088
1000 Independence Ave. S.W.
Washington, DC 20585

Jason Kiddy
Aither Engineering, Inc.
4865 Walden Lane
Lanham, MD 20706

M. Kramer
Foam Matrix, Inc.
PO Box 6394
Malibu, CA 90264

David Laino
Windward Engineering
8219 Glen Arbor Dr.
Rosedale, MD 21237-3379

Scott Larwood
1120 N. Stockton St.
Stockton, CA 95203

Bill Leighty
Alaska Applied Sciences, Inc.
PO Box 20993
Juneau, AK 99802-0993

Wendy Lin
GE Global Research
One Research Circle
Niskayuna, NY 12309

Steve Lockard
TPI Composites, Inc.
373 Market Street
Warren, RI 02885-0367

James Locke
AIRBUS North America Eng., Inc.
213 Mead Street
Wichita, KS 67202

James Lyons
Novus Energy Partners
201 North Union St., Suite 350
Alexandria, VA 22314

David Malcolm
Global Energy Concepts, LLC
1809 7th Ave., Suite 900
Seattle, WA 98101

John F. Mandell
Montana State University
302 Cableigh Hall
Bozeman, MT 59717

Tim McCoy
Global Energy Concepts, LLC
1809 7th Ave., Suite 900
Seattle, WA 98101

L. McKittrick
Montana State University
Dept. of Mechanical & Industrial Eng.
220 Roberts Hall
Bozeman, MT 59717

Amir Mikhail
Clipper Windpower Technology, Inc.
6305 Carpinteria Ave. Suite 300
Carpinteria, CA 93013

Patrick Moriarty
NREL/NWTC
1617 Cole Boulevard
Golden, CO 80401

Walt Musial
NREL/NWTC
1617 Cole Boulevard MS 3811
Golden, CO 80401

Library (5) NWTC
NREL/NWTC
1617 Cole Boulevard
Golden, CO 80401

Byron Neal
USDA - Agricultural Research Service
PO Drawer 10
Bushland, TX 79012

Steve Nolet
TPI Composites, Inc.
373 Market Street
Warren, RI 02885-0328

Richard Osgood
NREL/NWTC
1617 Cole Boulevard
Golden, CO 80401

Tim Olsen
Tim Olsen Consulting
1428 S. Humboldt St.
Denver, CO 80210

Robert Z. Poore
Global Energy Concepts, LLC
1809 7th Ave., Suite 900
Seattle, WA 98101

Cecelia M. Poshedly (5)
Office of Wind & Hydropower
Techologies
EE-2B Forrestal Building
U.S. Department of Energy
1000 Independence Ave. SW
Washington, DC 20585

Robert Preus
Abundant Renewable Energy
22700 NE Mountain Top Road
Newberg, OR 97132

Jim Richmond
MDEC
3368 Mountain Trail Ave.
Newberg Park, CA 91320

Michael Robinson
NREL/NWTC
1617 Cole Boulevard
Golden, CO 80401

Dan Sanchez
U.S. Department of Energy
NNSA/SSO
PO Box 5400 MS 0184
Albuquerque, NM 87185-0184

Scott Schreck
NREL/NWTC
1617 Cole Boulevard MS 3811
Golden, CO 80401

David Simms
NREL/NWTC
1617 Cole Boulevard MS 3811
Golden, CO 80401

Brian Smith
NREL/NWTC
1617 Cole Boulevard MS 3811
Golden, CO 80401

J. Sommer
Molded Fieber Glass Companies/West
9400 Holly Road
Adelanto, CA 92301

Ken Starcher
Alternative Energy Institute
West Texas A & M University
PO Box 248
Canyon, TX 79016

Fred Stoll
Webcore Technologies
8821 Washington Church Rd.
Miamisburg, OH 45342

Herbert J. Sutherland
HJS Consulting
1700 Camino Gusto NW
Albuquerque, NM 87107-2615

Andrew Swift
Texas Tech University
Civil Engineering
PO Box 41023
Lubbock, TX 79409-1023

J. Thompson
ATK Composite Structures
PO Box 160433 MS YC14
Clearfield, UT 84016-0433

Robert W. Thresher
NREL/NWTC
1617 Cole Boulevard MS 3811
Golden, CO 80401

Steve Tsai
Stanford University
Aeronautics & Astronautics
Durand Bldg. Room 381
Stanford, CA 94305-4035

William A. Vachon
W. A. Vachon & Associates
PO Box 149
Manchester, MA 01944

C.P. van Dam
Dept. of Mechanical & Aerospace Eng.
University of California, Davis
One Shields Avenue
Davis, CA 95616-5294

Jeroen van Dam
Windward Engineering
NREL/NWTC
1617 Cole Boulevard
Golden, CO 80401

Brian Vick
USDA - Agricultural Research Service
PO Drawer 10
Bushland, TX 79012

Carl Weinberg
Weinberg & Associates
42 Green Oaks Court
Walnut Creek, CA 94596-5808

Kyle Wetzel
Wetzel Engineering, Inc.
PO Box 4153
Lawrence, KS 66046-1153

Mike Zuteck
MDZ Consulting
601 Clear Lake Road
Clear Lake Shores, TX 77565

INTERNAL DISTRIBUTION:

MS 0557 D.T. Griffith, 1524
MS1124 J.R. Zayas, 6333
MS 1124 T.D. Ashwill, 6333
MS 1124 M.E. Barone, 06333
MS 1124 D.E. Berg, 6333 (10)
MS 1124 S.M. Gershin, 6333
MS 1124 R.R. Hill, 6333
MS 1124 W. Johnson, 6333
MS 1124 D.L. Laird, 6333
MS 1124 D.W. Lobitz, 6333
MS 1124 J. Paquette, 6333
MS 1124 M.A. Rumsey, 6333
MS 1124 J. Stinebaugh, 6333
MS 1124 P.S. Veers, 6333
MS 0899 Technical Library, 9536
(Electronic)

Sandia National Laboratories